Novel nanotweezers for high efficiency optical trapping at submicrometer scale

Politecnico di Bari

Department of Electrical and Information Engineering

ELECTRICAL AND INFORMATION ENGINEERING
Ph.D. Program
SSD: ING-INF/01 – ELECTRONICS

Final Dissertation

Novel nanotweezers for high efficiency optical trapping at submicrometer scale

---

by

DONATO CONTEDUCA

Referees:

Prof. Thomas F. KRAUSS

Prof. Richard DE LA RUE

Supervisor:

Prof. Caterina CIMINELLI

Coordinator of Ph.D Program:

Prof. Vittorio M. N. PASSARO

XXIX cycle, 2014-2016

Acknowledgments

First of all, I would like to thank my supervisor prof. Caterina Ciminelli for accepting me as a PhD student in her research group and for supporting me and my research activity during these years. Her supervision has been very professional and gratifying for me, contributing to enhance my experience in the field of integrated optics, since the first approach to the problem to the solution. I have really appreciated her humanity and perseverance, that will be a reference point for my life.

A special thank is also for prof. Mario Armenise for his suggestions, encouragements and critical observations during my master thesis and my PhD activity, that have improved my approach to the study.

I also owe a special thanks to prof. Thomas Krauss for his hospitality in his research group and his support during my master thesis and PhD activity. I have learnt a lot from our discussions. He has always prodded me and his impressive theoretical and experimental experience in integrated optics has helped me a lot.

Thanks to Ing. Dr. Francesco Dell'Olio, who helped me a lot during these years from a master student up to this goal. His teaching and suggestions have improved my work to reach always a higher level.

A thanks to all members (in the present and in the past) of the Optoelectronics Group of Politecnico di Bari. My PhD has gone very quickly thanks to our jokes, laughter and breaks. Work is a different place when you share it with passionate, hard-working and very friendly persons.

I could never forget to thank all members of the Photonics Group of the University of York. All time in your research group, with our discussions and meetings, has been very inspiring to me and I have learnt a lot from you, especially about the experimental work in a cleanroom for the fabrication of integrated optical devices and their optical characterization. A special thanks to Dr. Mark Scullion, because he followed me since the first day in the "trapping world" and I could learn so much thanks to his patience, humanity and availability.

As everybody knows: "*No man is an island entire of itself*" (John Donne), so I really would like to thank Giampaolo, Pepe, Paula and Bryan because we enjoyed a lot during my stay in York and I never felt "*an island"* far from my home thanks to these friends.

Finally, thanks to my family. This goal has been reached with their unconditional support and guidance through my life!

Most of all, thanks to Maria! I would not be the person that I am today without you in my life and there are not enough words to thank you in few lines. Your love, patience and support allow me to pass bad times and move forward in my life. These years, and all next steps together, will be never possible without you!

Donato Conteduca

Contents

List of Figures

List of Tables

Abstract

Trapping, manipulation, and sensing of particles at micro- and nanoscale have obtained a fundamental role for several applications and particularly in biomedical environments, such as oncology, proteomics and biology. Among life science application domain, the ability to trap matter at microscale, such as cells and bacteria, up to single molecule, protein and virus of few nanometers, allows to investigate many diseases (e.g. cancer early diagnosis, motility of bacteria and cells activity), and also the effects of new drugs on a single pathogen like a virus, prion or virion, in addition to the analysis of proteins interaction.

Optically-based techniques have been largely used to realize devices for trapping, typically called "optical tweezers", due to their several advantages compared to other trapping methods. Optical tweezers provide traps with high spatial resolution, and particularly contact-free manipulation, so obtaining a relevant decrease of risks of damage and disruption of the trapped matter. Such properties are very important for trapping of living matter in biomedical applications, in order to avoid changes of surface properties or alterations in the behavior of the target object, so affecting the results of the experiments.

A limitation of bulk optical tweezers is related to low values of optical forces that can be exerted, which poses a challenge for the manipulation of life matter at the nanoscale. In the last years, nanotweezers based on different technologies have been proposed in order to improve the trapping efficiency.

Higher values of optical forces have been obtained with integrated optical devices, and particularly photonic and plasmonic resonant cavities have demonstrated to enable trapping of living matter at the nanoscale, so interesting a strong research effort and becoming attractive for commercial devices.

In this work, an integrated photonic/plasmonic cavity, based on a bowtie nanoantenna vertically coupled to a 1D PhC cavity, has been proposed as hybrid nanotweezer, aiming at enhancing light-matter interaction and improving the trapping efficiency. The cavity provides ultra-high Q/V values with optical forces in the pN range for dielectric particles smaller than 100 nm. Such performance corresponds to high stability of the optical traps of beads at the nanoscale with long trapping time, potentially including also biological matter.

A good matching between simulated and experimental results of the hybrid cavity performance have been obtained. The suitability of the proposed device as an efficient hybrid nanotweezer has been demonstrated experimentally by the stable trapping condition of Au beads up to 200 nm observed for several minutes with sub-mW optical powers.

Introduction

Trapping techniques for manipulation of objects at micro and nanoscale have been strongly investigated in the last years, assuming a crucial role for many life science domains, such as medicine, biology, pharmacology and chemistry [1,2]. They have improved the performance obtained by other commercial techniques, which typically require bulky configurations and high power values [3].

Many trapping techniques have been proposed, which are suitable to trap and manipulate particles and living matter from several microns to few nanometers. In particular, optically-based detection schemes have demonstrated the best compromise in terms of high efficiency, compact volume and low value of energy consumption. Furthermore, devices used for optical manipulation provide stable trapping events for nanoparticles with a real time analysis, so covering the need of life scientists to manipulate smaller biological samples [4-6].

Optical tweezers are very advantageous for their ability to detect and manipulate target objects without a direct contact. The lack of touch or binding minimize risks of damage and disruption, preventing to affect surface properties of living matter, which is fundamental in biomedical applications, for example to investigate proteins interaction or virus properties [7].

It is very difficult to obtain high trapping efficiency with optical tweezers with bulk configurations, which are based on focusing a laser beam by optical lenses in order to improve light-matter interaction in small volumes [8]. This represents a critical issue for these devices, limiting their use in several applications in medicine, biology and chemistry, for which the trapping at nanoscale is necessary.

Recently, the spread of new technologies, fabrication techniques and materials has enhanced the integration of several devices on a single chip (Lab on a Chip), so allowing the realization of nanotweezers integrated with microfluidic channels [9]. Nanotweezers provide higher values of trapping forces, enabling the trapping at nanoscale and facilitating their use in nanomedicine (this term is related to the medical application of nanotechnology, including the study of nanomaterials, nanomachines for surgery, nanodevices for biosensing and nanodrugs for therapeutic applications) [10].

Nanotweezers have demonstrated to confine high energy values in very small volumes, which is a necessary condition to reach high trapping efficiency [11]. Therefore, such devices allow to trap selectively particles from few micrometers, such as small cells and bacteria [12,13], up to a single bead of few nanometers (i.e. proteins, DNA chains, small virus) [14,15]. It is very useful to diagnose human diseases, giving accurate information about its progression. In fact, the early detection of low values of concentration and small size of cells, such as cancer ones, bacteria or virus, facilitates a fast and careful medical prevention [16,17]. This would strongly decrease the mortality rate and also the expensive financial costs of health system for several diseases, i.e. cancer and genetic illnesses, related to the expenditure on care, emergency and surgeries, outpatients and drugs [18].

In the last years, optical nanotweezers have been also used in genetics and proteomics, due to their ability to trap matter at the single molecule level, allowing the study of coprotein interactions, protein-DNA and antigen-antibody bindings, detection of DNA strains and virions [19,20]. Such behaviour enables the analysis of the evolution of a life cycle of a single virus in order to define the disease's progress and to control the effects of drugs at single molecule level, so improving the efficiency of medical treatments [21]. This also justifies the rising and wide spread of the research interest towards nanotweezers, which is growing remarkably also due to their promising applications related to detection and analysis of genetic functionality and integrity, which is the basis of most human diseases. Furthermore, the direct trapping of particles of few nanometers without the need of labelling and tethering of target molecules is a strong advantage in comparison with the performance obtained by other commercial techniques [22]. Labels typically alter surface characteristics and activities of trapped objects (i.e. due to photobleaching and thermal effects) and tethering requires available binding sites for the surface attachment, modifying its properties and compromising the genetic information [23]. Several techniques and methods have been proposed to overcome these challenges, such as calorimetry, holographic techniques, enthalpic arrays and interferometric configurations, but they require large volumes, low sensitivity and long preparation times [24]. Therefore, the device integration with a real time analysis is prevented, making such methods unsuitable for several biomedical applications and particularly for the realization of point-of-care devices, unlike the compact and efficient nanotweezers [25].

The success of nanotweezers is also related to their versatility to be used for several applications and not limited only at biomedical environment. In fact, the trapping and manipulation of carbon nanotubes and graphene flakes have been used in electronics to realize chemical sensors, for example for the desalination of membranes, field emitters and integrated circuits [26,27]. The control on motion and spin of beads has been also investigated to explore the transitions between the classical and quantum world [28,29]. Nanoantenna used as plasmonic tweezers have been also proposed to obtain advances in magnetic recording for data storage and nanocamera, due to their ability to strongly confine electromagnetic energy and to provide heated regions in a volume at the nanoscale [30].

A description of several techniques and configurations of nanotweezers proposed in literature to enable trapping of particles at micro and also nanoscale has been included in the next chapter, so describing their performance, potential applications and limitations. Trapping methods with optical signals have been briefly discussed in Chapter 2, in order to put only in evidence the real and effective advantages of optical tweezers to the other methods. In Chapter 3, a discussion on theory and physical aspects of optically-based trapping techniques has been included, focusing on the different regimes as a function of geometrical and physical properties of the objects to trap.

A detail description of several configurations of optical and plasmonic nanotweezers proposed in literature is discussed in Chapter 4, focusing on the advantages obtained with hybrid nanotweezers as the best compromise among those configurations.

The design and numeric results of an ultra-high Q/V photonic/plasmonic cavity is proposed in Chapter 5. The experimental activity with the fabrication processes and techniques and the optical characterization is discussed in Chapter 6, demonstrating the good matching between numerical and experimental results.

In Chapter 7, the efficiency of the photonic/plasmonic cavity as hybrid nanotweezer for submicrometer particles has been verified, so demonstrating also the suitability of the proposed configuration for trapping at the nanoscale.

Finally, potential applications and future prospects of optical nanotweezers have been discussed to investigate environments where their spread is advantageous, such as biomedicine, and their effective impact in the worldwide market.

CHAPTER 2

Trapping techniques

Different techniques have been proposed and developed for trapping, probing and manipulating small particles at micro and nanoscale, such as optical [31,32], hydrodynamic [33,34], magnetic [35,36], acoustic [37] and dielectrophoretic traps [38,39]. An overview on different trapping techniques and configurations is reported to comprehend the physical mechanisms, their performance and drawbacks.

Finally, a brief description of optical tweezers with bulk structures for trapping at the microscale and their market review has been proposed. A detail description of integrated optical nanotweezer configurations, that enable trapping at the nanoscale, has been reported in Chapter 4.

2.1 Hydro-dynamical trapping

Propulsion forces that enable to transport objects can be obtained in a microchannel in which a liquid continuously flows inside [40]. The strength of these forces is strongly related by the shape and size of the channel and by the object's properties, because they affect the pressure of fluid in the channel. Different configurations of microchannels have been proposed to obtain sorting and trapping of particles at microscale [41]. In particular, the flow velocity strongly influences the intensity of forces acting on the particles, while the channel configuration affects their direction. Therefore, the flow streamlines change as a function of particles' size and fluid properties. This can be used to realize the separation of different objects and also their trapping in specific positions [42].

Different configurations of microchannels with a rectangular or circular transversal cross-section have been proposed to control particles' motion [43]. For example, multiorefices and microholes have been integrated in these structures to modify the fluid streamlines [44], in order to create microvortices, where particles can be attracted and then trapped as in a reservoir (see Fig. 2.1).

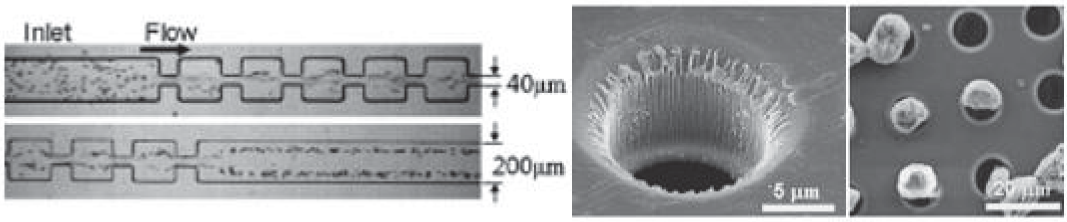

(a) (b)

Fig. 2.1. (a) Microparticles migrating through the multiorifice microchannel [43] and (b) trapping of LNCaP cell by nanoholes [44].

Trapping and manipulation of a single particle is challenging with hydrodynamic techniques. Recently, several devices with particular configurations of microchannels, that enable to predict the flow profile in each single trap, have been proposed. Kobel et al. in [45] demonstrated the trapping of a single cell with an optimized trap architectures with efficiency > 90% and a rate of cell loss of about 20%. Similar performance has been obtained by engineering the size and shape of the trap (see Fig. 2.2).

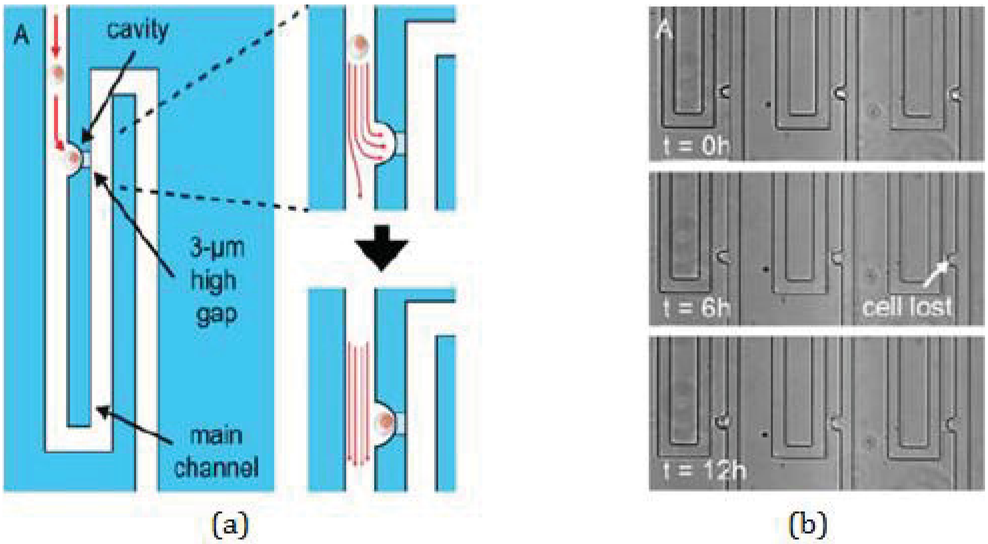

Fig. 2.2. (a) Schematic of the microchannel with a trapping site and (b) experimental verification of trapping of a single mammalian cell in particular condition of fluid motion.

Another important advantage of this configuration is that each trap region enables the confinement of a single cell, preventing other cell to remain inside, because of the change in the fluid motion around the trapped cell. Furthermore, the authors have demonstrated to obtain long trapping events, enabling the mother cell division in two small daughter cells directly in the trap. One of two daughter cell remains in the trap, while the other one is transported and then trapped into the next empty trap section, so allowing the detection and analysis of both of them to study their properties and their genetic code.

Despite the simple configuration of such devices and the ability of manipulation up to a single cell, characterized by high reliability and strong trapping efficiency, its limitation is related to the minimum size of the target object that can be trapped. High performance have been demonstrated with living cell at least of tens micrometers, but a stable and long trapping condition is very difficult with objects of only few micrometers or smaller. More complex design of trapping structure has been proposed to overcome such limitation, enabling to reduce the minimum size of the objects that can be immobilized in the single trap. For example, Probst et al. in [46] have demonstrated to stably trap a single *Escherichia coli* with a particular structure of the traps realized in the microchannel. The particular pattern proposed has been optimized to trap bacteria with a rod-shape, like *E. coli*, obtaining an efficiency of about 60% with single traps up to 87% with double traps (see Fig. 2.3).

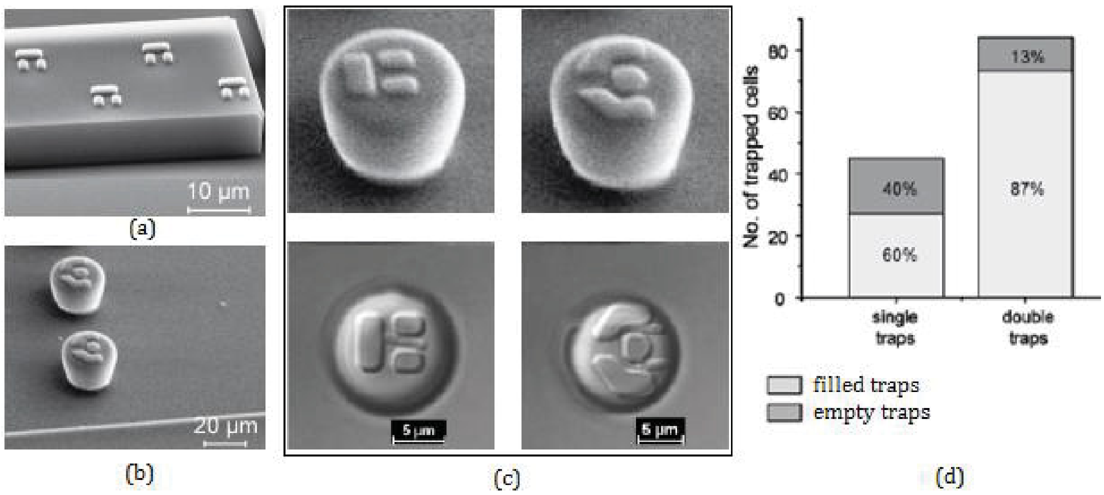

Fig. 2.3. Configuration of a single bacteria trap with (a) a rectangular and (b) cylindrical mechanical support. (c) SEM pictures of single and double trap sections before (top) and after (bottom) bacteria trapping. (d) Probability to confine bacteria in each single and double trap.

Several applications can require a pre-filtering of objects with different size and properties, aiming at carrying the target objects to the trapping sites to obtain a higher trapping efficiency. Tweezers exploiting the hydrodynamical trapping are very advantageous to satisfy such requirements, because the action of sorting and trapping can be obtained in an on-chip system. Sorting of different particles has been obtained by using channels with bifurcations and pinched regions [47], while a separation between the target objects has been demonstrated by multiorifice structures [48]. The multiorifice includes contraction and expansion cavities to provide two separate focused streams of particles with different size at the outlet, with enormous advantages for biological analysis, as demonstrated by Bhagat et al. in [49], where an extremely rare concentration of circulating tumor cells (CTCs) have been separated by the other particles flowing in the blood.

The drawback of hydrodynamic traps is related to the mechanical action of trapping, so requiring a direct contact of the target object with the trap, which can cause the damage or disruption of biological matter [50].

Several techniques have been proposed to allow non-contact trapping with hydrodynamic forces. In Ref. [51] two contra-directional laminar flows are used to create a stagnation point with a null flow, enabling trapping of nanoparticles up to 100 nm for few minutes. However, large displacements of about some microns for the trapped nanoparticles have been observed, which correspond to lower values of trapping stiffness compared to performance obtained with other techniques, such as the optical approach. Furthermore, some imperfections in the pattern of microchannel can delete the stagnation point, so obtaining only a radiation force on the particle that follows the fluid streamline.

2.2 Magnetic trapping

Magnetic field can be used also to control and manipulate with high efficiency the motion of sub-micrometer particles. Trapping of single cells and living matter have been also demonstrated by applying magnetic field with a desired spatial distribution. Such technique usually requires the binding between the target object to trap with large magnetic beads to allow an active control on their motion [52]. A typical configuration of systems used for magnetic trapping is shown in Fig. 2.4b. The tweezer is based on an array of several magnets and coils, that exert a magnetic field between magnets along a specific path, as a function of intensity of the magnetic field and the distance between magnets (Fig. 2.4a) [53]. The metal beads with functionalized surfaces are used as carriers for trapping and manipulation. By applying magnetic gradient fields, the magnetic markers can be easily manipulated, so enabling the motion of matter to detect in specific binding sites [54].

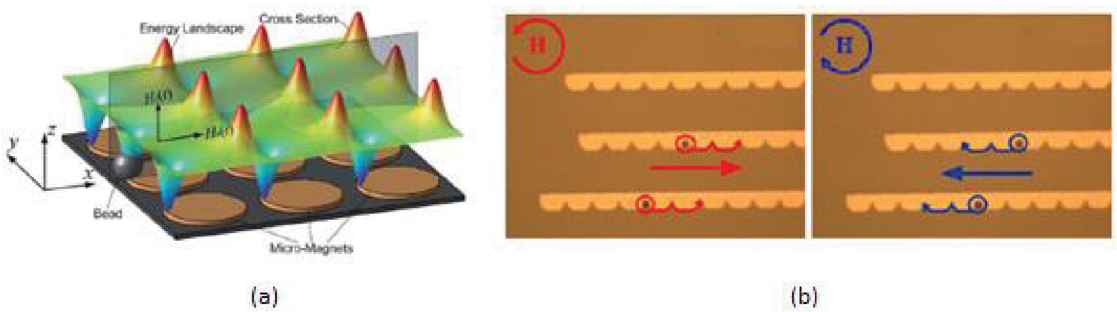

Fig. 2.4 (a) Schematic of a magnetostatic potential energy above an array of microdisk-magnets [53] and (b) motion of magnetic beads in forward and backward directions with a counter clockwise and clockwise direction of the magnetic field, respectively [52].

The direction of the magnetic particles is strongly affected by the properties of the applied magnetic field, as shown in Fig. 2.4b, where a forward and a backward motion can be obtained by applying a counter-clockwise and clockwise magnetic field, respectively [52]. Moreover, efficient separation of particles can be easily obtained with magnetic traps, by changing the driving frequency. In fact, beads move together at the same velocity for low driving frequencies, but above a critical threshold both drag properties and magnetic moment change, which corresponds to a net separation of magnetic beads as a function of their properties and size.

The main advantages of magnetic trapping are related to high values of stability for motion, the ability of separation and trapping of small objects, that allows to repeat measurements many times, and high scalability for the device integration on lab-on-a-chip systems with an improvement of sensitivity [54]. However, a similar behaviour also provides higher sensitivity to external parameters, such as changes in the viscosity and velocity of the fluid, high non linearity of magnetic forces and, particularly, a significant heating effect and the necessity of tethering of magnetic materials, that could also affect the properties of target objects to trap, such as cell viability. [55]. The strength of the magnetic field to apply is inversely proportional to the bead's size, in fact large magnetic field is required to trap small particles, which corresponds to high current electromagnets that can produce a relevant heating and risk of damage biological matter. Such limitation has been partly overcome by using soft magnetic structures in place of supermagnetic beads, which are less sensitive to heating [56,57], but this still represents the main drawback for the spread of a large use of magnetic tweezers for trapping at the nanoscale.

2.3 Dielectrophoretic trapping

Dielectrophoresis has been discovered by Pohl in 1960s [58]. This physical effect is based on the polarization of a particle under the influence of an electric field, so creating a dipole moment under the effect of the electric field gradient, as shown in Fig. 2.5. Particles can be either attracted or repelled from the region with the strongest energy gradient and the resulting force is called dielectrophoretic (DEP) force [59]. The intensity and the gradient of the applied electric field and bead's properties are the main parameters to define the force strength, while the particle's polarizability affects the positive or negative force behaviour. A positive DEP (pDEP) force corresponds to particles' motion to the region of high electric field strength (see Fig. 2.5), while negative DEP (nDEP) is related to opposite movements [60].

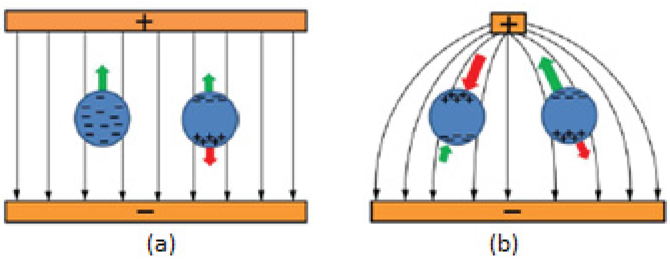

Fig. 2.5. DEP trapping of particles (charged and neutral) under (a) a uniform and (b) non-uniform electric field [60].

This effect has been largely used to manipulate the motion of beads at microscale, simply controlling the intensity of the electric field and the position of the point source.

Moreover, a higher control and also lower power dissipation have been already demonstrated by using AC voltage and insulator based DEP (iDEP) configuration, which include dielectric pillars that modify the distribution of electric field lines, so creating high field gradient in specific spatial positions [61].

DEP manipulation has proved to be very useful for trapping at microscale because it is contact-free with particles, fully controllable by changing frequency and magnitude of the electric field applied and it is also easy to interface with conventional electronics and to integrate in systems on chip [62]. In particular, efficient trapping of objects in a range of 1 μm – 1 mm has been proved. The dielectrophoretic effect has proven to be also suitable for trapping and manipulation of biological matter, such as cells and bacteria. However, particles with a size outside this range are difficult to trap due to the relevant gravity force for larger ones and the strong Brownian motion for objects at nanoscale. This is a drawback for dielectrophoresis technique, because very high values of electric field are necessary for a stable trapping condition, which corresponds to a voltage of several tens of volts with conventional configurations of electrodes [63].

The progress in nanofabrication allows values of gap of few nanometers between the electrodes, which corresponds to high values of electric field strong enough to trap nano-objects, but with lower values of applied voltage [64]. This behaviour enables trapping at nanoscale with DEP tweezers. Manipulation of small proteins and virus have been demonstrated, up to particles smaller than 100 nm [65] and detection of very low concentration of biological matter, such as DNA, up to 5 fM with voltage $V \leq 20$ V [66-68].

A relevant improvement of dielectrophoretic tweezer performance have been also demonstrated by using the light-induced dielectrophoresis (LIDEP), for which electrical contacts are created by the illumination of a photoconductor layer [69]. These optoelectronic tweezers provide manipulation of particles at micro and nanoscale with stronger trapping force and also lower AC voltage values [70,71].

2.4 Acoustic trapping

Acoustic forces have been largely used in biological applications for trapping, separation and sorting of particles and living matter at microscale [72,73]. This approach requires ultrasonic transducers deposited on the surface of a piezoelectric substrate, which generate surface acoustic waves (SAW) [74]. The ultrasonic standing waves have nodes and antinodes with a periodic spatial distribution where a mechanical pressure is exerted, so enabling trapping or repulsion of particles [75]. The position of the nodes and antinodes are affected by the frequency of the acoustic wave, which can be set to obtain the nodes in a specific position of the microchannel, so enabling microparticles separation. In fact, the magnitude of the acoustic forces depends on the particle size, density and compressibility, so particles with different size can be repositioned in different positions of the microchannel, obtaining an efficient sorting [76].

The first acoustic tweezers were based on the propagation of bulk acoustic waves (BAW) by using bulky transducers. This approach had several drawbacks, such as difficulty of integration in microchannels, due to the large volume of transducers, and also the necessity of microchannels in silicon or glass, and not with the conventional polymers (i.e. PDMS), because of their excellent acoustic reflection properties [76].

A stronger improvement of acoustic tweezers performance has been obtained by using surface acoustic waves (SAW), which propagate along the surface of an elastic material and confine higher energy values far from the surface of the substrate, so enhancing the interaction with the target objects to trap [73]. In Fig. 2.6 the operation principle of acoustic tweezer based on SAW proposed in [77] by Guo et al. has been reported. The system generates 3D trapping nodes for matter manipulation at microscale .

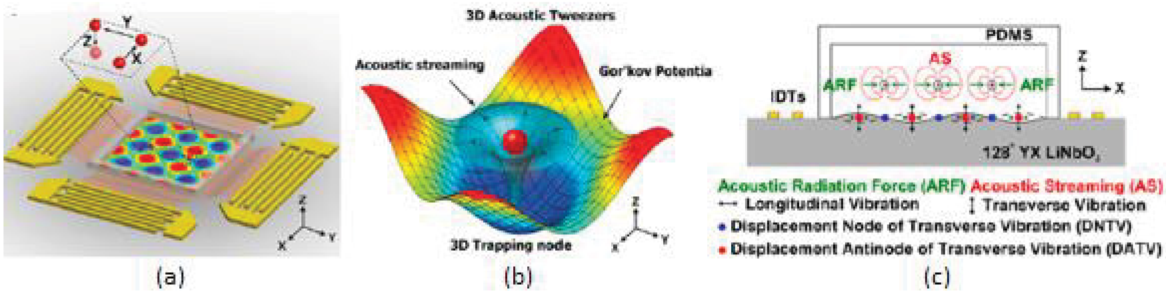

Fig. 2.6. (a) Configuration of a SAW-based tweezer proposed in [77] and (b) numerical simulation of the mapping of the acoustic field around a particle in a 3D trapping node. (c) Distribution of acoustic forces exherted on microparticles inserted in a microchannel.

The enhancement of the energy confinement provides the control and manipulation of a single microparticle and cell, unlike the BAW-based tweezers that can usually manipulate a cluster of particles [78], with also lower values of input power at least of a factor 20 in comparison with the bulky configurations, and several orders of magnitude with other trapping techniques, such as optic, electronic and optoelectronic ones [74, 79].

The resolution of the acoustic tweezers is the main drawback of such devices, because trapping is limited to microscale, making not possible manipulation of smaller objects. Therefore, acoustic tweezers have demonstrated to be very suitable for biological applications, such as trapping of bacteria and cells, due to high values of acoustic forces in pN range with very low power values, but at the same time trapping of proteins, virus and other biological matter and particles at nanoscale results too challenging to obtain by SAW-based trapping devices [74]. In the last years, trapping of sub-micron particles with low concentrations by using SAW has been investigated. Manipulation of such small particles has been obtained by trapping microparticles in the acoustic trap prior to the target objects at nanoscale, as proposed by Hammarstrom et al. in [80], who demonstrated to trap polymer beads of only 110 nm, by using 10 μm particle previously trapped. Such behaviour is due to a secondary acoustic force, given by the particle-particle interaction. This contribution is proportional to the volume of the particles that interacts, therefore a seed particle at microscale is necessary to exert an acoustic force strong enough to enable manipulation at nanoscale. This improvement of acoustic tweezers performance can be obtained at the expense of a previous trapping of large seed particles, so requiring a slower trapping process, unlike electric and optical traps with a faster process of manipulation at nanoscale.

2.5 Optical trapping

Optically-based techniques have demonstrated to exert high values of trapping forces, which are strong enough to control the motion and trap of objects at the microscale up to tens nanometers [3,81]. The pioneristic works with optical tweezer were introduced more than 30 years ago, in order to manipulate biological matter of few microns (e.g. cells), becoming very useful in several environments, such as medicine, biology, physics and chemistry [4].

The ability of trapping small object is given by a tightly focused laser beam, so obtaining high values of optical gradient in the beam waist. This provides to exert an attractive force, that pulls the bead approaching the laser beam to the region with the strongest energy confinement [82].

The theoretical background of optical trapping and a detailed description of the state-of-the-art of optical nanotweezers proposed in literature have been discussed in detail in the next chapters. Bulk configurations of optical tweezers have been proposed since thirty years ago to trap particles at the microscale up to mesoscopic objects [83]. Nowadays, such technology based on tight focusing of laser beam is mature, leading to the commercialization of several devices for multipurpose applications [84-88]. The advantages of such systems are related to high performance with reduced power consumption and low costs, compared to other instruments based on a different trapping approach. In Fig. 2.7, some configurations of commercial devices for optical trapping are shown.

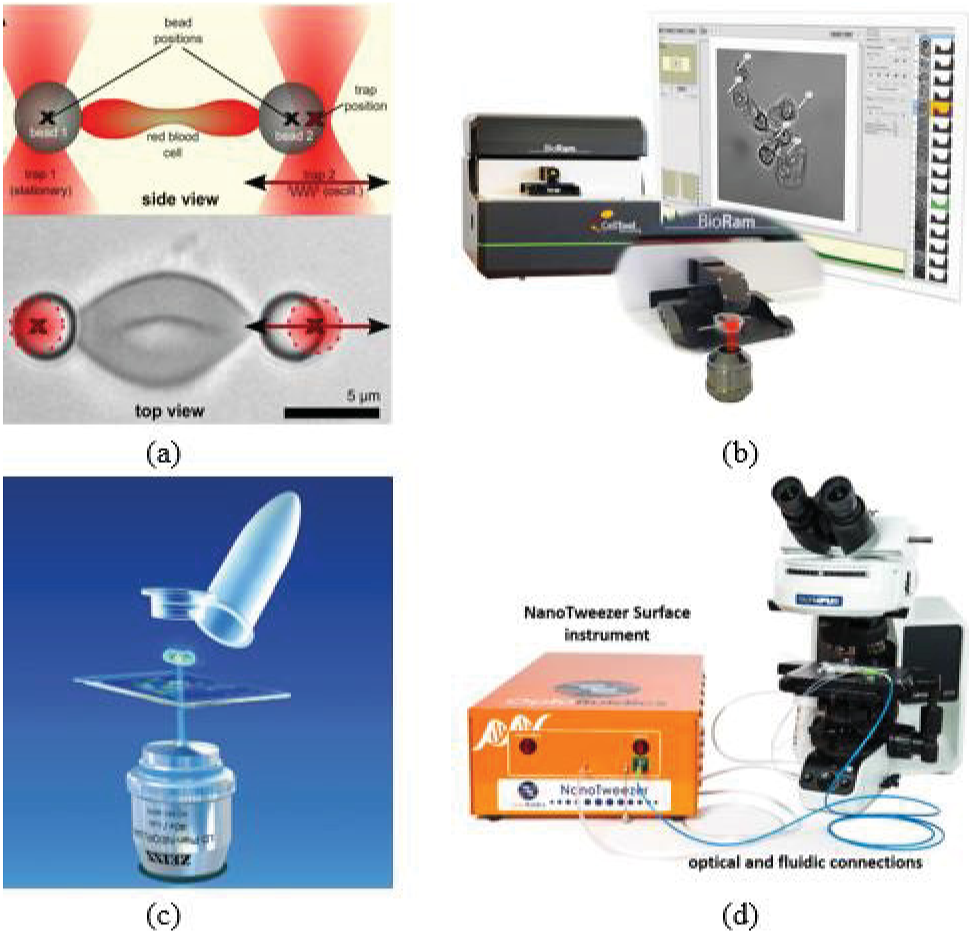

Fig. 2.7. (a) NanoTracker 2 of JPK instruments to trap and track particles from several µm down to 30 nm [84]. (b) BioRam system of CELLTool to trap cells and to analyse their properties by Raman Spectroscopy [85]. (c) PALM MicroTweezers of P.A.L.M. Microlaser technologies/ Zeiss for trapping and dissection biological matter at the microscale [86]. (d) NanoTweezer of Optofluidics for metal nanobeads and sub-micrometer biological matter with an integrated PhC cavity.

The free-space optical bulk tweezers have demonstrated to trap living matter, such as cells and bacteria, also allowing the manipulation with a control on their motion and dissection (Fig. 2.7a-c). It is also possible going further to the nanoscale, but such systems are not very efficient and require high values of optical power, due to a restricted optical gradient that they can provide. Instead, manipulation and trapping of particles smaller than 100 nm is easily obtained with Nanotweezer of Optofluidics (Fig. 2.7d), that includes an integrated PhC cavity as nanotweezer [88], unlike other systems with bulk configurations. This device strongly improves the nanotweezer efficiency, due to the stronger optical gradient compared to the values obtained by a simply focused laser beam, so demonstrating the clear advantages of integrated nanotweezers [89].

A more detailed description of the physical effects, configurations and performance obtained by integrated nanotweezers have been reported in the next chapters.

Chapter 3

Theory of optical trapping regimes

Different methods can be considered to predict the behavior of optical forces, because it depends on the particular environment in which the trapping sites are realized and, particularly, on the geometrical and physical properties of the target object. Therefore, a number of optical trapping regimes can be defined to study accurately the effect [90-92]. The simplest way to analyze optical forces with a diameter much bigger than the wavelength ($a >> \lambda$) is the Ray optics approach [93], while beads at the nanoscale ($a << \lambda$) can be approximated to a dipole and the most common method used in this condition is the Rayleigh approximation [94]. Both methods are not very accurate with particles comparable to the laser wavelength ($a \sim\lambda$), therefore a more rigorous method should be considered and the most used is the Lorenz-Mie regime [95]. A detail description of each optical trapping regime has been proposed in the next sections. Furthermore, a discussion about the main parameters that affect the trapping performance has been included in this chapter to have knowledge about the design criteria of an integrated optical device to enhance the efficiency as optical nanotweezer.

3.1 Ray optics regime

The Ray optics regime is the simplest and most intuitive method to describe the physical effect of optical trapping for large objects, because it is based on the reflection and refraction of rays incident on the object [96]. The early studies on optical tweezers proposed by Ashkin in the 1970's were based on a tightly focused laser beam to trap particles at the microscale [97]. Since the first configurations of optical tweezers, several improvements in the optical setup have been introduced to enhance the trapping efficiency. However, conventional optical tweezers based on bulk structures (e.g. a laser with high NA optical lenses) are able to trap matter at the microscale, and it is very difficult to overcome such limitation, due to low values of optical gradient that can be reached [98]. Assuming a typical optical wavelength in the visible range or in the near infrared, when the target object to trap is several microns, such as a cell, the condition $a >> \lambda$ is verified and the Ray optics regime results valid.

The Ray optic regime assumes that incident rays change their direction due to reflection and refraction, when they impinge on a bead with a different refractive index than the surrounding medium, as shown in Fig. 3.1. Such behaviour results in a force on the particle due to the exchange of momentum [99]. This physical effect can be explained by the Fresnel equations, which describe the fraction of reflected and refracted light at the boundaries of the object. The refracted light produces the gradient force which attracts the object into the focus (Fig. 3.1a and Fig. 3.1b], while the force by reflected rays acts in the opposite direction and pushes the particle away from the focus [Fig. 3.1c] [100, 8].

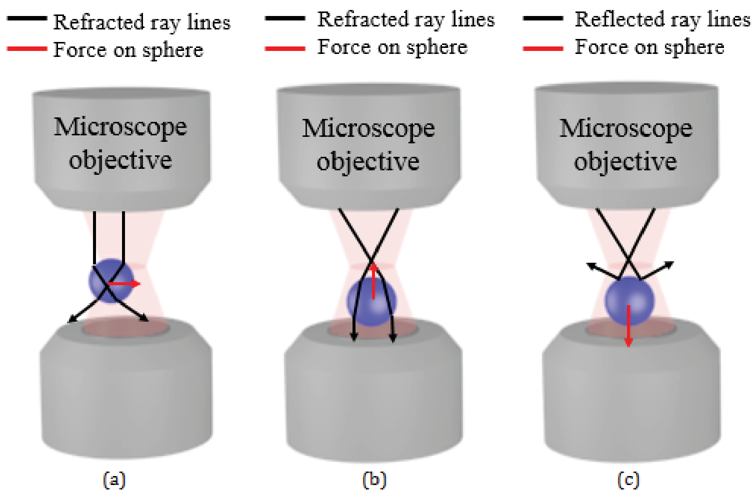

Fig. 3.1. Forces acting on a microparticle described by the ray optics approach. An attracting force results from the refracted rays when the particle is (a) laterally displaced from the beam waist or (b) placed behind the light focus. (c) Reflected rays provide an opposite force on the particle in the same direction of the light propagation, pushing it away from the trapping site.

The light passes through the object when the incident rays are focused exactly in the middle of the spherical particle, without any resulting force. If the particle hit by the incident ray is off-centre, then the emergent rays are refracted, which results in a momentum transfer from the incident light to the particle, as shown in Fig. 3.1a. The resulting force pushes the particle towards the focus of the laser beam. The magnitude of this force scales as the gradient of the beam profile (hence "gradient force"), which increases with the numerical aperture of optical system [101].

A similar behaviour with a resulting restoring force can be observed when the object is displaced along the axis of the optical lens, as illustrated in Fig. 3.1b. At the same time, light reflections provide a force in the direction of the light propagation and opposite to the attractive force, which pushes away the particle from the trapping site (Fig. 3.1c). A stable trapping condition can be achieved if the gradient force acting on the particle is higher than the effect of absorption and scattering force.

This physical behaviour is verified by the Fresnel equations in presence of a strong interaction between the particle and the laser beam, which is typically obtained with large particles. Therefore, it has been demonstrated the reason why ray optics regime is assumed only with objects that verify the condition $a >> \lambda$. In fact, this condition is not still valid for particles of few nanometers (a < λ), because only a small amount of light interacts with the bead, so changing the relationship between the optical force and object's size, as shown in Fig. 3. This demonstrates the unsuitability of the ray optics regime to study the optical forces on particles at the nanoscale [8].

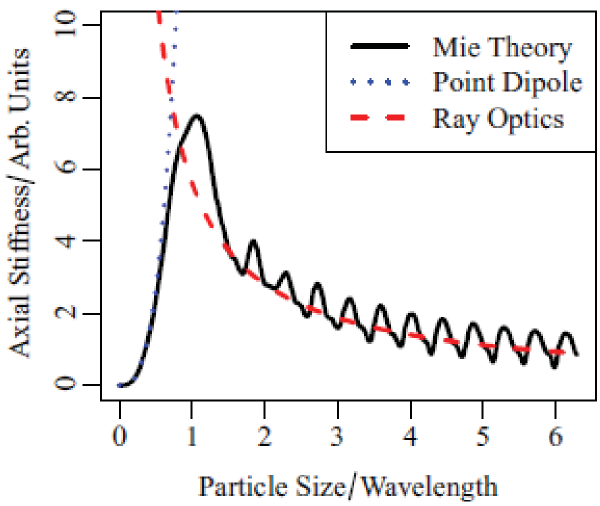

Fig. 3.2. Optical stiffness k (directly proportional to the trapping force F and the particle's displacement x (F = k·x)) as a function of the particle's size, calculated by using three different theoretical approaches:ray optics, Mie theory and Rayleigh dipole approximation [8].

3.2 Rayleigh regime

The trapping force is strongly affected by the target object's size. In particular, for large particles ($a > \lambda$) has been verified a decrease of trapping force as the particle's size increases. As discussed above, it can be demonstrated by the enhancement of scattering and absorption effects, which are opposite to the gradient force, resulting in a lower trapping efficiency. On the contrary, the behaviour of optical force changes when the bead becomes much smaller than the wavelength ($a << \lambda$) [102]. The Ray optics regime is not still valid, because a different physical behavior is verified. In fact, there is a relevant decrease of scattering and absorption forces because of smaller scattering and absorption cross-section values [103]. However, also a strong decrease of trapping efficiency has been verified, demonstrated by the fact that the gradient force is proportional to the third power of the particle's radius. At the same time, the thermal effects and, therefore, the Brownian motion, become more evident on the bead's motion for smaller size, so strongly reducing the trapping effect when the particle is at the nanoscale.

The Rayleigh approximation is used to analyse the behaviour of optical forces on particles at the nanoscale ($a < \lambda$). In this regime the field is assumed constant across the bead and induces an oscillating dipole in a small dielectric object [104]. The particle then becomes polarized with a dipole moment described by:

$$\vec{p} = \alpha \vec{E} \tag{1}$$

where $\vec{E}$ is the electric field vector, and α is the particle's polarizability, which quantifies the strength of interaction with the optical field, and can be calculated by:

$$\alpha = \frac{\alpha_0}{1 - \frac{ik^3 \alpha_0}{6\pi\varepsilon_0}} \tag{2}$$

with k the field wavevector and α_0 the point-like particle polarizability obtained by the Clausius-Mossotti relation, expressed by:

$$\alpha_0 = 4\pi a^3 (\varepsilon - \varepsilon_m) / (\varepsilon + 2\varepsilon_m) \tag{3}$$

ε and ε_m the relative permittivity of the particle and the surrounding medium, respectively. Therefore, the strength of light-particle interaction is influenced by the dielectric contrast between the target object and the surrounding medium (physical properties) and by the size of the particle (geometrical properties) [3].

The Rayleigh approximation assumes that a certain fraction of photons focused on the nanoparticle are either scattered or absorbed. This interaction provides a momentum transfer to the nanoparticle, which generates the forces F_{scatt} and F_{abs} and pushes the object in the direction of the optical propagation with a net forward velocity [105]. The scattering force calculated assuming the Rayleigh approximation for a nanoparticle can be expressed by:

$$F_{scatt} = \frac{8\pi^3 I_0 \alpha^2 \varepsilon_m}{3c\lambda^4} \tag{4}$$

where I_0 is the incident light intensity, c is the speed of light and ε_m is the relative permittivity of the surrounding medium. The absorption force is given by:

$$F_{abs} = \frac{2\pi\varepsilon_m I_0 \,\mathrm{Im}(\alpha)}{c\lambda} \tag{5}$$

where Im(α) is the imaginary part of the particle polarizability.

Scattering and absorption forces provide the total force along the propagation direction, also called radiation pressure.

In contrast, the gradient force acts on the nanoparticle in the direction perpendicular to the propagation direction, in order to attract the object, and is given by [106]:

$$F_{grad} = \frac{2\pi\alpha\nabla I_0}{c} \tag{6}$$

The optical force on particles at the nanoscale is linearly proportional to the polarizability, which corresponds to a gradient force as a function of the third power of the bead's radius. This condition has been validated with a size range of particles from few nanometers to a couple of hundred nanometers. The gradient force causes an attractive action on particles with a refractive index higher than the surrounding medium, due to a positive value of polarizability, as demonstrated by Eq. 6.

The optical gradient is maximized in regions with a strong decay of the optical intensity ∇I_0, which corresponds to the site with the strongest trapping efficiency. However, if the refractive index of the bead is lower than the value of the surrounding medium, the polarizability is negative and a net repulsive force is obtained, which pulls away the particle from the region with high optical gradient, as confirmed by Eq. 6 [107]. It is clear that the energy distribution, together with the physical and geometrical properties of the trapped object, are the main factors that affect the trapping efficiency.

This behavior confirms the challenge of trapping objects at the nanoscale, because the polarizability scales as a factor of the third power of the bead's radius. Furthermore, the ease of manipulation of metal nanoparticles respect to dielectric ones is also verified by Eq. 6, because of a higher polarizability α due to a stronger refractive index contrast.

The accuracy of the Rayleigh approximation reduces if the particle's size becomes comparable to the wavelength used in the experiments ($a \sim \lambda$) (see Fig. 9), because the condition related to a constant field across the particle is not preserved. In this condition, the gradient force is not still a function of a^3 as for nanoparticles, but follows a weak dependence ($\sim a^2$) for particle's size comparable to the wavelength [104].

On the contrary, if the target object is very small up to few nanometers, the effect of gradient force becomes stronger than the scattering one. In fact, the ratio F_{grad}/F_{scatt}, is proportional to $1/a^3$, because F_{grad} and F_{scatt} are proportional to α and α^2, respectively, (see Eq. 4 and Eq. 6), which should corresponds to an improvement of the trapping effect as the particle size decreases. However, the decrease of F_{grad} for very small particles corresponds to a considerably weaker attraction of the bead (See Fig. 9), while the effect of Brownian motion, that counteract to the trapping force, becomes more effective (as clearly described in the next sections), confirming a net worsening of the trapping efficiency as the particle size strongly decreases.

3.3 Lorenz-Mie regime

Rayleigh approximation and Ray optics method are not accurate to calculate the value of optical forces when the particle's size is comparable to the laser wavelength ($a \sim \lambda$). A more rigorous analytical model is necessary to evaluate the value of the optical force and the Lorenz-Mie theory has demonstrated to be the most accurate approach in this trapping regime [108].

The method is based on the calculation of scattering of a plane wave by an object, and the resulting force is given by the decomposition of the trapping field in plane waves. Unlike the ray optics, a coherent trapping light is assumed in Lorenz-Mie regime and, furthermore, both size and shape of the target object to trap are considered in the force evaluation, on the contrary to Rayleigh approximation. These assumptions require to solve equations that are power demanding, particularly for not spherical objects. Several methods have been proposed to simplify the evaluation of optical forces, e.g. the T-matrix formalism [109].

The main limitation of Lorenz-Mie theory is related to the assumption of plane-wave illumination to estimate optical forces, which is not really viable to obtain by optical tweezers, and particularly for strongly focused beams as typically required for trapping at the nanoscale. A more complex form of such method, so called Generalized Lorentz-Mie theory (GLMT), has been introduced to overcome such limitation, assuming any arbitrary illumination in the trapping system and object's shape [110]. This improvement in the model provides higher accuracy in the solution, so obtaining a good matching between the results obtained with the GLMT and Rayleigh approximation for the calculation of optical forces exerted on particles at the nanoscale.

GLMT can be used to evaluate the incident light field E_0, the scattered wave E_s and the field within the object to trap E_i, which are functions of the incident field's coefficients, scattering and interior field's ones, respectively, that depends on the properties of the beam and on the size and composition of the object. A detailed description of this complex analytical method has been proposed in [110]. The electric field components are used to define the radiation trapping efficiency Q, as discussed in [111], and therefore, the trapping force F is given by:

$$F = \left(\frac{n_{medium} P}{c} \right) Q \tag{7}$$

where c is the speed of light in vacuum, n_{medium} is the refractive index of the medium and P is the beam power [111]. The accuracy of the model has been verified by a good agreement between the values of the optical forces estimated experimentally and the results obtained by Lorenz-Mie regime observed for particles respecting the condition

$a < \lambda$, and also with bigger size ($a \sim w_0$, w_0 is the beam waist). In contrast, a non-negligible mismatch is obtained evaluating optical forces in the axial direction for particles with $a \sim 0.4w_0$, because the electromagnetic field is no longer uniform across the particle, as assumed by Rayleigh theory [112].

The GLMT is the most accurate technique for force evaluation, but also very computation demanding. Therefore, easier analytical methods like the Rayleigh approximation and ray optics are largely used, as a function of the particle shape, when GLMT is not necessarily required to calculate the optical force.

3.4 Maxwell Stress Tensor Method

In particular condition with complicated configurations of the system, related to the properties of the target object and the trapping site, numerical methods represent the best choice to calculate accurately the volumetric distribution of optical forces acting on a particle .

The Maxwell Stress Tensor (MST) method is a general numerical method used to calculate optical forces on arbitrary particles and for any type of light source [113]. The force typically depends on the properties of both optical source and target object. The time average force $\langle \boldsymbol{F} \rangle$ on a particle obtained with MST is:

$$\langle \boldsymbol{F} \rangle = \int_S \left\langle \overleftrightarrow{T}(\boldsymbol{r},t)\mathbf{n}\mathrm{dS} \right\rangle \tag{8}$$

where $\mathbf{n}$ is the outgoing vector normal to the surface S of the particle and $\overleftrightarrow{T}$ is the Maxwell stress tensor, which can be expressed by:

$$\overleftrightarrow{\boldsymbol{T}} = \frac{1}{2}\mathrm{Re}\left[\left(\varepsilon_0\varepsilon\boldsymbol{E}(\boldsymbol{r})\boldsymbol{E}(\boldsymbol{r})^* + \mu_0\mu\boldsymbol{H}(\boldsymbol{r})\boldsymbol{H}(\boldsymbol{r})^*\right) - \frac{1}{2}(\varepsilon_0\varepsilon|\boldsymbol{E}(\boldsymbol{r})|^2 + \mu_0\mu|\boldsymbol{H}(\boldsymbol{r})|^2)\overleftrightarrow{\boldsymbol{I}}\right] \quad (9)$$

with μ_0 and μ the magnetic susceptibility of vacuum and the surrounding medium, respectively, $\boldsymbol{E}$ and $\boldsymbol{H}$ the electric and magnetic field vectors and $\overleftrightarrow{I}$ the unit matrix tensor [113]. The components of the electric and magnetic field can be calculated analytically in particular conditions (i.e. by applying the GLMT method) or generally by numerical methods, such as Finite Element Method (FEM) and Finite Difference Time Domain (FDTD). The knowledge of the distribution of *E* and *H* fields at the surface *S* of the target object allows the evaluation of the optical force on the target object.

A good agreement between values of optical forces calculated with the numerical method MST and those obtained using the most general analytical approach GLMT, has been verified [114].

3.5 Main parameters of optical trapping

The physical principle of optical trapping assumes that the attraction of an object is allowed if the gradient force exceeds the scattering and the absorption effects. The resulting force pulls the target object to the equilibrium point in the focal region, where a net force balance is obtained. If the particle is displaced from its stable position, a restoring force arises on the bead proportional to the offset from the equilibrium point, so enhancing as the distance increases until reaching a maximum. In fact, a rapid decrease of the restoring force occurs when the distance from the equilibrium point becomes too large, because the energy gradient is weak very far from the beam focus. This behavior is very similar to a harmonic oscillator, with the optical force acting as a spring force and given by Hooke's law [115]:

$$F_{trap} = k \cdot x \tag{10}$$

where k is the optical stiffness and x represents the particle's displacement from the equilibrium point. The value of the trap stiffness is calculated along the three coordinates, assuming the lowest value as the reference to define the limit of the optical trap. The stiffness gives information about the trapping efficiency [116]. Assuming a value of the trapping force F_{trap}, a high value of the optical stiffness corresponds to small fluctuations of the particle around the equilibrium point, as required for a stable trapping condition, according to Eq. 10. This condition is necessary to reduce the effects of the Brownian motion on the particle's motion and also improve the detection accuracy of the target object. The Langevin equation describes the motion of the particle under the effect of the optical force [117, 118]:

$$m\frac{\partial^2 x}{\partial t^2} + \gamma_0 \frac{\partial x}{\partial t} + kx = (2k_b T \gamma_0)^{1/2} W(t) \tag{11}$$

where γ_0 is the friction coefficient (=6πη*a, a* is the particle's size and η the viscosity), T is the temperature and k_B the Boltzmann constant, while *W(t)* denotes the stochastic process of the target object as a function of time. The term kx in Eq. 11 represents the optical trap's influence with k the trapping stiffness, while the term $2k_B T\gamma_0$ is related to the random Gaussian noise and includes the effects of Brownian motion that affects the particle's motion, like a noise contribution.

The target object can be assumed as an overdamped system with short oscillation frequencies, due to the presence of the fluid medium [118]. The viscosity effect is dominant because the particles are usually in a laminar flow, which corresponds to low values of Reynolds number. The laminar flow condition is necessary to reduce the effect of Brownian motion on the target object as it makes easier to trap particles [119]. Turbulence becomes more relevant with a decrease of the particle size, making it more difficult to achieve stable trapping. The motion of the particle in a microfluidic channel can be described by Stokes' drag equation, which corresponds to a propulsion force in the same direction of the fluid flow:

$$F_{drag} = \gamma_0 \frac{\partial x}{\partial t} = \gamma_0 v \qquad (12)$$

with v the particle velocity [106]. The Langevin equation takes the effect of Brownian motion into account for a rigorous description of forces affecting the velocity and trajectory of the particle's motion. The Brownian motion is a diffusion process that affects the particle's displacement x. The diffusion coefficient D is predominant for this effect, given by the Stokes-Einstein's equation [120]:

$$D = \frac{K_b T}{6\pi\eta a} \qquad (13)$$

The diffusion coefficient D is inversely proportional to the particle size, which means that the Brownian motion is more relevant in the Rayleigh regime. Therefore, the nanobeads move faster and with larger displacements around the equilibrium point, so reducing the stability of the optical trap, corresponding to a decrease of the trapping efficiency [121]. This condition confirms that trapping and manipulation of particles at the nanoscale is more challenging. In fact, despite the parameter F_{grad}/F_{scatt} increases with a decrease of the bead's size as a function of a^3, as obtained by Eq. 4 and Eq. 6, however the trapping efficiency worsens because the trapping force is strongly reduced for the enhanced effects that oppose to the attractive action on the bead. In fact, a worsening of three orders of magnitude of the gradient force is obtained with a decrease of a factor 10 of the particle's size. At the same time, an increase of the diffusion coefficient of one order of magnitude and, therefore, of the effect of the Brownian motion, is also obtained, which becomes comparable or even stronger than the attracting force, with a relevant decrease of the trapping efficiency.

The temperature assumes a fundamental role in trapping applications to define the particle's motion, related to the probability to bring and stably hold the target object in the trap. The particle's fluctuation is related to the temperature T_c obtained around the optical trap, according to the Equipartition theorem:

$$k_b T_c = k\left\langle x^2 \right\rangle \quad (14)$$

where $<x^2>$ is the particle's mean squared displacement from the equilibrium point. This equation also expresses that for a given temperature value in the system, a stronger trapping stiffness reduces particle fluctuations around the equilibrium point, enabling higher control on its positioning. The temperature increase is typically due to the strong electromagnetic confinement in the optical trap, as confirmed by the equation:

$$\kappa_T \nabla^2 T_c = \frac{\omega}{2} \mathrm{Im}(\varepsilon) \mathrm{x} |\mathbf{E}|^2 (\vec{r}) \quad (15)$$

An enhancement of the optical force can be obtained by increasing the input power. However, it also corresponds to a relevant increase of temperature, as confirmed by Eq. 15, because the term $|\mathbf{E}|^2$ is directly proportional to the input power. Therefore higher values of input power do not provide higher trapping efficiency, because the Brownian motion becomes more relevant. This consideration leads to the optical stability, which is defined as:

$$S = \int_{r_0}^{\infty} F_{tot} dr \Big/ k_B T \tag{16}$$

F_{tot} is the resulting force exerted on the particle, *r* is the spatial coordinate and the term $\int_{r_0}^{\infty} F_{tot} dr$ represents the work necessary to carry the particle from a free position to the equilibrium point r_0, while the term $k_B T_c$ is the thermal energy. The radiation force is opposite to the gradient force, so it is necessary that the latter is dominant on the absorption and scattering contributions to optimize F_{tot} and enhance the optical stability [105]. An increase of stability corresponds to longer trapping time, because of the Kramers' escape rate [122]:

$$t_{trap} \propto \exp\left(\frac{U}{K_b T}\right) \tag{17}$$

where $U(=\int_{r_0}^{\infty} F_{tot} dr)$ is the trap potential depth. Several applications require long trapping times to provide the detection and the manipulation of the target object. Therefore, it is necessary that the potential depth U be higher than the thermal energy to trap the target particle. $S \geq 10$ is typically assumed as the stable trapping condition, where the bead is trapped while the laser is kept on. The bead is released when the laser is switched off [119].

High value of optical stability S is obtained by optimizing the trap potential depth U and minimizing the thermal energy. An enhancement of the gradient force is necessary to verify such condition. For a given target particle flowing in a fluid, the gradient force can be optimized by using higher values of the input optical power. However, this choice does not corresponds to higher trapping efficiency, because an increase of the absorption force, particularly with metal particles, is obtained and corresponds to a lower resulting force F_{tot}. Furthermore, an increase of the temperature is also verified with higher values of power, as given by Eq. 15, so obtaining a higher thermal energy with a consequent decrease of the optical stability (see Eq. 16) [123]. Therefore, the best approach to enhance the trapping efficiency is to maximize the gradient intensity ∇I_0, because stronger gradient force can be obtained without increase the input power, so not affecting the thermal energy of the trapping system [106]. This confirms the higher efficiency of the integrated optical devices used as optical tweezer rather than the bulk structures, due to their ability to provide stronger energy confinement and optical gradient. For this reason, similar devices have demonstrated to be very useful for trapping of particle at the nanoscale, and also living matter for biomedical application, because of higher trapping efficiency together with lower risk of photodamage [124].

A detail description of configurations of integrated optical devices used as optical nanotweezers has been reported in the next chapter, in order to compare their performance and to define the design criteria to realize an efficient optical nanotweezer.

CHAPTER 4

State-of-the-art of integrated optical nanotweezers for trapping of sub-micron particles

Free-space optical tweezers have been briefly discussed in Chapter 2, in order to clarify the effective advantages of optically-based trapping techniques compared to performance obtained with other methods. However, a great limitation of such devices is related to the unavailability of trapping matter at the nanoscale, particularly dielectric objects and living matter, because the optical gradient obtained in free-space by a laser beam focused by optical lenses with high numerical aperture is not strong enough to exert optical forces suitable for manipulation of such small objects.

Different strategies have been proposed to afford trapping at the nanoscale with bulk optical tweezers [125], such as oil-immersed optical lenses to provide higher values of *NA* [126], or by including other optical components in the trapping setup, such as galvanometer-mounted mirrors, acousto-optic deflectors, spatial light modulators (SLMs), holographic techniques to obtain unusual optical beams, such as Laguerre-Gaussian modes and Bessel modes with a circular symmetry or Airy beams [127], or diffractive or polarizing elements, that give higher control and allow the manipulation of optical beams. [128]. Unfortunately, all these techniques have disadvantages. For example, oil-immersed lenses, which provide an *NA* up to 1.7 [129], are typically affected by optical aberration [130], while optical tweezers controlled by SLMs are characterized by low response time [131] and holographic techniques are difficult to implement, due to the complexity of the experimental setup [24]. All these solutions are also quite bulky, making difficult the integration of the trapping system in a compact point-of-care device.

Recently, integrated optical devices exploiting near-field optical trapping have offered a solution to overcome limitations of conventional free-space optical tweezers [3]. A stronger electromagnetic energy gradient is provided with near-field devices, because the field exponentially decays from the surface where the light is confined. The sharp exponential decay generates a strong trapping force, much higher than values obtained with free-space optical tweezers, so enabling manipulation at the nanoscale with safe values of optical power. Stable trapping conditions have been obtained for the manipulation of dielectric nanoparticles, making such devices very useful for several applications in medicine and biology [2].

Integrated optical devices used for trapping at the nanoscale are known as nanotweezers. In this chapter a detailed and critical analysis of the state-of-the-art of different configurations of optical nanotweezers has been discussed to have a clear and useful comparison among such devices, in order to define the most suitable trapping technique and device configuration to provide high trapping efficiency at the nanoscale.

4.1 Optical waveguides and nanowires

Optical waveguide are used for trapping and propulsion of microparticles up to nanoscale range, aiming at improving the performance provided by the bulk optical tweezers and limiting their diffraction limit [132].

Light propagates inside the optical waveguide and the evanescent field enables a radiation pressure along the waveguide surface with a propulsion of particles on the surface in the direction of light propagation [133]. This allows to control the motion of particles and can be very useful to obtain an active and effective sorting of particles in very small volumes. The first experiments to control the sub-micron particles' motion with optical waveguides used as optical tweezers have been done since 20 years ago. In particular, interesting results were obtained with metal beads, due to their higher values of polarizability which makes easier their manipulation. The control on motion of 1 μm metal particles has been demonstrated in [134] and an improvement of performance for the bead's propulsion with optical waveguides has been also verified, so allowing manipulation of objects up to 50 nm [135].

Manipulation of dielectric particles and living matter is more difficult because a weaker gradient force can be obtained due to lower polarizability. It has been demonstrated the control of micrometer-size dielectric particles and living matter, such as red blood cells and bacteria [136,137] (see Fig. 4.1)

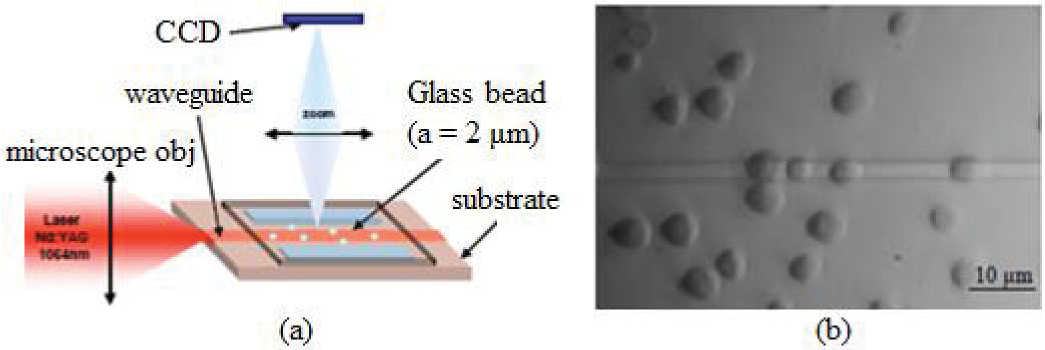

Fig. 4.1. (a) Experimental setup and (b) microscope image of the optical tweezer used in [137] for trapping of yeast cells

The configuration of a loop waveguide has been also proposed for the purpose of trapping microparticles, as shown in Fig. 11, and not limiting at their propulsion along the surface, as typically happens with a simple optical waveguide [138]. The folding of the waveguides to create a narrow slot provides strong energy confinement, aiming at trapping dielectric microparticles down to 1 μm.

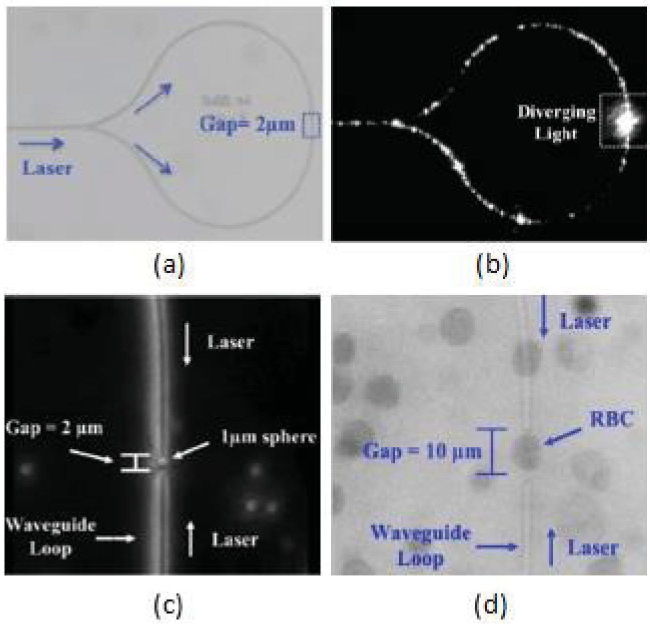

Fig. 4.2. (a) Configuration of the optical waveguide loop with a gap of 2 μm and (b) scattering light from the waveguides and the gap. (c) Optical trapping of polystyrene microparticle of 1 μm and (d) red blood cells (RBC) of 7-8 μm with a gap of 10 μm [138].

As described in Fig. 4.2, the light propagates in both arms of the loop, so propelling the microparticles to the gap placed between the waveguides, where a strong energy confinement has been also verified in that region, due to the narrow gap width (2 μm). A strong trapping force, compared to values obtained by the evanescent field around the channelled waveguides, has been obtained, so enabling stable trapping in the slot region. The main advantage of this optical tweezer is related to the ease of integration of the waveguide loop with microfluidic channels, that makes the on-chip system very useful for single cell detection and also to analyse the interaction of multiple cells (see Fig. 4.2c). Such configuration has been also used for a stable trapping of red blood cells with a disk-shape (1 μm thickness and width of about 8 μm) [138].

An accurate control on the fabrication and use of fluidics has demonstrated to assume an important role in optical tweezers performance, because the tighter control over the particle movement facilitates the particles flow very close to the surface of waveguide and, therefore, maximizes their interaction with the evanescent field, so improving the probability to trap particles with high efficiency of manipulation and propulsion. The strong control on channel size and also flat surfaces prevent undesired effects and changes in fluid flow, which can increase Brownian motion of particles and also change their direction of propagation. Moreover, the fabrication of valves, micropumps and mixers in the microchannels has enabled the integration of several optical tweezers on a single chip with a higher control on the fluid motion, due to the ability to manipulate pressure and fluid direction, in which the particles can flow [139-142]. This behavior is very useful for simultaneous analysis for sensing applications in chemical, biological and medical environments [143,144].

However, the limitation of optical waveguides used as optical nanotweezer is related to the small amount of evanescent field obtained, that directly interacts with the target object. In fact, the strong light confinement in the core of the waveguides prevents to obtain high values of optical gradient and, therefore, also the values of trapping force that can be exerted is limited.

Different techniques have been proposed to overcome such issue, in order to enable trapping of sub-micrometer dielectric particles with this simple configuration of optical tweezers.

A remarkable enhancement of trapping efficiency has been obtained by using optical nanowires, because they provide a more relevant contribution of evanescent field, due to their smaller area, which corresponds to stronger optical gradient.

Trapping of dielectric nanoparticles (i.e. polystyrene or glass of about 400 nm) and metal beads with size a < 100 nm with a higher stability than performance of conventional optical waveguides has been demonstrated [133].

Recently, these configurations have been used to simplify particles' detection and their analysis. Kong et al. introduced a new nanophotonic approach combining near-field optical trapping and Surface Enhanced Raman Spectroscopy (SERS) to detect up to a single metal nanoparticle, exploiting both the strong energy confinement in the nanowire and higher scattering from the metal beads (Fig. 4.3) [133]. The optical nanowire provides the trapping of the metal bead, while the scattering obtained by the particle’s surface is useful to collect the Raman signal, so using the system to the simultaneous detection of nanoparticles and for their characterization, as shown in Fig. 4.3c.

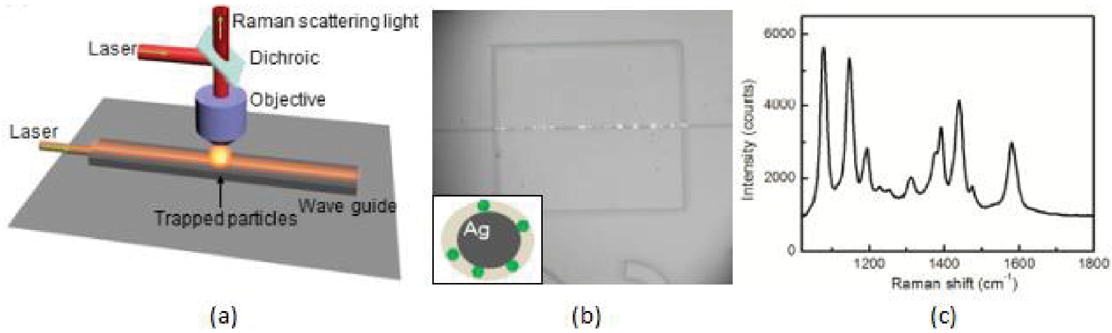

Fig. 4.3 (a) Setup of the nanotweezer SERS system. (b) Trapping of single poly (allylamine) coated Ag NPs with adsorbed 4-aminothiophenol (4-ATP) molecules using a 1064 nm laser. (c) Far-field SERS spectra excited by 785 nm laser [133].

A similar configuration has been demonstrated by Schein et al. in [145], who exploit the near-field light scattering technique for the analysis of nanoparticle-surface interactions, making it possible to manipulate 50 nm size Au nanoparticles.

As already observed with optical waveguides, novel configurations and particular techniques have been proposed to enhance the efficiency of nanotweezers based on optical nanowires for particles’ manipulation and trapping up to the nanoscale and living matter.

Soltani et al. in [146] proposed a platform with a nanophotonic standing wave array trap (nSWAT) to obtain a 3D confinement of DNA strands. The device includes a waveguide split in two arms. The same light intensity propagates in both arms and the interference of two counter-propagating waves provides the formation of a standing wave with 3D optical traps exactly in the anti-nodes (see Fig. 4.4)

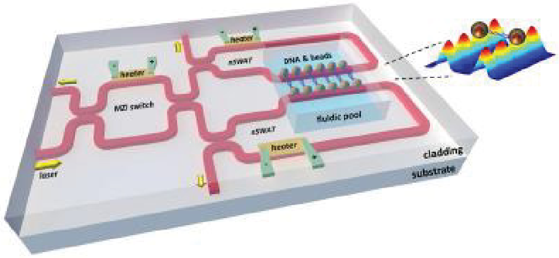

Fig. 4.4. Configuration of the nSWAT. The inset shows an array of traps for a DNA molecule by using two beads with a colored 3D plot of calculated energy density of standing waves [146].

The nSWAT provides an array of optical traps (one for each anti-node in the standing wave). Longer waveguides provides a larger number of traps, but require higher optical input power to prevent high optical loss with a consequent decrease of trapping efficiency. Trapping of DNA chain by using two polystyrene beads of 490 nm, at which the DNA is tethered with streptavidin, has been demonstrated. The beads are trapped in the antinodes, so holding the DNA molecule in a fixed position to be easily detected. The binding between DNA and polystyrene beads is necessary because optical forces exerted by the waveguides are not so strong to trap directly DNA chains of few nanometers.

In the last years, the development in nanofabrication techniques has provided the realization of sub-100 nm slotted waveguides. These configurations allow to enhance the electromagnetic energy confinement in a very small volume, which corresponds to high values of optical gradient in the slot with a strong trapping efficiency, much higher than performance typically obtained with optical nanowires [147].

The main advantage of slotted waveguides is the strong energy confinement in a region filled by fluid, where it is possible the direct interaction with the target object to trap, unlike optical waveguides, for which the evanescent field responsible for the trapping action represents only a small amount of the total energy propagating in the waveguide. This enhancement of trapping strength has been confirmed experimentally by slotted configurations able to trap particles at the nanoscale [148]. Yang et al. obtained a stable trapping condition for gold nanoparticles up to 20 nm. However, the polarizability of dielectric nanoparticles is almost one order of magnitude lower than metal beads, which corresponds to weaker optical forces, so making more difficult the trapping with high efficiency [148].

Yang et al. have also demonstrated experimentally the ability of trapping an individual strand of YOYO-1 tagged 48 kb long λ-DNA molecule [147]. A stable trapping condition has been demonstrated with a slot width of 60 nm, but requiring an input power at least of 250 mW, as shown in Fig. 4.5.

Such power value required for a stable trapping condition could damage the trapped DNA for very long exposure time at laser beam, due to a high energy density in that region.

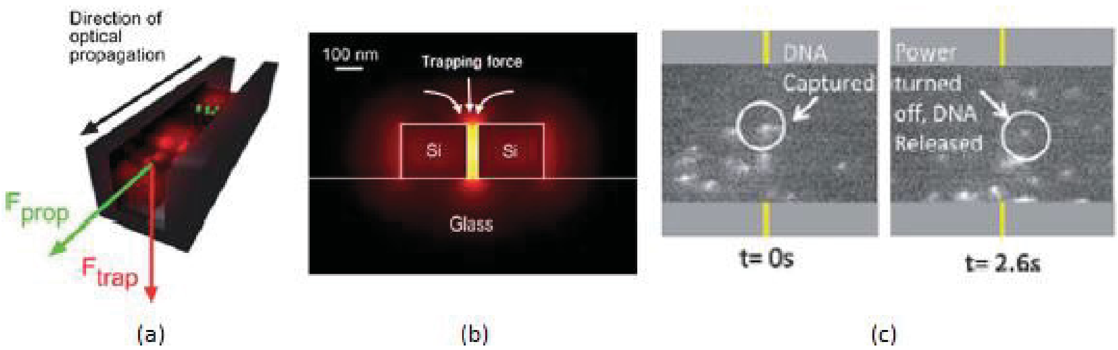

Fig. 4.5. (a) Schematic and (b) mode distribution of the slotted waveguide. (c) Trapping (left) and release (right) of YOYO tagged 48 kb λ-DNA with a slot width of 60 nm [147].

As already observed with optical nanowires, also slotted waveguides enable the propulsion of trapped particles along the direction of light propagation, while their confinement in a specific region is still a challenge to obtain with these configurations. However, this behaviour is very useful to improve the action of sorting by using optical techniques. In fact, the separation of particles with different properties and size can be obtained easily, due to the stronger trapping effect verified in slotted structures. For instance, the higher trapping efficiency of slotted waveguides useful for active sorting of dielectric nanoparticles has been verified by Lin et al. in [149]. The configuration includes a 3-dB optical splitter consisting of a ridge waveguide and a slotted waveguide, as shown in Fig. 4.6.

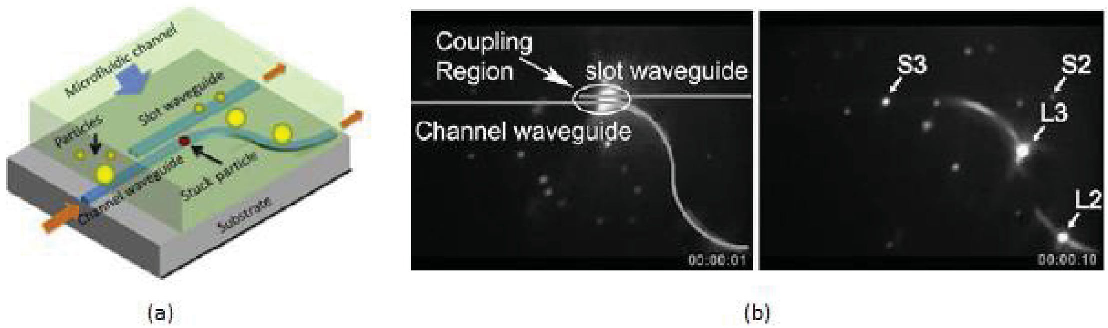

Fig. 4.6. (a) Configuration of the platform for passive sorting. (b) Experimental demonstration of sorting with the smaller particles of 320 nm (S) propelled along the slotted waveguide and bigger ones (L) propagating in the ridge waveguide [149].

After trapping polystyrene particles, their propulsion along the waveguide is verified until the coupling region, where only smaller nanoparticles can be trapped and moved forward in the slotted waveguide, while the bigger ones remain on the larger ridge waveguide. An efficient and passive sorting between polystyrene particles with a size of 2 μm and 320 nm with an input power of 20 mW has been experimentally verified [149], as shown in Fig. 4.6b and Fig. 4.6c.

4.2 Optical dielectric resonators

A stable trapping condition with long trapping time for dielectric particles and living matter at nanoscale (<100 nm) is prevented by using optical nanowires or slotted waveguides, due to an optical gradient that is not strong enough to attract so small beads, as discussed in the previous section. In fact, only manipulation of metal objects has been verified, enabling the control of motion of particles up to 20 nm, with values of input power P_{in} < 20 mW [147]. Instead, trapping of dielectric nanoparticles can be obtained with an optical power $P_{in} \gg 100$ mW, related to a consequent strong enhancement of thermal effects that can also destroy or damage the trapped living matter [115].

Integrated optical resonators provide high spectral and spatial energy confinement, due to high values of Q-factor and low mode volume, which corresponds to high values of the Q/V ratio [150]. A similar behaviour enables strong light-matter interaction, because high energy values are typically obtained in a sub-wavelength region, so providing remarkable optical gradients with strong enhancement of optical forces, compared to the performance of non-resonant optical devices. In fact, trapping of dielectric nanoparticles with low values of optical input power has been verified, unlike slotted optical waveguides, so providing manipulation at the nanoscale together with long trapping time, that simplifies the target detection and manipulation [151].

Several configurations of integrated optical resonant cavities have been proposed as optical nanotweezer to enhance the trapping efficiency, in order to allow trapping at sub-micron level up to few nanometers.

4.2.1 Whispering-Gallery-Mode Resonators

The Whispering-Gallery-Mode (WGM) were the first resonant cavities used for applications of trapping and manipulation of particles at the micro- and nanoscale, due to their high reliability of fabrication process, ease of integration and their ability to confine strong energy values, which is useful to exert strong trapping forces.

The working principle of such cavities is based on the coupling of light from the bus waveguide to the microring, where light constructively interferes in the resonator, so enhancing the evanescent field and obtaining longer interaction time between light and matter, which makes microring resonators very suitable for biosensing, chemical sensing and obviously optical trapping applications [152-154].

High values of Q/V have been obtained with WGM cavities, which corresponds to strong light-matter interaction. In particular, ring resonators are the most used among WGM configurations for their ease of fabrication and optical characterization and reliable performance.

Integrated microring resonators provide $Q/V > 10^5 (\lambda/n)^{-3}$ with a footprint $A < 0.1$ mm^2, which corresponds to high values of the optical gradient field at resonance. Manipulation of dielectric microparticles' motion has been demonstrated theoretically [155] and also experimentally [156-158]. In particular, silicon technology provides higher values of Q-factor, due to the optical properties of the material and the maturity of fabrication process, which allows to minimize imperfections that cause optical losses [159]. High optical forces can be obtained, so enabling high-stability trapping events with low optical input power. These configurations have been used to achieve efficient particle sorting with a straight propagation of particles along the bus in OFF-resonance and their transport in the round pattern in ON-resonance. For instance, in [159] a stable trapping of polystyrene microparticles of 1.1 μm in the microring has been verified with a footprint of the resonator of about 100 μm^2 and an input power of 5 mW, which is much lower than power values used with bulk optical tweezers. In Fig. 4.7, the value of trapping force as a function of the input power has been reported [159].

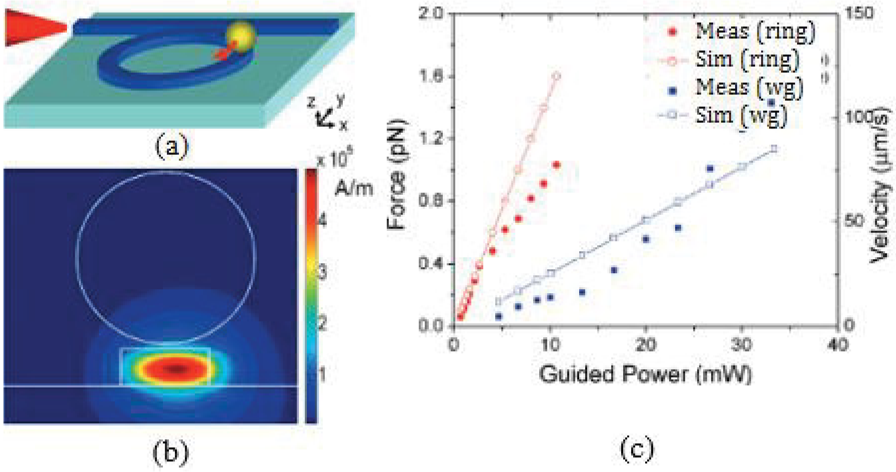

Fig. 4.7. (a) Configuration and (b) FEM simulations of the microring resonator as optical nanotweezer for microparticle trapping proposed in [159]. (c) Behavior of optical force F as a function of the input power.

Trapping of sub-micrometer dielectric particles has been demonstrated with different configurations of Whispering Gallery Mode (WGM) resonators, such as microdisks and microspheres, but at the expense of larger footprint and complex manufacturing process [160].

4.2.2 Photonic crystal cavities

Photonic crystals (PhC) cavities have demonstrated to enhance the figure of merit Q/V, with higher values of Q-factor and smaller mode volume compared to the values obtained with microring cavities [161,162]. The strong photons confinement in ultra-narrow regions makes PhC cavities particularly suitable for optical trapping, due to high values of optical gradient and low optical losses [119]. Such properties of PhCs allow their use in several applications, such as biosensing [163,164] chemical sensing [165,166], and also in optical communication systems [167].

The strong optical gradient obtained with PhC cavities allows to realize efficient optical nanotweezers and several configurations have been already proposed in the literature. An advantage of PhC cavities is related to slow light, which has been demonstrated to be very useful for manipulation of sub-micrometer particles, as confirmed by Scullion et al. in [168]. A strong enhancement in guiding velocity of sub-micrometer particles has been observed by exploiting the slow-light effect in the PhC cavity. A different behavior of trapping effects on dielectric particles up to 500 nm has been verified by a different control of the operative wavelength of the exciting laser, corresponding to a different particle velocity that changes as a function of the wavelength assumed in input of the device, as shown in Fig. 4.8.

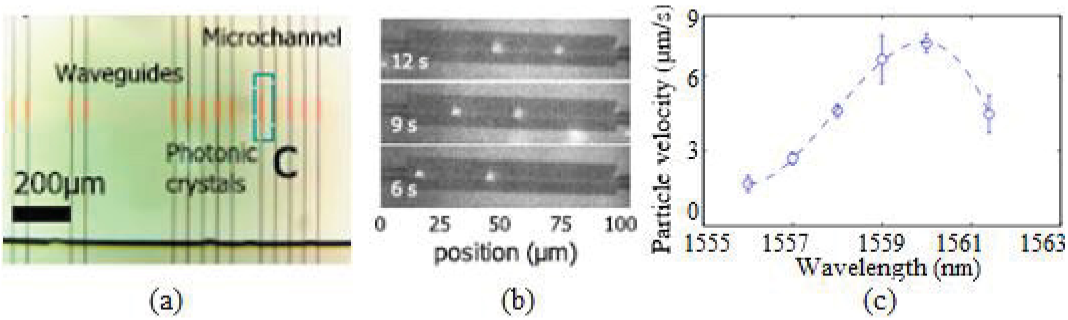

Fig. 4.8. (a) PhC waveguides integrated in an optofluidic chip for sub-micrometer particle trapping. (b) Time-lapse images of optical guiding of dielectric particles along the PhC waveguides and (c) particle velocity as a function of the laser wavelength [168].

The slow-light effect enhances light-matter interaction, so obtaining higher values of optical forces. Therefore, unlike optical waveguides which require high values of input power ($P_{in} \gg 10$ mW) to control the motion of micrometer particles, PhC waveguides allows to guide polystyrene particles at nanoscale ($a < 500$ nm) with a low input power

P_{in} = 2.5 mW, which corresponds to a decrease of about one order of magnitude of power consumption [168].

A further advantage of photonic crystal cavities, rather than performance obtained with WGM cavities, is the ability of confining strong energy values in a very small volume, so enabling trapping of target objects in a specific position and not limiting to their propulsion [13]. This enhancement of the gradient force allows to strongly reduce the optical power without affecting the trapping efficiency. For instance, Leest et al. proposed the first experiment on trapping of living matter by using a 2D PhC cavity [13], verifying the suitability of the resonant cavity for an efficient trapping of a single bacteria Escherichia coli. The bacteria was stably trapped with very low input power (P_{in} < 1 mW), which is a necessary condition to prevent photodamage of the living cell. Higher values of optical force are necessary to enable trapping of smaller objects. A solution to satisfy such requirement has been obtained by using PhC slotted structures. In fact, the simultaneous effect due to presence of the slotted waveguide with a width < 100 nm and a resonant cavity with a high Q-factor enables strong optical energy confinement inside the slot in the defect region, so allowing a 3D trapping of small nanoparticles, as demonstrated by Mirsadeghi et al. in [169] (see Fig. 4.9). Trapping events of Au nanoparticle with a diameter as small as 24 nm has been experimentally verified with an input power P_{in} = 750 μW, which corresponds to a decrease of about three orders of magnitude compared to the results obtained in [135] with the propulsion of similar Au nanoparticles by using a simple optical waveguide. However, even if the particles are attracted by the gradient force, the trapping stiffness is low as demonstrated experimentally by fast and evident changes of the resonance transmission, related to oscillations of the trapped objects from the equilibrium point, which are due to small size of the nanobeads and low power values.

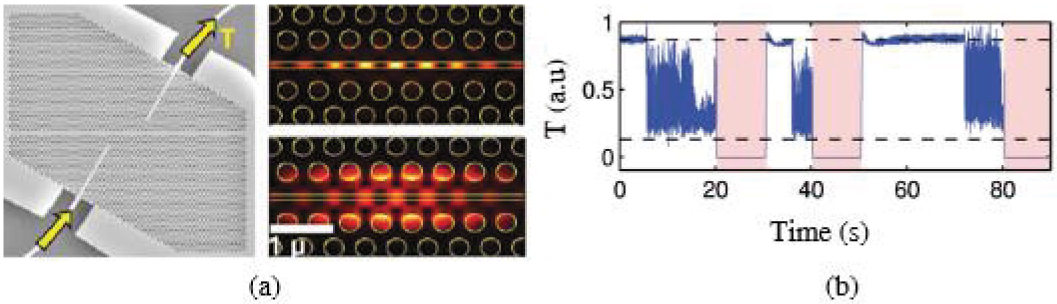

Fig. 4.9. (a) SEM figure and FDTD simulation of 2D slotted PhC cavity. (b) Time-dependent optical transmission with oscillations due to trapping events. The shaded regions indicate when the laser is turned off to release the transiently trapped particles. An input power of 0.75 mW in the PhC cavity has been assumed for the meausurements [169].

In the last years, hollow PhC cavities have been also used for nanoparticle trapping. Descharmes et al. proposed in [170] a PhC waveguide with a large hole inside the PhC and close to the waveguide. The larger hole represents the defect necessary to obtain a resonant behaviour (Fig. 4.10). The size and position of the hole from the waveguide influences the Q-factor and resonance transmission of the cavity.

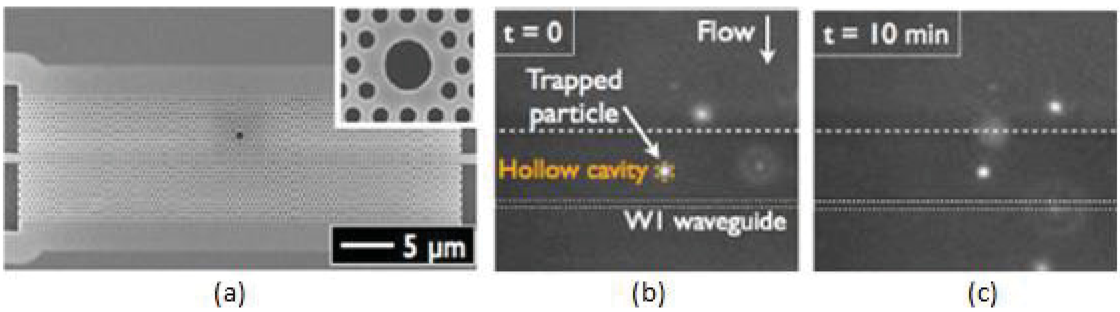

Fig. 4.10. (a) SEM picture of the hollow PhC cavity. (b) Trapping of 500 nm polystyrene particle at t = 0 and (c) after t = 10 min [170].

The optical energy is mostly confined in the hollow cavity large 700 nm with a strong optical gradient inside the defect. A very stable optical trap for dielectric particles of about 500 nm has been demonstrated with ultra-low optical power. In fact, trapping or release of polystyrene particles can be obtained on demand, as shown in Fig. 4.10b and Fig. 4.10c, with high efficiency, as confirmed by long trapping time up to several minutes and a very low input power of only 120 μW. The minimum size of particles that can be trapped is 250 nm, requiring a power at least of 360 μW. Trapping of smaller particles represents an issue because of the challenge to obtain a stronger optical gradient inside the hole. In fact, the energy is maximum at the surface of the hollow cavity and quickly decreases in the center of the hole, so making more difficult the interaction of very small nanoparticles with the electromagnetic energy confined in the hollow cavity [170].

The enhancement of the trapping force can be obtained by decreasing the mode volume of the cavity. This can be obtained by using 1D PhC microcavities consisting of a single row of holes in a photonic wire, because the resonant mode is stronger limited laterally than the 2D counterpart of PhC. Such property, together with high values of Q-factor, determines a relevant enhancement of light-matter interaction [171]. Q-factor exceeding 10^5 have already been experimentally obtained by properly tapering the holes' size and position in order to reduce mismatch between the waveguide mode and the Bloch mode in the photonic crystal cavity [172,173], expecting values up to $Q \sim 10^9$ theoretically [174]. Moreover, mode volume $V < 10^{-1} (\lambda/n)^3$ have been demonstrated [175], which is almost an order of magnitude lower than values obtained by 2D PhCs. Values of the figure of merit Q/V ~ 10^7 $(\lambda/n)^{-3}$ have been achieved [176], which is comparable with the 2D PhC performance, but with the advantage of stronger energy confinement, which corresponds to higher optical gradients and improves the suitability of such devices as optical nanotweezer.

Lin et al in [14] proposed a 1D PhC cavity in SOI technology with periodic holes' size that gradually increases from the middle to the outer region and a cavity in the middle is created by shifting holes outward. Such cavity provides Q-factor of about 2×10^3 and the strong energy confinement in the cavity allows trapping of polystyrene nanoparticle as large as 110 nm. This result corresponds to a decrease of the size of the smallest detectable beads of about a factor 2 in comparison with the performance obtained with a microdonut resonator, in addition to a more compact device footprint (~10 μm^2). An enhancement of the tweezer performance has been verified by Mandal et al. in [177] by assuming a more accurate tapering approach for the cavity design, so verifying stable trapping of polystyrene nanoparticle up to 50 nm for long trapping time with a release only on demand (tunring-off the laser or with a reverse flow in the channel) with very low input optical power (P_{in} = 1.7 mW), as shown in Fig. 4.11.

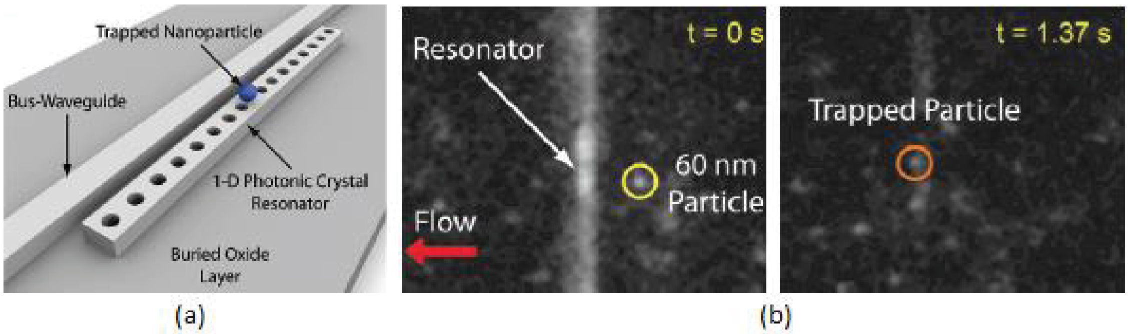

Fig. 4.11. (a) Schematic of the 1D PhC photonic crystal resonator. (b) Trapping of 60 nm polystyrene nanoparticle at resonance [177].

Such cavities are characterized by a strong energy confinement in the core material with a higher refractive index with a small amount of evanescent field, which effectively acts to generate optical forces. Such limitation can be overcome by optimizing the photonic crystal configuration aiming at confining the optical energy in the region with lower refractive index, so enhancing the interaction between the particles and the cavity mode. Chen et al. proposed a 1D PhC cavity in Si_3N_4 technology with a very small hole in the middle of the cavity between two identical tapered Bragg mirrors in order to satisfy such requirement (see Fig. 4.12) [178]. The small hole in the middle of the cavity acts as an inner cavity with a strong light intensity. Higher values of optical stability (S = 12) and optical stiffness have been calculated, enabling trapping of Wilson disease proteins and also polystyrene nanoparticles up to 22 nm with P_{in} = 10 mW with a negligible temperature enhancement ($\Delta T \sim 0.3$ K), due to low values of optical absorption in Si_3N_4.

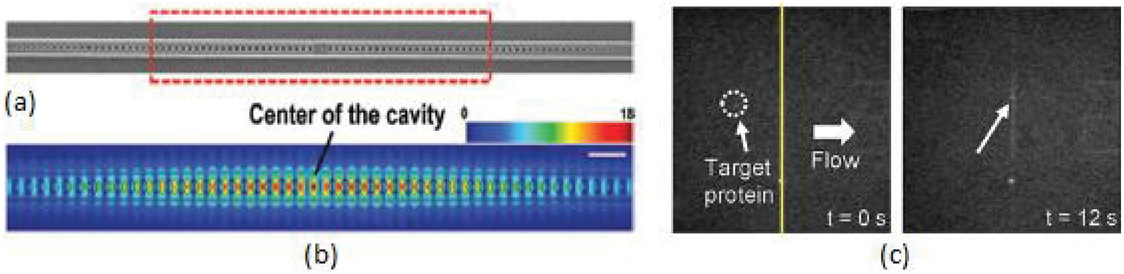

Fig. 4.12. (a) SEM image of the PhC microcavity plus hole (MH) and (b) electric field distribution at resonance. (c) Trapping event of Wilson disease protein [178].

Another strategy to confine light in the material with lower refractive index is with slotted waveguide embedded in a 1D PhC cavity. This configuration provides a relevant decrease of mode volume with a strong energy confinement in a very small region. For instance, Wang et al. have proposed a 1D PhC slotted cavity with a mode volume $V < 10^{-1} (\lambda/n)^3$ (Fig. 4.13) [175]. The strong energy confinement in the slot makes such cavity suitable for biosensing applications and optical trapping. In particular, trapping events of single 20 nm polystyrene nanoparticle have been observed, corresponding to a shift of few pm of the resonance wavelength and a “jump” of resonance transmission when a particle approaches the cavity, due to the gradient force that pulls the bead toward the slot. However, the strong Brownian motion due to the very small size of the nanoparticle prevents long trapping time and changes in the resonance transmission for only few seconds have been observed with beads smaller than 30 nm (see Fig. 4.13).

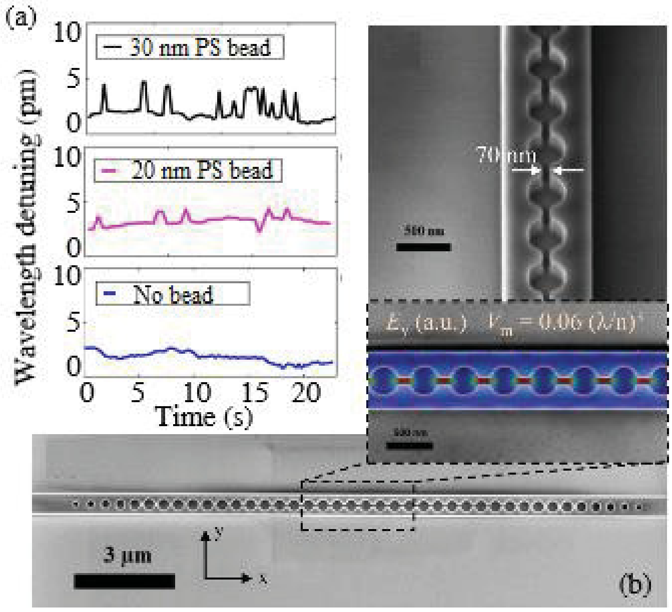

Fig. 4.13. (a) Wavelength detuning for each trapping event of polystyrene nanobead and (b) SEM image of the 1D PhC slotted cavity with a magnification of the slot and electric field distribution in the inset [175].

Recently, Liang et al. have proposed the first air-mode photonic crystal nanobeam cavity at telecom wavelength (Fig. 4.14). The strongest advantage of such cavity is the ultra-high Q/V (> 10^7 $(\lambda/n)^{-3}$), due to high values of Q-factor (>10^5) and very small mode volume (10^{-2} $(\lambda/n)^3$), even lower than those obtained by slotted configurations [176]. The high energy confinement in the air allows to exert strong trapping force in the cavity region, providing trapping of Au nanoparticles up to 1.8 nm and, potentially, polystyrene beads of only 3 nm with only P_{in} ~ 1mW. Such performance obtained with air-mode PhC cavity confirms an improvement of manipulating nanoscale objects of about one order of magnitude smaller than other PhC cavities and enables detection of sample concentration up to 1 fM.

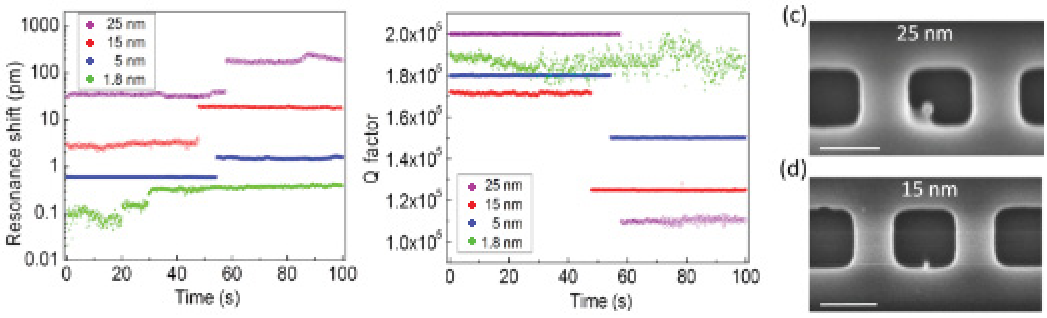

Fig. 4.14. (a) Resonance shift and (b) Q-factor gbehavior as a function of the size of the metal nanoparticle trapped in the air-mode photonic crystal cavity. (c) SEM image of the PhC nanobeam cavity with a trapping event of (c) 25 nm and (d) 15 nm Au bead [176].

4.3 Plasmonic nanostructures

Plasmonic nanostructures have been largely used to manipulate objects at micro and nanoscale, because of their ability to overcome diffraction limits typical of dielectric configurations, so enabling a strong sub-wavelength energy confinement [179]. A peculiarity of plasmonic devices is the strong energy confinement observed at the interface between metal and dielectric layers, with sharp exponential decay from the metal surface [180]. This behavior represents an evident advantage for several applications, such as optical communications [181, 182], optical imaging [183], energy harvesting [184], nanoelectronics [185, 186] and, particularly, sensing and optical trapping for applications in biology, chemistry and medicine [187, 188]. Plasmonic biosensors have demonstrated to improve sensitivity up to the detection of a single molecule [189, 190].

The configurations of plamonic cavities used as plasmonic tweezers are: nanoantenna and nanoapertures.

4.3.1 Plasmonic nanoantenna

Nanoantenna are plasmonic cavities with a resonant behavior, and a strong energy confinement around the metal surfaces is obtained, corresponding to strong light-matter interaction in sub-micrometer volumes. The simplest configuration of nanoantenna is the monopole, which consists of a single metallic nanoparticle, where electromagnetic field is strongly confined at the surface [191]. A configuration of monopole nanoantenna has been proposed for trapping by Cetin et al. in [192], as shown in Fig. 4.15.

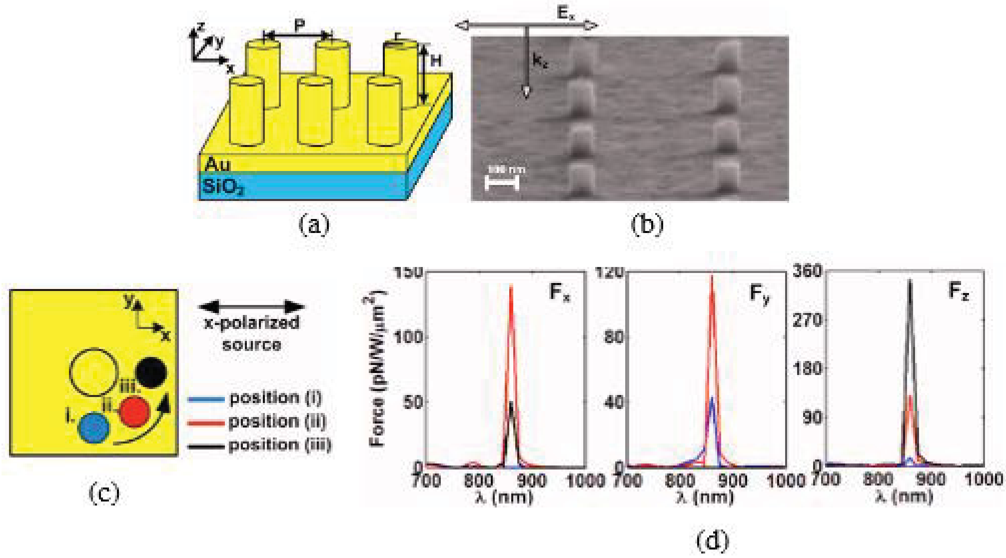

Fig. 4.15. (a) Schematic and (b) SEM figure of an array of monopole nanoantenna. (c) Different position of the trapped object with a diameter of 200 nm around the monopole and (d) relative forces along three directions.

The remarkable enhancement of the energy confinement in sub-wavelength region typical of plasmonic nanoantenna makes such cavities suitable to provide efficient and stable optical traps [193, 194]. Furthermore, the optical stiffness is very high in optical nanoantenna, corresponding to a strong attracting force. However, the trapping length scales inversely to the optical stiffness, therefore it is necessary that particles flow very close to the nanoantenna to be trapped, unlike dielectric configurations with a longer decay length of the evanescent field [195].

Several patterns of nanoantenna have been proposed as plasmonic naotweezers with high performance, such as dimers, dipole and bowtie structures. The narrow gap between two metal structures provides a strong enhancement of the optical energy of about two orders of magnitude than values obtained by a simple monopole [196].

A plasmonic dimer consists of a pair of metal nanoparticles, with a circular or elliptical shape, separated to each other by a narrow dielectric gap [197]. The advantage of such cavity is the ease of fabrication and high control over the gap width due to progress in manufacturing of nanostructures, which improves the accuracy and device reliability together with a strong energy confinement inside the nanoscale gap [198].

Grigorenko et al. have proposed in [190] an array of gold dimers excited by normal incident light, as shown in Fig. 4.16.

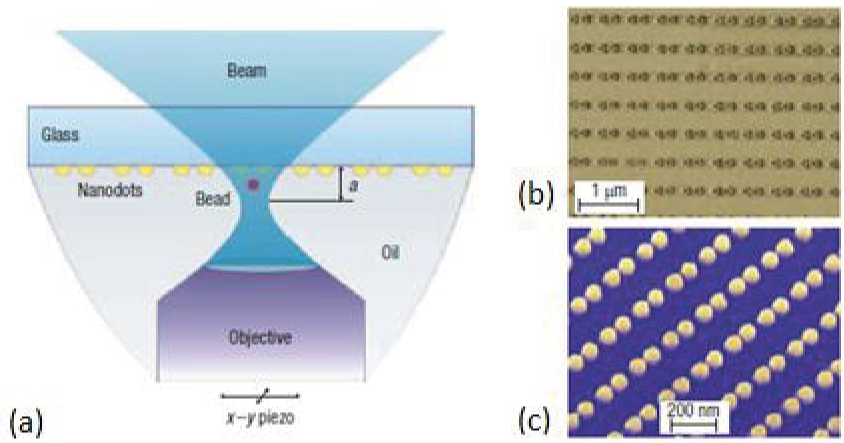

Fig. 4.16 (a) Schematics of the plasmonic nanotweezer proposed in [190]. (b,c) Micrographs of the device with different lattice constants.

Typical values of the Q-factor of plasmonic cavities are Q ~ 10, which are much lower than dielectric resonant cavities performance. This behavior is due to high values of optical losses for the presence of metal with higher absorption effect, but at the same time, the small gap of about 100 nm between the metal structures of the dimer provides a strong energy confinement ($V \ll (\lambda/n)^3$), which corresponds to high values of Q/V ($> 10^4 (\lambda/n)^{-3}$) and, therefore, strong light-matter interaction. However, trapping efficiency is not very high with dimers because of rounded corners of the metal blocks, so preventing an extreme energy confinement in the cavity. Trapping of 200 nm polystyrene beads has been demonstrated with an input optical power at least of 440 mW [190]. Even if the power value is high, the laser is focused in order to lighten several nanoantennna, which corresponds to an energy density that minimizes the thermal heating without affecting the plasmonic tweezer performance.

Recently, several dimers configurations have been proposed with higher performance, due to the development in nanofabrication techniques with the realization of smaller gap with an exponential increase of the energy confinement. This corresponds to higher values of trapping force with lower values of optical power, making possible also the trapping of living matter. Galloway et al. have proposed in [199] a gold dimer to stably trap Bovine Serum Albumin (BSA) protein without damage.

The device proposed in [105] has demonstrated to be suitable for light-assisted molecular immobilization, which enables chemical interaction between different biological matter with a high spatial resolution of the immobilization, thanks to the action of optical gradient. In fact, even if the protein immobilization is allowed by the molecular binding, this effect is based on light-assisted molecular immobilization. In fact, the use of plasmonic cavities allows to reach strong energy confinement in volumes at the nanoscale, exactly in the dimers gap. It is clear that the optical near field governs the protein immobilization because the streptavidin-coated gold colloids are attracted by the hot-spots with a strong energy confinement in the nanoantenna gap and interact with the cavities, demonstrating that the protein binding is triggered by the enhanced plasmonic fields. The interaction of biotin and streptavidin-coated gold colloids, which are simultaneously trapped in the nanoantenna gap, has been verified experimentally with an input power of only 0.5 mW and negligible thermal heating (see Fig. 4.17).

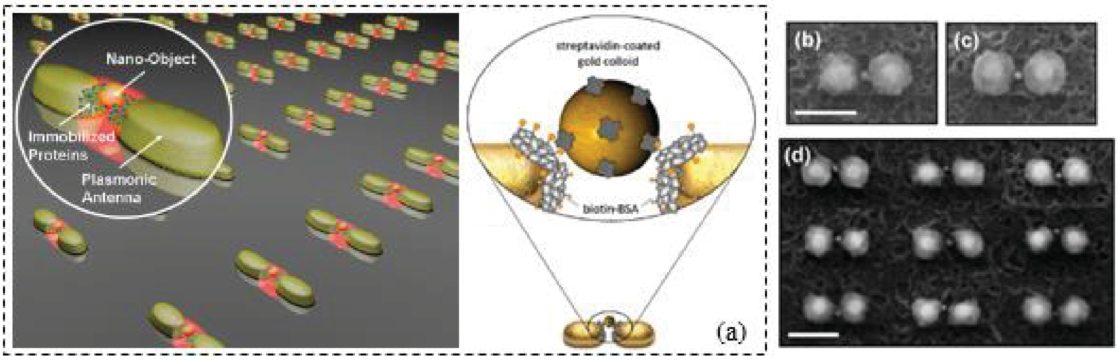

Fig. 4.17. Schematic of the array of dimers nanoantenna used for light-assisted molecular immobilization with a magnification of the interaction between bioting and streptavidin injside the narrow gap of the nanoantenna in the insets. (b,c) SEM images showing binding of a single and (d) an array of dimers for binding of gold nanoparticle in the gap (scale bar = 150 nm).

Dipole nanoantenna are realized by two metal arms separated by a narrow gap with a similar structure of dimers, but with a rectangular or square shape of each arm, that provides higher values of energy confinement due to their sharp corners. A higher control on their spectral response has been observed, because changes of the length of metal blocks and gap width cause a different resonance behavior. Dipole nanoantenna have been largely studied, aiming at optimizing their size and surface quality to enhance trapping efficiency [200]. Trapping of metal and dielectric beads, and biological matter smaller than 100 nm has been verified [201]. For instance, Zhang et al. in [201] have calculated an optical stability S > 5 and a remarkable red-shift of the resonance wavelength of about 50 nm when a single 20 nm Au nanoparticle is trapped inside the gap of only 25 nm. The extraordinary light-matter interaction also allows trapping also particle of 10 nm beds, observing a resonance shift of about 20 nm in presence of each trapping event (see Fig. 4.18).

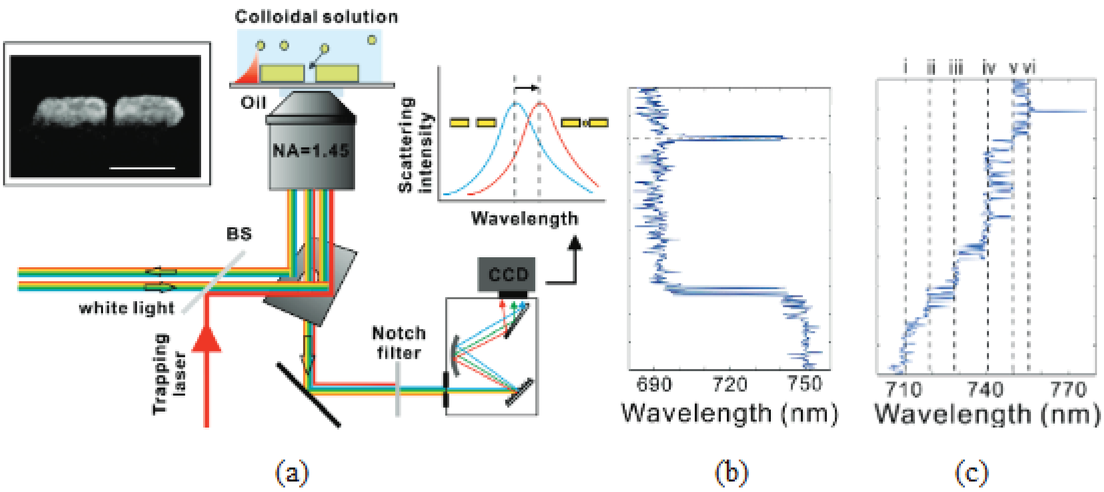

Fig. 4.18. Configuration of the optical setup and the dipole nanoantenna (in the inset) for trapping of a single Au nanoparticle. Resonance shift observed after a trapping event of a single (b) 20 nm Au bead with a gap of 25 nm and (c) 10 nm Au bead with a gap of 15 nm.

Low values of input power have been used without affecting the stability of the optical traps. For instance, a stable trapping of Escherichia Coli for several hours has been demonstrated with dipole naoantenna by Righini et al. in [5] with an input power of 300 mW to excite a large array of dipole structures [5](see Fig. 4.19), corresponding to an optical intensity of only 10^9 W/m^2 for each plasmonic cavity, which is almost an order of magnitude lower than the damage threshold of bacteria [202].

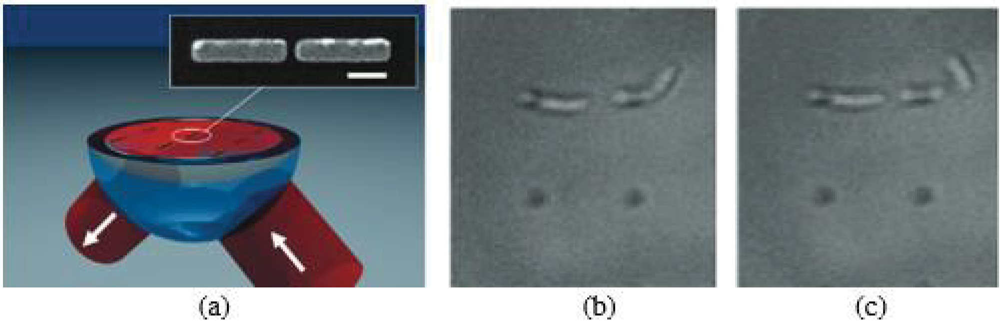

Fig. 4.19. Schematic of the optical setup used for optical trapping of living bacteria with dipole nanoantenna. (b,c) A sequence of bacteria trapping recorded over two hours [5].

In the last years, the bowtie nanoantenna, consisting of a triangular shape of two metal arms separated by a narrow gap, have received a rising interest [203]. Theoretical studies have demonstrated that dipole nanoantenna provide stronger energy peaks than bowtie configurations, but at the same time they are also characterized by multiple optical traps in the external edges of the metal arms and not only in the gap. On the contrary, bowtie structures are not affected by multiple trapping sites as for dipole nanoantennas, because the light is tightly focused in a single spot inside the gap, in specific condition of light polarization, and low energy confinement is typically observed at the other corners, which corresponds to a higher sensitivity of the resonant nanoantenna [200, 203]. This represents a strong advantage for plasmonic nanotweezers, because the position of the optical trap is well defined with a higher trapping efficiency and the fluctuations of trapped objects are typically less evident. Such behavior makes bowtie nanoantenna very suitable for trapping of small objects and also living matter [204]. Roxworthy et al.

have proposed an array of bowtie nanoantenna to trap, stack, and sort dielectric nanoparticle with an input power lower than 1 mW [205, 206]. An improvement of energy confinement up to a factor 4 has been obtained by using pillar-supported bowtie nanoantenna (p-BNA), where the plasmonic cavities are elevated from the substrate, as proposed by Chen et al. in [207] (see Fig. 4.20). This corresponds to a potential enhancement of trapping force and also refractive index sensitivity, achieving up to S = 1763 nm/RIU, which is two times greater than performance obtained by using simple bowties, allowing trapping and sensing of single molecule.

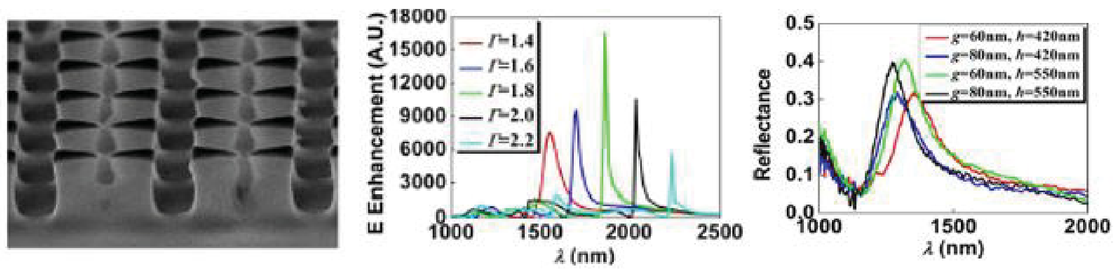

Fig. 4.20. (a) SEM image of p-BNA. (b) Near-field intensity enhancement spectra calculated by FDTD simulations and (c) experimentally obtained near-IR reflection spectra [207].

4.3.2 Metal nanoholes

A strong energy confinement with a consequent enhancement of trapping forces has been achieved by focusing a laser beam into a nanoaperture in a metal film, so overcoming the diffraction limit typical of dielectric configurations [208]. This perturbation of the local electromagnetic energy distribution strongly affects the motion of particles around the nanoaperture, thereby enabling trapping at the nanoscale. The trapped particle has itself a strong influence on the local electromagnetic field with an active role in the trapping action. This effect is called self-induced back-action (SIBA) optical trapping and enhances the trapping efficiency with a strong localization of single particle exactly in the nanohole where the optical gradient is maximum [209]. Unlike the plasmonic nanoantenna, nanoapertures have not a resonant behavior, therefore they require very small gap to enhance light confinement in order to exert high values of optical forces. This insensitivity to wavelength translates into lower sensitivity to thermal effects (a temperature increase < 1K is typically observed with nanoparticle trapping [210]).

Changes in the optical transmission is the physical effect observed in presence of a trapping event of a bead inside the nanohole. An increase of transmission is given with a trapped bead with a higher refractive index of the fluid inside the nanoaperture, therefore the optical characterization of the plasmonic nanotweezer is based on the analysis of the transmission values to confirm a trapping event and the range of such changes quantify the size of the bead and its optical properties.

Several configurations of plasmonic tweezers based on nanoapertures have already been shown in the literature, such as single nanoholes [211], rectangular slits [212] coaxial apertures [213], and double nanoholes (DNH) [214,215] (see Fig. 4.21).

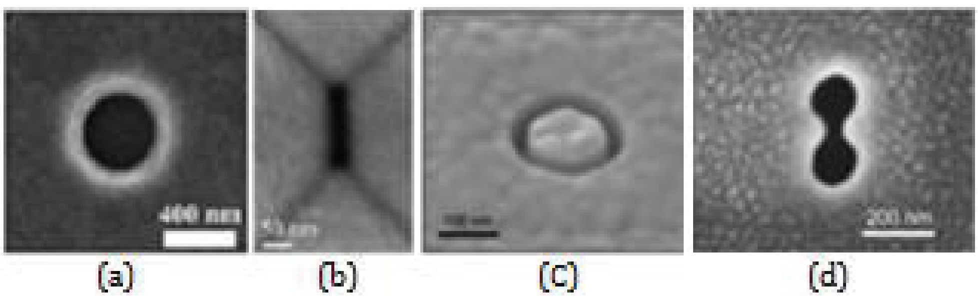

Fig. 4.21. Configurations of nanoapertures with (a) single nanohole [211], (b) rectangular slit [212], (c) coaxial shape [213], and (d) double nanohole [214] proposed as plasmonic nanotweezer.

The simplest configuration of plasmonic nanoapertures is based on a circular nanohole in which a laser beam is tightly focused, as the configuration proposed by Kim et al. in [211]. Stable trapping of a single DNA molecule has been obtained for at least t = 1 min. Furthermore, it has been verified that DNA of different lengths can be differentiated through the measurement of scattering signals, so leading to several DNA sensor applications.

The minimum size of particles that can be stably trapped in the aperture is strongly dependent on the size of the nanohole. Narrower gap are necessary to further enhance the trapping efficiency of the device. Among such configurations, double nanoholes (DNH) have demonstrated the highest trapping efficiency [216]. DNH consists of two circular nanoholes close to each other, thus forming a cusp with an ultra-thin gap between them (< 30 nm), as shown in Fig. 4.21d. This configuration enables an extreme energy confinement within the cusp, with a sharp and strong optical gradient around the ultra-thin gap of the DNH and enabling to trap nanoparticles of only few nanometers. This behavior makes such device useful for manipulation at the single molecule level with high spatial confinement and long trapping time. In particular, Pang et al. in [214, 215] realized trapping of a single BSA protein (~ 3 nm) and 12 nm silica beads with a signal-to-noise ratio SNR > 30 with a trapping time longer than 80 seconds. Zehtabi-Oskuie et al. in [217] verified the trapping of streptavidin with an optical intensity of 10^9 W/m^2. Moreover, such devices have been also used to study binding between DNA and protein [218], protein-antibody co-trapping [219] and protein unzipping [220], because of their ability in single particle detection and trapping, thus allowing accurate and high-resolution biological and chemical analysis without requiring tethering or labels.

The limitation of metal nanoholes compared to performance obtained with plasmonic nanoantenna is the absence of a resonant behavior, that causes lower values of trapping stiffness (k = 0.2 pN/nm·W [121]). This makes more difficult the trapping of the target object close to the nanoaperture, so requiring negligible effects of Brownian motion together with a perfect focusing of laser beam in the gap, in order to allow the attraction effect when the bead is exactly in that position. Higher values of input power of several milliwatts should be applied to enhance the trapping stiffness, because k increases linearly with power laser, but at the expense of thermal effects that would affect the Brownian motion of the nanoparticles around the nanohole, without any improvement in the trapping efficiency.

Recently, DNH plasmonic nanotweezers fabricated at the tip of a tapered optical fiber have been proposed. For instance, Berthelot et al. in [221] and Gelfand et al. [220] have proposed a tapered optical fiber with a DNH at the tip to trap nanoparticles for several minutes with low optical power (P_{in} ~ 700 μW) together with the ability of moving them over tens of micrometers, thereby achieving extreme control over the 3D manipulation of objects at the nanoscale (see Fig. 4.22).

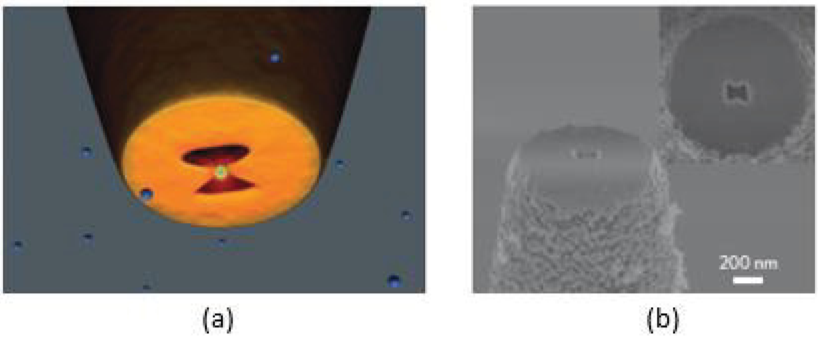

Fig. 4.22. (a) Schematic and (b) SEM image of DNH patterned at the extremity of a tapered optical fiber [221].

4.5 Hybrid devices

In the last years, a strong research interest has been observed in study and realization of hybrid configurations, with the integration of dielectric and metal structures in the same device, especially to realize high performance resonant cavities [222]. The reason is that photonic/plasmonic configurations have demonstrated to exploit advantages and peculiarity of dielectric devices, such as low loss propagation and high quality factor in resonant cavities, together with extreme optical confinement, typical of plasmonic structures [223, 224]. Such behavior corresponds to strong light-matter interaction, due to high energy confinement in very small subwavelength regions together with lower optical losses than values obtained with plasmonic configurations.

Several configurations of hybrid devices have been proposed with the aim of optimizing the enhancement of the energy confinement to be suitable for several applications, such as optical communications [225, 226], optical information storage [227] and, most of all, molecular sensing, [222] optical trapping, detection and manipulation [228, 229]. Some of these hybrid devices have been reported in Fig. 4.23.

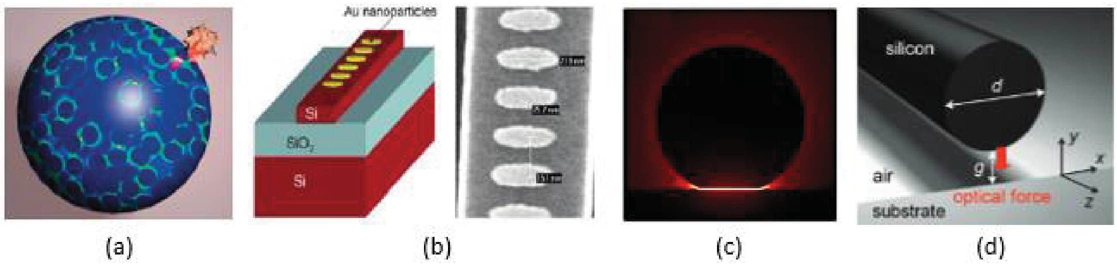

Fig. 4.23. Configurations of different hybrid cavities to obtain high gradient of optical field and strong light-matter interaction [229, 228, 222, 224].

WGM cavities have been largely used for biosensing, due to their high values of Q-factor, corresponding to relevant sensitivity with very low limit of detection (LOD) [230, 231]. Their performance have been strongly improved with hybrid configurations, where small metal nanoparticles are bound to the dielectric WGM cavity to create hotspots with ax extreme subwavelength energy confinement. The metal nanoparticles allow trapping of small beads up to a single molecule [231]. Dantham et al. have demonstrated ultra-sensitive detection with a hybrid WGM microcavity in [232] where nanoshell gold microspheres are directly bounded to the WGM cavity surface, as shown in Fig. 4.24. The binding is due to the gradient force that draws them to the equator of the resonant cavity. The nanoshell is able to attract a BSA protein and a single thyroid cancer marker (Tg) with masses of 0.11 ag and 1 ag, respectively, and their stable trapping onto the WGM surface is given by the proper salt concentration in the sorrounding medium, aiming at increasing the conductivity of the solution and so, decreasing the effects of the repulsive force for particles at the nanoscale. This effect of optical forces is typically called "carousel trap", for which attractive optical gradient forces remarkably enhance the transport to the sensing region of the target object to detect, overcoming limitations given by the diffusion of such small detecting area. The nanoshell is able to trap a BSA protein and a single thyroid cancer marker (Tg) with masses of 0.11 ag and 1 ag, respectively, which corresponds to an improvement of limit of detection of several orders of magnitude, due to both high Q-factor of the WGM cavity and the strong energy localization at the nanoshell. The stronger interaction between the hybrid cavity and the single molecule has been also confirmed by the enhancement of the shift of resonance wavelength of 240 % and 1500% for the Tg and BSA, respectively, for each trapping event in presence of the nanoshell with the bump.

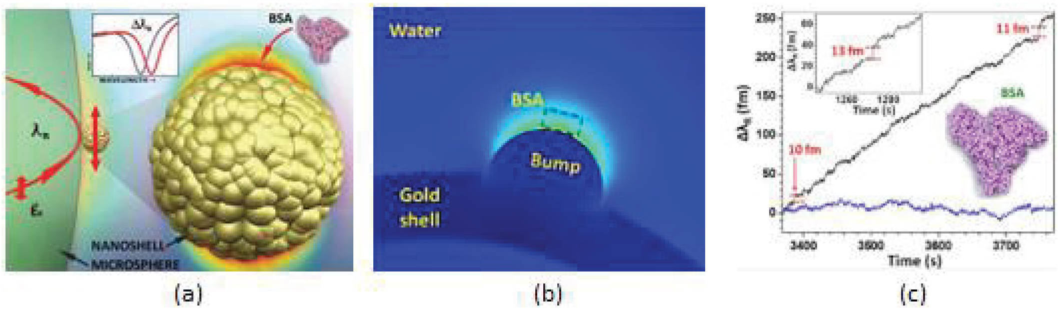

Fig. 4.24. (a) Schematic of the hybrid WGM microcavity with an integrated gold nsanoshell. (b) FEM simulation of the energy distribution around the nanoshell and (c) experimental results on resonance shift with and without the nanoshell [232].

Photonic/plasmonic nanotweeers based on the integration of optical nanowires with plasmonic structures have demonstrated stable trapping of particles at nanoscale. O'Dell et al. have proposed a cavity with a multi-walled carbon nanotubes adsorbed onto a silicon waveguide [233], as shown in Fig. 4.25. The evanescent field of the optical waveguide is strong enough to adsorb a single-wall carbon nanotube (SWCNT) with a plasmonic behavior. A strong enhancement of both the electromagnetic energy and the gradient field has been obtained at the surface of the SWCNT, several orders of magnitude stronger than the evanescent field of a simple dielectric waveguide. This corresponds to an improvement of the trapping forces exerted around the plasmonic structure. Moreover, the adsorption of the SWCNT allows that nanoparticles can be trapped and not only propelled along the waveguide, which represents a limit of dielectric waveguides used as optical nanotweezers.

Trapping of polystyrene beads of about 500 nm has been demonstrated experimentally for several seconds, until the laser is switched off, confirming high values of optical stability. It has been demonstrated by FEM simulations that light-matter interaction calculated around the SWCNT is so strong to trap potentially dielectric bead of only 10 nm, which is an unexpected result to reach by using a simple nanowire.

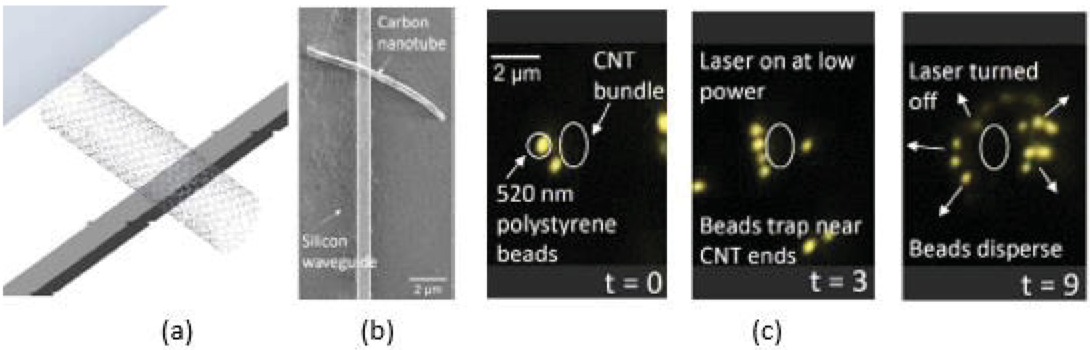

Fig. 4.25. (a) Schematic and (b) SEM image of the hybrid configuration with the adsorption of a SWCNT onto a silicon waveguide surface. (c) Trapping events of 520 nm polystyrene beads on the SWCNT [233].

Lin et al. have proposed a hybrid cavity based on the integration of a bowtie nanoantenna on a silicon waveguide [234], aiming at funneling the photonic mode of the nanowire into a plasmonic resonant mode of the bowtie, highly confined within the narrow gap at resonance (Fig. 4.26a). The strong enhancement of the optical energy in the gap provides the trapping of polystyrene nanoparticles up to 20 nm. The threshold power used to obtain a stable trapping condition ($S \geq 10$) for these particle's size is $P_{in} = 10$ mW with a negligible thermal enhancement. This performance confirms an improvement of trapping efficiency obtained with the hybrid configuration in comparison with that evaluated without the integration of the bowtie.

A similar approach with a hybrid configuration has been also proposed by Ying et al. in a theoretical study [235]. Several plasmonic nanoantenna with different lengths are placed in cascade onto a dielectric waveguide, as shown in Fig. 4.26b, which resonate at different wavelengths.

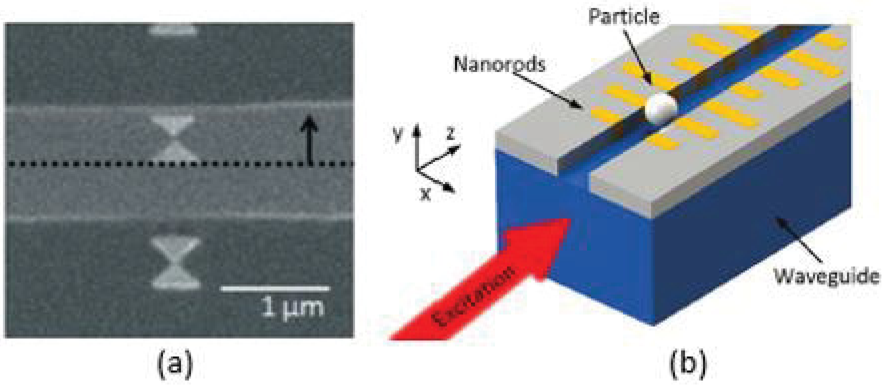

Fig. 4.26. Hybrid nanotweezers for nanoparticle trapping with the integration of a (a) bowtie [234] and (b) dipole nanoantenna array on a dielectric waveguide [235].

The particle propagates along the waveguide between the nanoantenna, until it reaches the plasmonic cavity in resonance, where the strong energy confinement enables the trapping event. Therefore, Ying et al. have demonstrated to control the particle motion with the hybrid cavity and switch its position only by changing the resonance of laser beam focused on the nanoantenna, so expecting to obtain an efficient conveyor for a polystyrene nanobead of only 40 nm.

A strong enhancement of light-matter interaction has been demonstrated by using an hybrid cavity with a plasmonic bowtie placed on a 1D PhC cavity, so exploiting the high

Q-factor of the photonic crystal and also the subwavelength confinement in the bowtie simultaneously [236, 237].

In particular, Ciminelli et al. have proposed a theoretical study in [236] where a photonic/plasmonic nanotweezer with an Au bowtie nanoantenna vertically coupled to a 1D PhC dielectric cavity, as shown in Fig. 4.27. The resonance matching for both cavities provides to enhance the coupling efficiency from the PhC to the bowtie, so obtaining a high gradient force around the nanoantenna due to ultra-high value of Q/V up to 10^7 $(\lambda/n)^{-3}$, together with high values of resonance transmission (T > 30 %), which represents a fundamental advantage of the hybrid configuration rather than plasmonic ones.

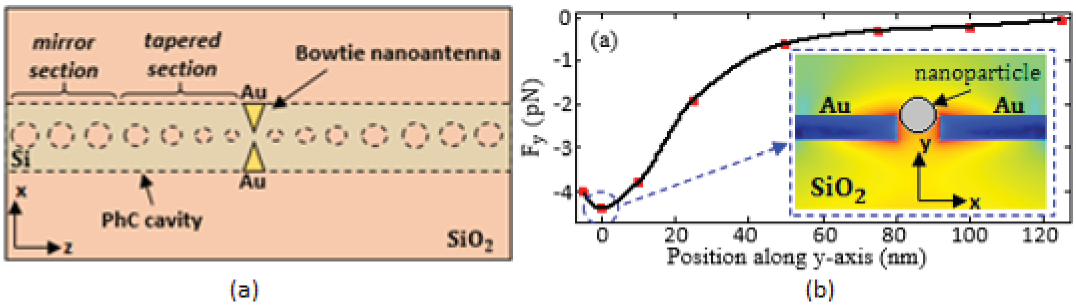

Fig. 4.27. (a) Top view of the photonic/plasmonic cavity with an Au bowtie vertically coupled to a 1D PhC. (b) Results of 3D FEM simulation of optical forces exherted on 40 nm polystyrene nanoparticle with an in imput power of 1mW [236].

The strong energy confinement in the bowtie, due to high efficient funneling of optical energy from the PhC at resonance, allows trapping of 40 nm polystyrene nanoparticle with a very high optical stability (S = 30), so expecting long trapping time with low input power (P_{in} = 1 mW). Furthermore, the high values of the potential energy much greater than 10 K_BT with low optical power have demonstrated the ability of the photonic/plasmonic cavity to trap smaller nanoparticles, making the device suitable for application in medicine and biology for single protein trapping [236].

We have reported in Tab. 1 the state-of-the-art of the integrated pohotonic, plasmonic and hybrid nanotweezers for a comparison of performance, in order to identify the most suitable configuration to exploit an efficient trapping condition at sub-micrometer scale and nanoscale.

Tab. 1. Performance of integrated nanotweezers with dielectric, plasmonic and hybrid configurations.

Config.	Type	Particle size	Particle material	Power	Performance	Trapping time
2D PhC cavity [13]	Dielectric	2 μm	E. coli (biological)	1 mW	S ≥ 10 k = 7.6 pN/nm·W	> 5 min
Microsphere resonator [160]	Dielectric	280 nm	Silica (dielectric)	0.23 mW	S = 5.5	> 20 min
2D PhC cavity [170]	Dielectric	250 nm	Polystyrene (dielectric)	0.36 mW	S ≥ 10	> 10 min
Slotted waveguide [147]	Dielectric	75 nm	Polystyrene (dielectric)	250 mW	S ≥ 10 k = 0.3 pN/nm·W F = -25pN (@ P = 1W)	-
Optical nanowires [145]	Dielectric	50 nm	Au (metal)	3 mW	S = 6	10 sec
1D PhC with bowtie nanoantenna [236]	Hybrid	40 nm	Polystyrene (dielectric)	1 mW	S = 30 k = 90 pN/nm·W F = -4.4pN (@ P = 1 mW)	> 30 min (expected)
2D PhC cavity [169]	Dielectric	24 nm	Au (metal)	0.75 mW	S ≥ 10	> 40 sec
1D slotted PhC [175]	Dielectric	20 nm	Polystyrene (dielectric)	-	-	~1 sec
Slotted waveguide [147]	Dielectric	-	λ DNA 48kb (biological)	250 mW	S ≥ 10	> 3 sec
1D PhC [176]	Dielectric	5 nm	Au (metal)	1 mW	S = 30	> 60 sec
1D PhC [176]	Dielectric	3 nm	Polystyrene (dielectric)	1 mW	S ≥ 10	> 60 sec

1D PhC [178]	Dielectric	-	Cy5-labeled Wilson disease protein (biological)	10 mW	S = 12	>25 sec
Microsphere resonator with nanoshell [232]	Hybrid	3 nm	BSA protein (biological) Thyroid Carcinoma marker (biological)	0.05 mW	-	> 120 sec
Nanohole [211]	Plasmonic	-	DNA molecule (biological)	7.8 mW	S ≥ 10	40 sec
Double nanohole (DNH) [214]	Plasmonic	3 nm	BSA protein (biological)	3.5 mW	S = 10 K = 0.2pN/nm·W	> 90 sec
Nanoantenna [199]	Plasmonic	3 nm	BSA protein (biological)	0.5 mW	S ≥ 10	-
1D PhC [176]	Dielectric	1.8 nm	Au (metal)	1 mW	S = 10	> 60 sec

In the next chapter, the optimized design of the photonic/plasmonic cavity with an ultra-high Q/V and the experimental results as hybrid nanotweezer have been discussed. The physical concept is the same of that proposed in Ref. [150]. The device configuration has been optimized to obtain high cavity performance with a high reliability for the fabrication step.

CHAPTER 5

Design of the hybrid cavity for optical trapping applications

5.1 Device configuration

The photonic/plasmonic device includes a 1D PhC dielectric microcavity embedded in a silicon (Si) photonic wire, which is vertically coupled to an Au bowtie nanoantenna, as shown in Fig. 5.1 [236].

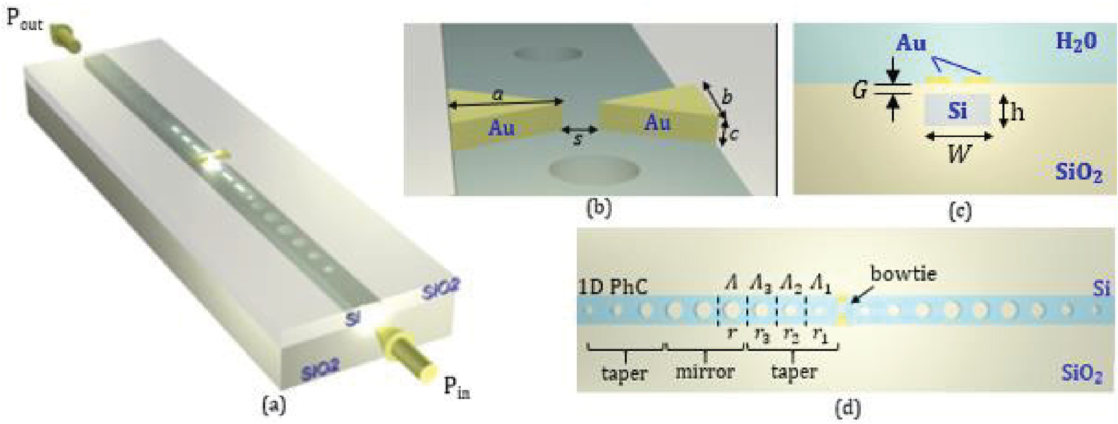

Fig. 5.1. (a) Hybrid cavity configuration with (b) a magnification of the bowtie nanoantenna. (c) Cross-section and (d) top-view of the cavity with the alignment of the bowtie to the PhC dielectric structure.

The width and the thickness of the Si wire, placed on 3 μm buried oxide, are $W = 490$ nm and $h = 220$ nm, respectively. The cavity is realized by two mirror sections, each consisting of N mirror holes with the same radius r and period Λ, and a tapering section in the middle of the cavity (see Fig. 5.1). The tapered section has been designed to improve the matching between the nanowire mode and the Bloch mode in the photonic crystal structure aiming at reducing the coupling loss [26]. Both holes' radii and periods are not uniform in the tapering section and they have been chosen to obtain a resonance condition around λ = 1550 nm and, particularly, to optimize the energy confinement in the cavity together with a resonance transmission of the 1D PhC dielectric cavity higher than T = 90 %. This is necessary to overcome the remarkable optical loss obtained when the plasmonic nanostructure is placed above the PhC in the hybrid configuration.

A plasmonic bowtie nanoantenna is placed above the PhC to enable the vertical funnelling of light from the dielectric cavity to the metal structure, in order to obtain strong energy confinement in the bowtie, so strongly decreasing the cavity mode volume with relevant values of optical transmission. A silica layer has been placed between the bowtie and the PhC cavity to decrease optical losses.

We have assumed water as the surrounding medium, in order to simulate the interaction of nanoparticles with the cavity and to study the efficiency of the cavity for optical trapping.

5. 2 Design of 1D PhC dielectric cavity

For the design of the mirror section of the 1D PhC dielectric cavity a fixed period and radius has been considered, equal to Λ = 390 nm and r = 130 nm, respectively, in order to obtain a large photonic bandgap that includes the wavelength of 1550 nm. The number of the mirror holes N affects the cavity performance; a large number provides a stronger mirror strength. The presence of the tapering section destroys the translational symmetry in the photonic crystal, so obtaining a resonance condition in the photonic bandgap, which is a function of the properties of the tapered holes.

The key parameter considered to optimize the cavity performance is the filling fraction $FF_i = \pi r_i^2/(W \cdot \Lambda_i)$. Different tapering approaches have been investigated, by assuming a fixed value, linear or quadratic increase of the FF_i from the cavity to the mirror. The best cavity performance has been calculated with a linear increase of both FF_i and Λ_i, corresponding to a quadratic increase of the holes' radii r_i. In fact, this tapering approach allows to obtain a Gaussian attenuation profile of $|E|^2$, so optimizing the matching condition between the guided mode in the nanowire and the Bloch mode in the photonic crystal structure, with a consequent decrease of the optical loss and an enhancement of the resonance transmission.

A parametric analysis was carried out to define the set of value of r_i, Λ_i, N and N_t to optimize the cavity performance, obtaining a high resonance transmission $T > 90\%$, with a Q-factor at least of few thousands and strong energy confinement in the cavity, aiming at obtaining strong energy confinement necessary for the vertical coupling to the bowtie. We have calculated the influence of r_i and Λ_i on the cavity performance, assuming for the former parameter a minimum value of r_1 = 60 nm, imposed by the fabrication tolerances, while for the latter one, the minimum value of Λ_1 is 300 nm. A smaller period has not been investigated, because the distance between the central holes becomes too narrow (< 200 nm), so making the deposition of the bowtie above the PhC cavity more challenging during the fabrication process.

The cavity performance, in terms of Q-factor, resonance transmission T, Q/V and resonance wavelength, have been calculated by 3D FEM simulations as a function of different value of r_1 and Λ_1 (see Fig. 5.2). Any change in the set of values (r_1, Λ_1)

corresponds to different values of the whole set of r_i and Λ_i, according to the specific tapering approach previously described. For instance, a choice of (r_1, Λ_1) = (70 nm, 320 nm) corresponds to r_2 = 84 nm, r_3 = 96 nm, r_4 = 108 nm, r_5 = 119 nm and Λ_2 = 334 nm, Λ_3 = 348 nm, Λ_4 = 362 nm, Λ_5 = 376 nm, by assuming a number of tapered holes N_t = 5. We have assumed the cavity excited by a fundamental TE mode. The dispersion properties of materials has been taken into account (e.g. n_{Si} = 3.478 and n_{SiO2} = 1.444, respectively, at λ = 1550 nm). The water absorption has been also used in the model, so considering also the imaginary part of the refractive index of water (e.g. n_{H20} = 1.318 and k_{H20} = 9×10^{-5} at λ = 1550 nm).

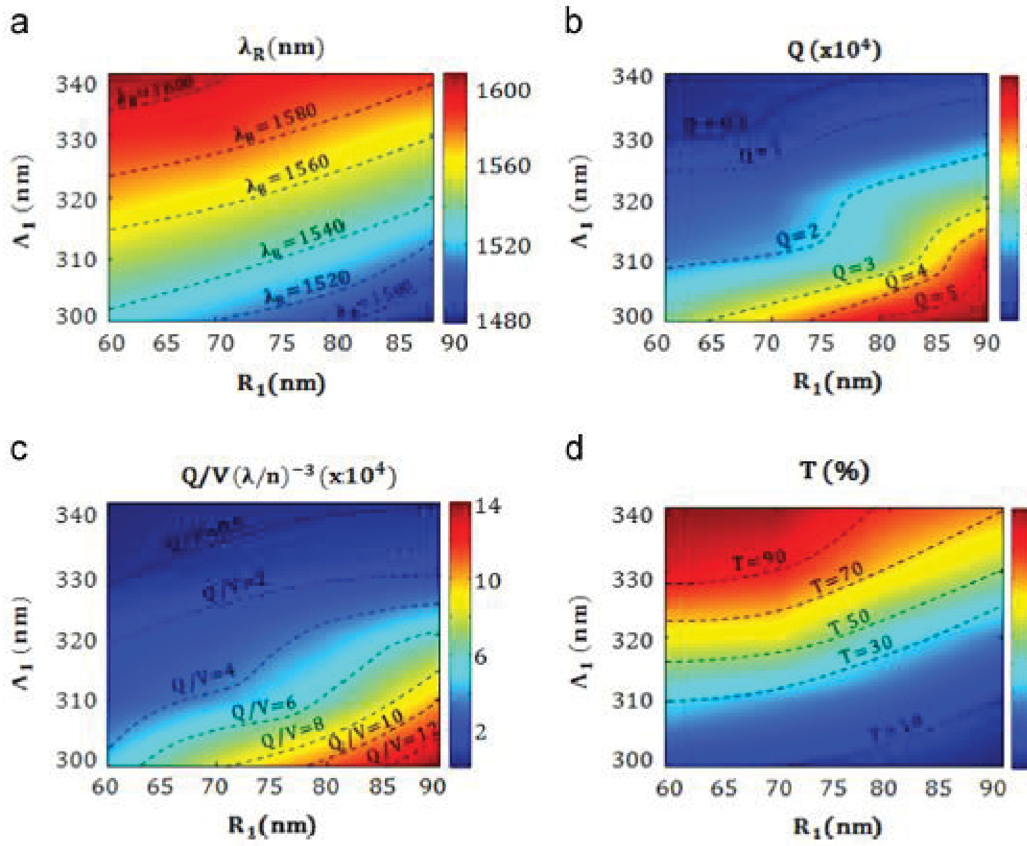

Fig. 5.2. (a) Resonance wavelength, (b) Q-factor, (c) Q/V ratio and resonance transmission as a function of the couple (R1, Λ1) with N_t = 5.

A significant improvement of the Q-factor has been observed by increasing the size of r_1 and Λ_1, as shown in Fig. 5.2. For example, with r_1 = 90 nm and Λ_1 = 300 nm and N_t = 5, a Q-factor > 5×10^4 has been calculated, corresponding to Q/V = 1.2×10^4 $(\lambda/n)^{-3}$. This condition has been obtained at the expense of very low values of resonance transmission (T < 10%), which is not suitable for the integration of the PhC dielectric cavity in the hybrid configuration, because the bowtie causes strong optical loss. On the contrary, high values of resonance transmission (T > 90 %) can be obtained in the opposite situation, with small values of r_1 and large period Λ_1, but unfortunately this corresponds to lower values of Q-factor. A resonance transmission T ~ 93 % has been calculated with r_1 = 60 nm and Λ_1 = 340 nm, but the Q-factor is lower than 10^3, corresponding to Q/V = 2×10^3 $(\lambda/n)^{-3}$. So, even if the requirement of the resonance transmission (T> 90%) is satisfied, this pattern is not suitable for the design of the hybrid cavity, because the Q/V is very low and not suitable to exert high optical forces.

Another critical requirement is the resonance wavelength, because a resonance condition close to 1550 nm for the design. Those cases discussed before correspond to a shift of resonance condition of about 50 nm from the target point, which make those patterns unsuitable.

As shown in Fig. 5.2, a resonance condition close to 1550 nm is obtained with a cavity pattern that provides a resonance transmission not higher than 60%. A similar result demonstrates that a different configuration should be assumed to satisfy all requirements for the dielectric cavity.

In particular, a different number of holes in the cavity has been taken into account in 3D FEM simulations to realize their effective influence on the cavity performance.

The first case deals with the simulation of the PhC cavity with a different value of the mirror holes ranging from $N = 3$ to $N = 9$, keeping fixed the number of the tapered holes at $N_t = 5$, $r_1 = 70$ nm and $\Lambda_1 = 330$ nm.

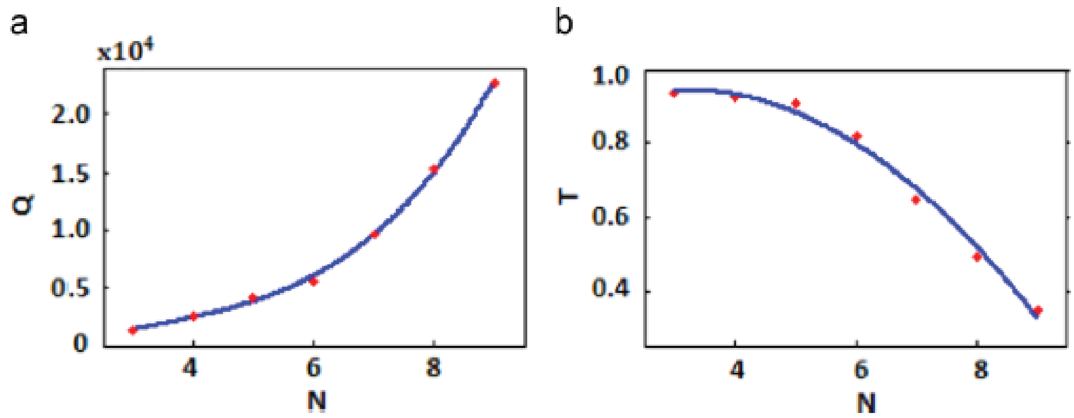

Fig. 5.3. (a) Q-factor and (b) resonance transmission behaviour as a function of N with $N_t = 5$, $r_1 = 70$ nm and $\Lambda_1 = 330$ nm.

As shown in Fig. 5.3, the Q-factor increases as N increases, due to a stronger effect of the PhC cavity realized with more periods, as typically observed with a simple 1D Bragg grating device. Therefore, an increase more than one order of magnitude from $Q = 2x10^3$ with $N = 3$ to $Q = 2.3x10^4$ with $N = 9$ has been calculated. However, the resonance transmission also decreases from T = 90% to T = 35% by ranging the number of the mirror holes in that range. The resonance transmission is kept almost constant up to $N = 5$ and then decreases quickly for higher values of N.

A similar behaviour has been also observed by changing the number of the tapered holes N_t, as shown in Fig. 5.4.

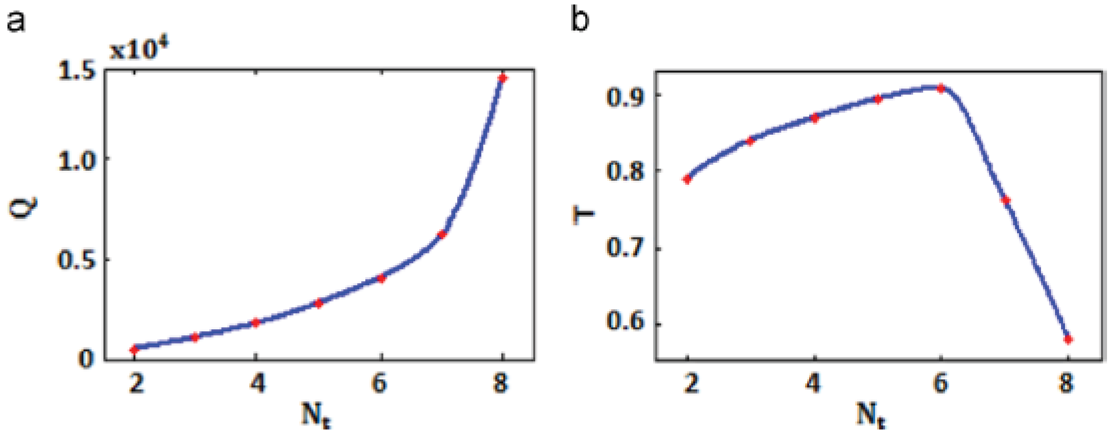

Fig. 5.4. (a) Q-factor and (b) resonance transmission behaviour as a function of N_t, by assuming $N = 5$, $r_1 = 70$ nm and $\Lambda_1 = 330$ nm.

An increase of the Q-factor is obtained with a large number of the tapered holes, with a faster behaviour than that observed with an increase of mirror holes. It can be explained by a better mode matching between the guided mode in the nanowire and the Bloch mode in the cavity. However, a relevant decrease of the resonant transmission is calculated with high values of N_t, providing T < 60% with $N_t = 8$.

In both cases, the results by 3D FEM simulations have demonstrated that is necessary to consider a limited number of the holes in the cavity to provide T > 90%, but at the expense of a decrease of the Q-factor. Therefore, different configurations of the holes' pattern have been investigated, in order to optimize the cavity performance.

An important advantage of the proposed configuration is related to the mode distribution in the cavity at the resonance condition, shown in Fig. 5.5.

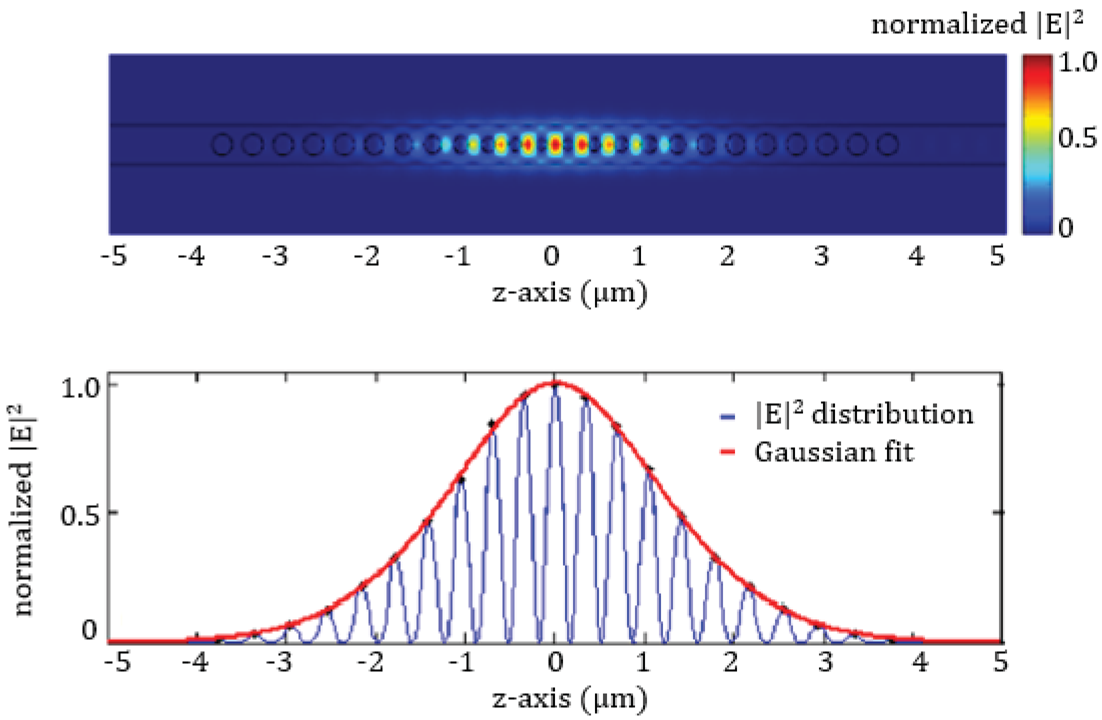

Fig. 5.5. Gaussian distribution of the energy confined in the PhC dielectric cavity at resonance.

It is evident the Gaussian distribution of the resonant mode in the cavity. Such condition corresponds to the best matching between the guided mode in the nanowire and the cavity mode, so minimizing optical loss with a consequent optimization of the resonance transmission. This demonstrates the high values of T calculated, also higher than 90% with Q-factor of few thousands. The maximum value of the energy distribution is in the middle of the cavity, exactly where the nanoantenna is placed in the hybrid configuration.

Another important parameter investigated for the design of the PhC structure is the cavity defect. The design assumed for the PhC cavity provides a resonant behaviour by tapering the holes' radii and periods, without any defect within the central holes. If we introduce a defect $d \neq 0$, an improvement of resonance transmission has been calculated, but with a relevant decrease of the Q-factor. This can be justified by the fact that the defect introduces a further phase shift in the cavity, so destroying the interference condition between the transmitted and reflected light. This corresponds to a lower mirror strength of the PhC with a higher transmitted component and weaker cavity effect, related to a lower value of Q-factor. In fact, a strong decrease of the energy peaks confined in the cavity have been calculated by increasing the defect *d*, so reducing the energy that can funnel into the bowtie with the hybrid configuration, so worsening the efficiency of the photonic/plasmonic cavity as nanotweezer (see Fig. 5.6).

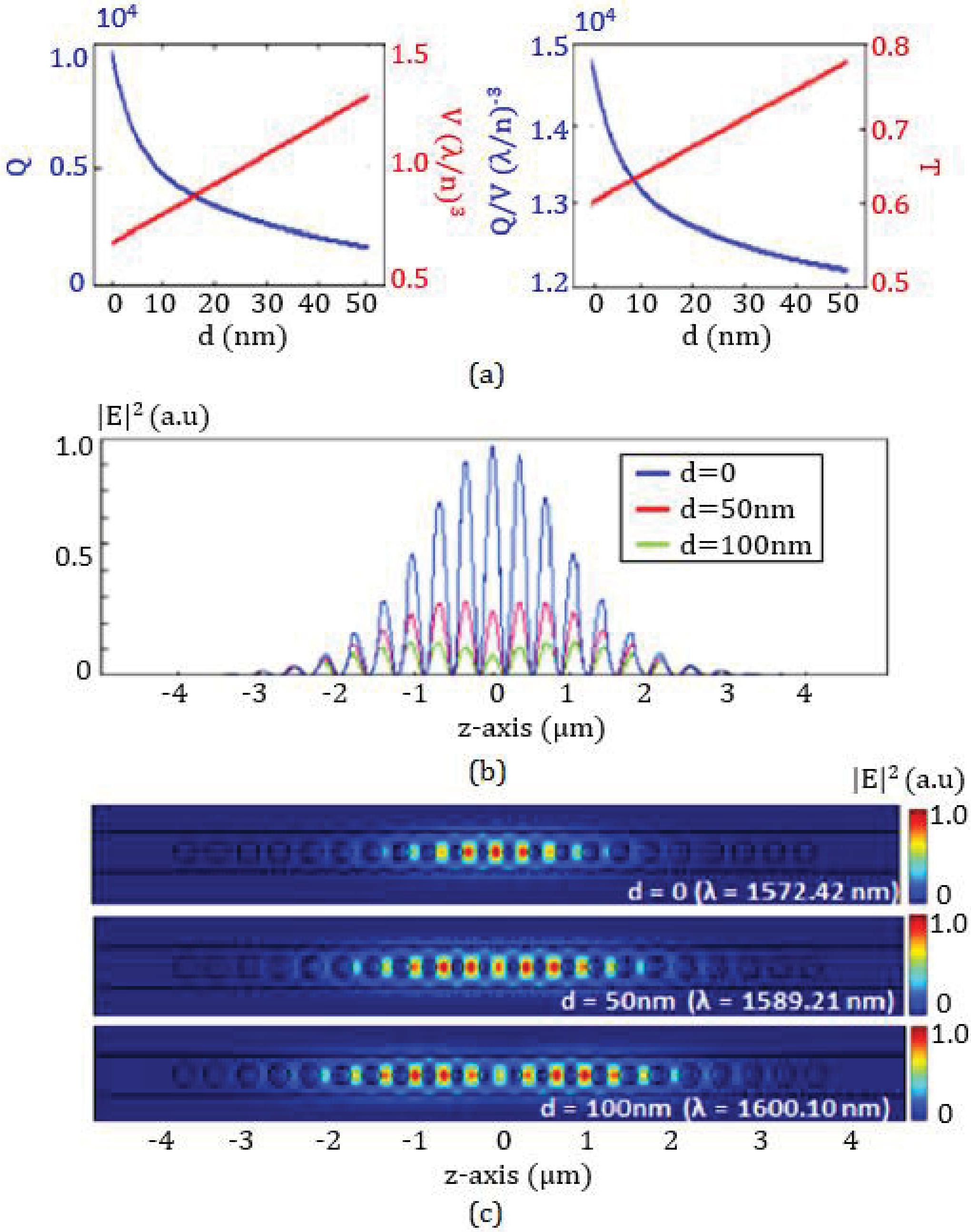

Fig. 5.6. (a) Cavity performance as a function of the defect cavity d. b)-(c) $|E|^2$ distribution in the cavity at resonance for a value of d equal to 0, 50nm, and 100nm normalized to the maximum $|E|^2$ peak (d=0 nm).

Therefore, the case $d = 0$ has been assumed as the best condition in terms of energy confinement and Q-factor, and a proper tapering approach has to be considered to keep high the resonance transmission, in order to prevent the strong effect of optical loss due to the presence of the nanoantenna in the hybrid configuration.

The width of the nanowire has been reduced from $W = 490$ nm to $W = 460$ nm to have a blue-shift in resonance without affecting optical loss. Furthermore, the number of the holes in the mirror and tapering sections has been reduced, in order to provide very-high values of the resonance transmission. In Fig. 5.7 the transmission spectrum of the cavity with $N = 3$ and $N_t = 3$ has been reported, assuming $r_1 = 90$ nm, $\Lambda_1 = 330$ nm, $r = 130$ nm and $\Lambda = 390$ nm with the same tapering approach discussed previously.

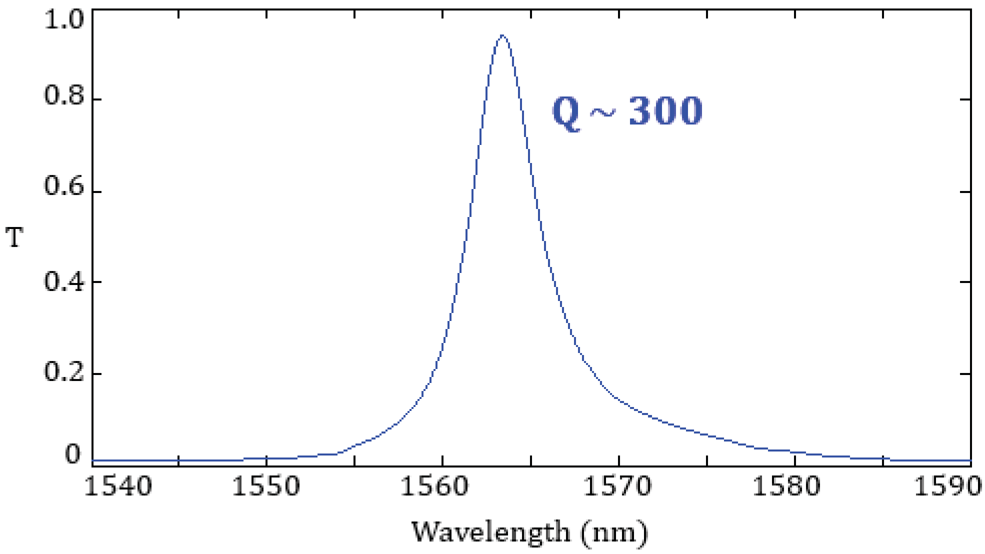

Fig. 5.7. Transmission spectrum of the PhC dielectric cavity with $N = N_t = 3$.

The cavity provides a resonance transmission T = 93% with a resonance condition λ ~ 1560 nm, very close to target value of 1550 nm. A relevant advantage obtained with this pattern is related to the energy confinement in the cavity, which is strongly focused in the middle of the cavity, as required for an efficient condition of the vertical coupling (see Fig. 5.8). Such confinement is also better than that obtained with $N_t = 7$, for which the conversion from the waveguide mode to the Bloch mode in the cavity happens slowly and this corresponds to higher values of Q-factor, but at the same time this results in a wider energy distribution also in the lateral sections of the cavity, so worsening the vertical coupling with the bowtie nanoantenna.

The PhC structure assumed with $N = N_t = 3$ provides Q = 3x10^2 and V = 0.7 $(\lambda/n)^3$, with Q/V = 4.3x10^2 $(\lambda/n)^{-3}$. Such performance confirms that, even if the condition of the resonance condition and the transmission value satisfy the requirements for the PhC cavity design, however, this pattern is unsuitable for using the device as optical nanotweezer, because the Q-factor, and therefore light-matter interaction, are too low.

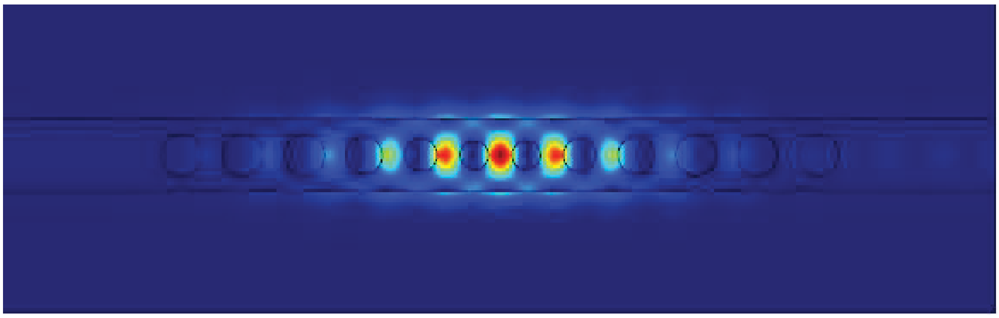

Fig. 5.8. Mode distribution at resonance condition in the PhC dielectric cavity with $N = N_t = 3$.

This issue has been overcome by assuming a different configuration of the PhC, simply introducing in the structure a symmetric tapering section at the output of the mirror holes. In this condition, the guided mode is slightly adapted to the Bloch mode in input and also slightly re-converted into the nanowire mode at the output of the cavity. This corresponds to lower optical loss together with an enhancement of the Q-factor, without affecting the resonance transmission. The configuration and performance of this PhC structure have been proposed in Fig. 5.9.

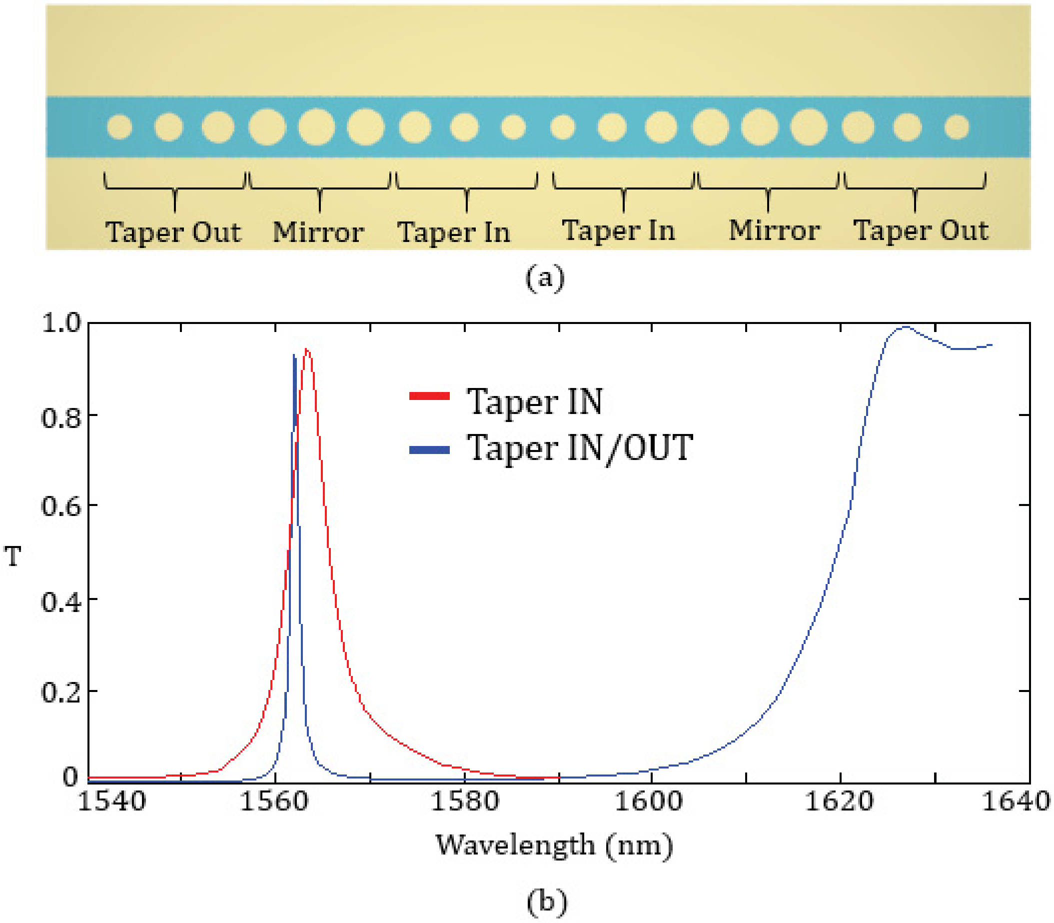

Fig. 5.9. (a) Configuration of the PhC cavity with input/output tapering sections with $N_t = 3$ and $N = 3$. (b) Transmission spectra of the PhC cavity with and without the output tapering section.

In Fig. 5.9b a comparison between the PhC with and without the tapering section at the output has been reported, in order to make evident the effective advantage of this new tapering pattern.

A Q-factor of 1.8×10^3 with a resonance transmission of 93% have been calculated with in/out symmetric tapering sections, confirming almost the same value of the resonance transmission and mode volume ($Q/V = 2.6 \times 10^3 (\lambda/n)^{-3}$). An improvement of the Q-factor by a factor six is obtained, compared to the cavity performance without the output tapering section.

A parametric analysis on the holes' radii and periods have been carried out by 3D FEM simulations, as already done previously with different values of N_t and N, obtaining a similar behaviour. Therefore, the best compromise in terms of the Q-factor, high resonance transmission and strong energy confinement has been assumed with $r_1 = 90$ nm, $\Lambda_1 = 330$ nm, $r = 130$ nm and $\Lambda = 390$ nm.

The Q-factor of 1.8×10^3 is suitable for the target application of trapping, because it is strong enough to prevent the evident effect of optical loss with the integration of the plasmonic nanoantenna, so obtaining remarkable values of light-matter interaction, as required for strong optical force. Furthermore, values of Q-factor that are too high make the control of the operating wavelength for the optical nanotweezer more difficult due to a shift in resonance during a trapping event, as described in detail in the next chapters. The design parameter of the 1D PhC cavity and its performance have been reported in Tab. 2.

Tab. 2. Parameters of the 1D PhC dielectric cavity and performance obtained by 3D FEM simulations.

Parameters	**Values**
N	3
N_t	3
r_1	90 nm
R	130 nm
Λ_1	330 nm
Λ	390 nm
D	0
G	130 nm
Performance	
λ_R	1562.01 nm
Q	1.8×10^3
T	93%
V	$0.7\ (\lambda/n)^3$
Q/V	$2.6\ \times 10^3\ (\lambda/n)^{-3}$

5. 3 Design of the bowtie nanoantenna

The configuration of the photonic/plasmonic cavity includes an Au bowtie nanoantenna vertically coupled to the PhC structure. The bowtie structure is realized by two triangular metal structure close to each other, in order to create a narrow gap in which the optical energy results strongly confined (see Fig. 5.10).

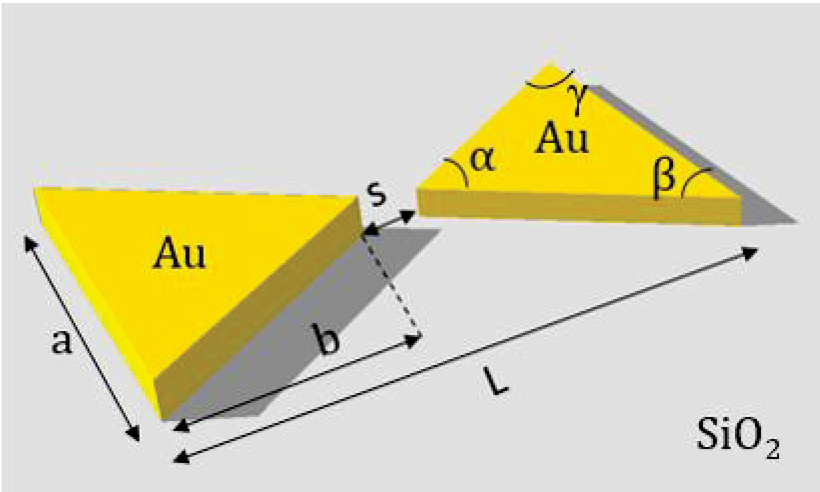

Fig. 5.10. Schematic of the bowtie nanoantenna used to realize the hydrid cavity.

The strong energy confinement is obtained because light propagating in the PhC faces a strong refractive index contrast in the region of the bowtie, exactly at the interfaces between gold and dielectric materials. The continuity of the normal component of the electric flux density D has to be verified ($\hat{n} \cdot (D_{diel} - D_{met}) = 0$), this corresponds to a strong light confinement in the material with the lower relative permittivity, which is the water surrounding medium within the bowtie slot in this particular configuration. This physical principle demonstrates the light funnelling from the PhC to the bowtie at the resonance condition. If the wavelength of light in input of the device does not match with the resonance condition, the PhC acts as a mirror and light is totally reflected, so the interaction with the bowtie is prevented. On the contrary, at resonance, light is focused between the central holes under the bowtie and this allows to funnel light to the nanoantenna. The coupling efficiency is improved if there is a resonance matching between both cavities. In fact, a longer interaction of light between the PhC and the bowtie is obtained in this condition and stronger energy values can be confined in the metal slot if the operating wavelength is the same of the resonance condition of the PhC and the bowtie.

The bowtie configuration has been chosen in place of a dipole one, because it provides a higher sensitivity. In fact, even if stronger energy peaks can be obtained by using the dipole structure realized by two rectangular strips, in this study a bowtie nanoantenna has been assumed because it affords a better localization of the optical energy inside the gap, with a weaker field confinement at the external edges compared to the dipole performance.

The size of each triangular structure and the gap slot s remarkably affect the bowtie performance (see Fig. 5.10). In particular, a thickness c = 30 nm has been considered, because thicker values cause stronger optical losses without any improvement in energy confinement. On the contrary, a thinner Au layer affects remarkably the energy confinement, so worsening the light trapping efficiency. The parameters a and b are the transversal and longitudinal directions of the bowtie compared to the direction of light propagation, as shown in Fig. 5.10. They affect the energy confinement and optical loss, but particularly the resonance condition.

The design of the hybrid cavity requires the matching between the resonance of PhC cavity and bowtie, in order to maximize the light funnelling into the nanoantenna. The bowtie size have been chosen to satisfy such requirement. Different configurations can be considered aiming at providing the resonance around 1550 nm, however the necessity of the alignment of the bowtie to the PhC structure, exactly between the central holes, limits the number of different patterns that can be investigated. In fact, it is necessary that the nanoantenna does not cover the PhC holes, in order to reduce optical loss. Fabrication tolerances have been also considered for the design of the nanoantenna. Small values of angles α, β or γ, which define the bowtie shape, are difficult to realize. The risk of not precious shape and round corners could affect the energy confinement in the bowtie, so limiting light trapping and limiting the trapping efficiency.

The minimum value of angle that we have assumed for the design of the bowtie in order to allow the fabrication with high reliability is at least of 45°.

Another important parameter that affects the resonance condition is the total length of the nanoantnenna *L* (see Fig. 5.10). We have assumed a value $L < 500$ nm, which corresponds almost to the width of the nanowire where the PhC is realized. This choice is due to the fact that larger values of the bowtie length cause higher optical loss, because the absorption and scattering are stronger in the structure when the bowtie is larger than the nanowire width.

Moreover, light confinement is strongly related to the slot size. A very narrow slot provides strong energy confinement, but also the optical loss becomes more relevant, so decreasing the detection resolution of the hybrid cavity. On the contrary, large values of s prevent the slot effect, so making useless the bowtie because only optical loss can be obtained without any energy enhancement as typically obtained with a nanoantenna. A slot s = 40 nm has been assumed as the best compromise in terms of energy confinement and optical loss. This corresponds to $b \sim 230$ nm, according to the design steps considered. Lower values of b are not suitable for the design, because it becomes too difficult to afford the requirement of the resonance at 1550 nm unless of using large values of the other parameter a, but at the expense of a more challenging fabrication process and also higher optical loss.

So, a gap value s = 40 nm and a transversal length b of each triangular structure of 220 nm have been considered for the design of the bowtie.

A parametric analysis on the parameter a has been carried out to define the geometry of the bowtie in order to satisfy the resonance condition close to 1550 nm, minimizing optical loss and simplifying the fabrication process.

The scheme of the system simulated by 3D FEM simulation to study the nanoantenna behaviour has been reported in Fig. 5.11.

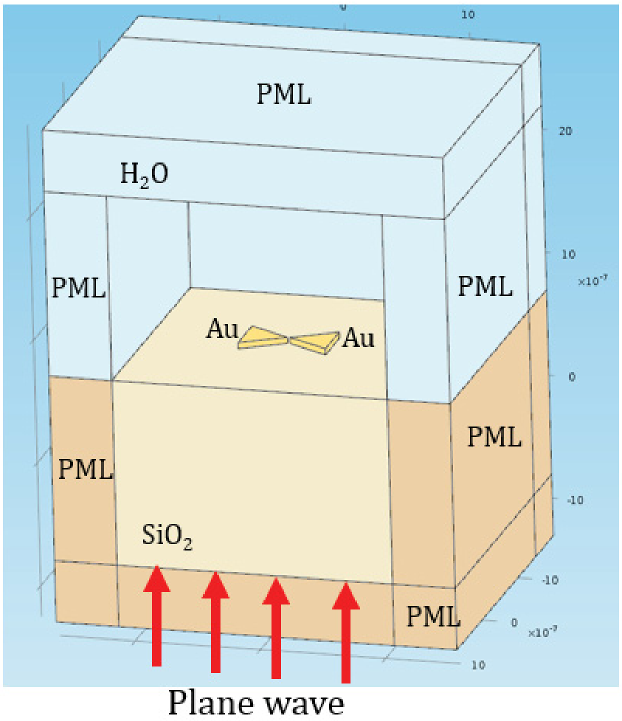

Fig. 5.11. Configuration assumed for FEM simulations of the bowtie nanoantenna.

We have assumed the bowtie nanoantenna placed on a silica substrate. An out-of-plane input condition has been considered with light directly focused from the bottom of the substrate, as in the configuration of the hybrid cavity where light is funnelled from the PhC. A plane-wave polarized along the principal axis of the bowtie has been assumed in input. The incident intensity in the computational domain is 700 mW/μm^2. The Perfect Matching Layer (PML) has been considered around the cavity, in order to prevent any effect of undesired reflections at the boundaries of the computational volume.

3D FEM simulations have been carried out to obtain the transmission spectrum of the bowtie. The Lorenz-Drude model has been used to simulate the optical properties of gold. In Tab. 3, the geometrical parameters of the bowtie assumed to obtain the best compromise in terms of resonance condition, strong energy confinement, reduced optical loss and high reliable fabrication process have been reported.

Tab. 3. Parameters value of the bowtie nanoantenna resonating at 1.5 μm.

Parameter	Value
a	350 nm
b	220nm
c	30 nm

Parameter	Value
s	40 nm
α	77°
β = *γ*	52°

The bowtie transmission spectrum has been reported in Fig. 5.12.

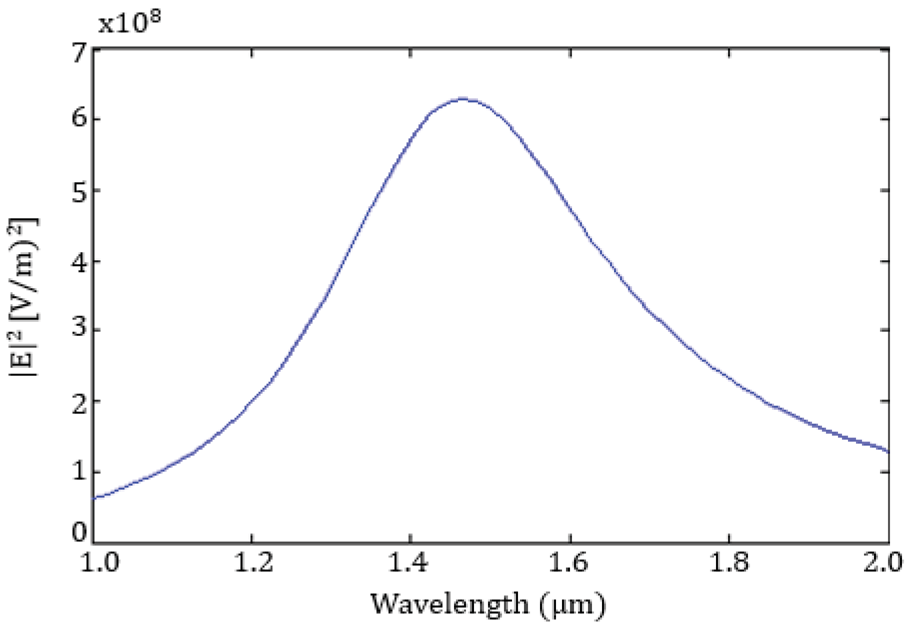

Fig. 5.12. Energy enhancement in the plasmonic bowtie nanoantenna.

A strong enhancement of the energy confinement in the bowtie has been observed at resonance compared to the values calculated far from the resonance, confirmed by the low value of the mode volume $V = 5x10^{-4} (\lambda/n)^{-3}$ and corresponding to $Q/V \sim 10^4(\lambda/n)^{-3}$. As discussed before, the resonance matching of both cavities allows the optimization of light-matter interaction. The maximum enhancement of the energy confinement in the bowtie with this configuration has been calculated at around $\lambda = 1500$ nm with a good matching with the PhC resonance condition, so allowing a high coupling efficiency, because the Q-factor of the bowtie is only $Q < 10$ with a FWHM ~ 400 nm. This corresponds to a decrease of the energy enhancement smaller than 5% compared to the maximum value obtained at around 1550 nm.

5.4 Design of the photonic/plasmonic cavity

The single configurations of the PhC cavity and the bowtie nanoantenna have been designed to optimize the performance and their interaction. In this section, the integration of both cavities in the same device has been considered in order to realize the photonic/plasmonic cavity.

As discussed in the previous section, the PhC cavity has been totally embedded in silica. The silica thickness G above the nanowire defines the distance between the PhC and the bowtie. The value of G strongly affects the optical loss and the coupling efficiency. The maximum coupling efficiency can be obtained if the bowtie is placed directly on the PhC, which corresponds to $G = 0$. However, a remarkable drop of the resonance transmission more than 90% is obtained with this pattern, which makes useless the cavity because of the unacceptable detection resolution.

The resonance transmission increases as the gap *G* becomes larger, however the maximum value of the energy confined strongly decreases. This behavior corresponds to higher values of the Q-factor, due to a decrease of losses, together with a more relevant enhancement of the mode volume, resulting in a decrease of the Q/V with a worsening of light-matter interaction in the cavity. Therefore, an optimal value of *G* should be calculated to reach a compromise between the resonance transmission and light-matter interaction for the design of the photonic/plasmonic cavity.

We have considered a configuration of the hybrid cavity that should provide at least $T \geq 20\%$, in order to obtain a good detection resolution with a strong advantage respect to the simple plasmonic nanoantenna.

The evanescent field in the PhC cavity extend about 150 nm. Therefore, the fast increase of the resonance transmission from that value is justified by the fact that there is not a strong interaction between the PhC and the bowtie anymore. On the contrary, for values of gap $G < 150$ nm the optical energy can be funnelled and the effect becomes stronger as the gap decreases, corresponding to an improvement of the Q/V (the mode volume decreases faster than the Q-factor), but the resonance transmission is very low ($T < 10\%$) for $G < 100$ nm. We have calculated that $G = 130$ nm is the gap value for which the condition $T > 20\%$ is satisfied. In particular, $T = 26\%$ has been obtained with $Q = 9.5 \times 10^2$ and a resonance condition at 1563 nm, with a red-shift of about 1 nm from the value obtained with the PhC dielectric cavity, due to a higher value of the effective index for the presence of the Au bowtie. The cavity performance are shown in Fig. 5.13.

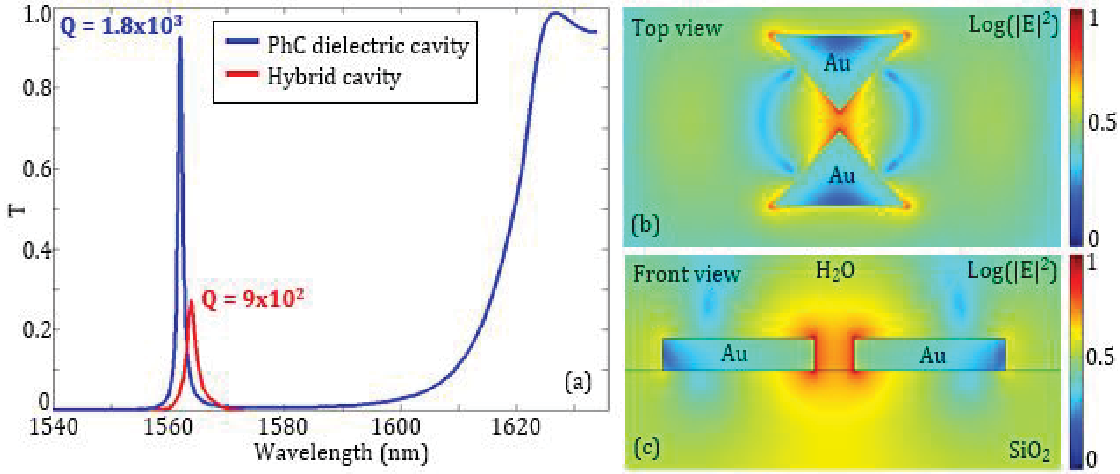

Fig. 5.13. Transmission spectrum of the 1D PhC dielectric cavity (blue curve) and hybrid cavity (red curve); (b) top view and (c) cross-section of the hybrid cavity at resonance.

For the hybrid cavity, Q only drops by a factor 2 compared to the PhC cavity (Q = $9x10^2$); the transmission drops by a factor 3.6 up to T = 26 %, as shown in Fig. 5.13. The mode volume remains almost unaltered to that of the single nanoantenna, exactly we calculate V = $6x10^{-4}$ $(\lambda/n)^3$. This results in a remarkably high Q/V = 1.5 $x10^6$ $(\lambda/n)^{-3}$ and energy confinement in the bowtie. The strong optical gradient in the bowtie gap, as shown in Fig. 5.13b and Fig. 5.13c, confirms the efficient energy transfer from the PhC to the bowtie. In addition to strong light-matter interaction, the high detection resolution obtained (T = 26%) makes the hybrid cavity very suitable for optical trapping applications.

The performance of the hybrid cavity are much better than the single PhC dielectric structure and the single bowtie, so demonstrating the relevant advantages obtained if we put the two together.

The position of the bowtie nanoantenna and its separation from the PhC structure strongly affect the performance of the hybrid cavity. A misalignment of the nanoantenna by about 100 nm along any direction increases the on-resonance transmission and the Q-factor, but it reduces the energy confined in the hotspot, so worsening the bowtie effect. A larger misalignement prevents the energy coupling from the PhC to the bowtie, so obtaining only higher optical loss in this case, without any improvement of light-matter interaction.

In simulation, the cavity behavior in presence of a misalignment between the bowtie and the PhC has been calculated. In fact, a relevant drop of the coupling efficiency is obtained when the nanoantenna is not exactly in the middle of the cavity above the central holes. 3D FEM simulations have demonstrated that $Q/V > 10^5 (\lambda/n)^{-3}$, assumed as the condition of strong light-matter interaction, have been obtained with a maximum misalignement of the bowtie of ± 50 nm in both longitudinal and transversal directions. Furthermore, if the misalignment is along long-axis of the PhC, in addition to the relevant increase of mode volume, also a drop in transmission is calculated because the metal is placed above the holes, so strongly affecting optical losses in the cavity.

The energy confinement in the bowtie also depends on the gap with s. When s decreases from s = 60 nm to s=40 nm, the resonance transmission and the Q-factor decrease slightly, but the energy density in the bowtie goes up, which is also reflected by a decrease in the Q/V of about 20% with s = 60 nm (Q/V = 1.2×10^6 $(\lambda/n)^{-3}$), compared to results obtained with s = 40 nm.

The very high confinement of the optical energy at the metal tips makes the cavity very sensitive to the pattern of the metal structure, and particularly to the sharpness of the tips. We also evaluated the cavity performance with rounded corners of the metal bowtie, as shown in Fig. 5.14. A relevant increase of the mode volume is achieved by increasing the radius r of the rounded corners, leading to a decrease in the Q/V ratio. A Q/V > 10^5 $(\lambda/n)^{-3}$ has been calculated with rounded tips of 10 nm, which is a typical value that can be obtained by the conventional fabrication steps, so confirming strong light-matter interaction also with a realistic configuration of the bowtie.

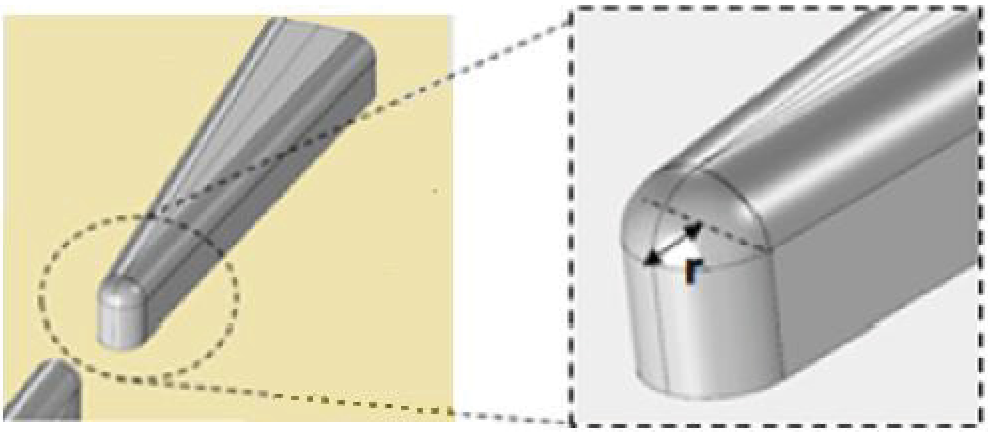

Fig. 5.14. Configuration of the bowtie in the photonic/plasmonic cavity with rounded tips.

Chapter 6. Fabrication and optical characterization of the hybrid cavity

6.1 Device fabrication

The fabrication of the photonic/plasmonic cavity has been discussed in this section. The experimental activity has been carried out at Photonics Group of University of York.

A Silicon-on-Insulator (SOI) wafer with 220 nm silicon layer on 3 μm thick buried oxide has been used to realize the PhC dielectric cavity.

All fabrication steps of the hybrid cavity have been reported in Fig. 6.1.

Fig. 6.1. Fabrication process of the optofluidic chip with the integration of the hybrid cavity in a PDMS microchannel.

The spin coating of the positive e-beam resist AR-P 6200.13 on SOI wafer at 5000 rpm and baking on the hot plate at 180°C for 5 min have been done to obtain a final resist thickness of 350 nm (Fig. 6.1a).

The pattern of the PhC dielectric cavity has been defined by using Electron-beam lithography with a RAITH "Voyager" system. In our own recipe, an electron dose of 130 $\mu C/mm^2$ with a current of 300 pA has been assumed for the exposure of the AR-P resist. Then, the resist is developed for 2 min by xylene (Fig. 6.1b).

The PhC dielectric structure is obtained by Reactive Ion Etching (RIE) with a gas mixture of CHF3:SF6 with a flow of 14.5 sccm and 12.5 sccm, respectively (Fig. 6.1c).

SEM pictures of a PhC dielectric cavity with an input/output tapering section have been reported in Fig. 6.2.

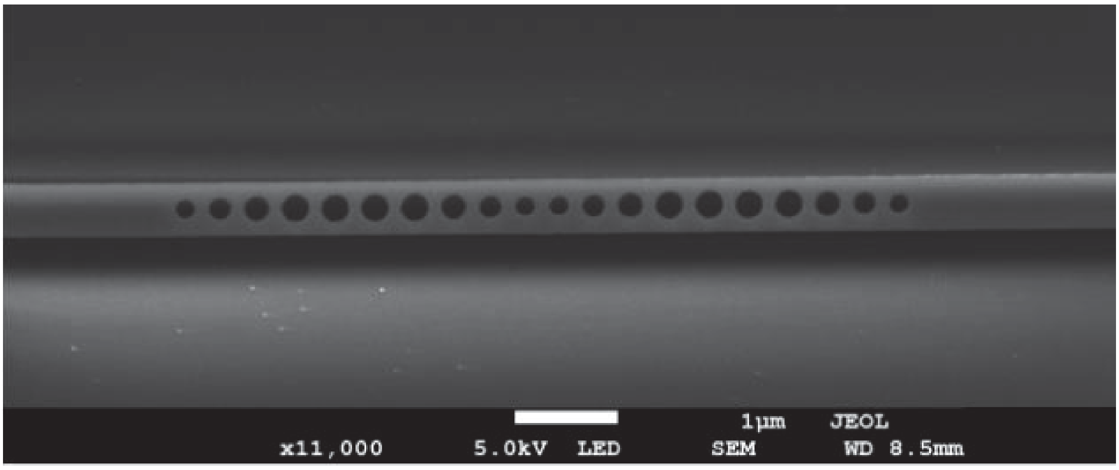

Fig. 6.2. SEM picture of the PhC dielectric cavity with input/output tapering section

As described in the previous sections, the PhC structure is totally embedded in a silica layer. In order to simplify the fabrication process, Flowable oxide (FOx) at liquid phase is spin coated above the sample with the PhC cavity at 2200 rpm and then baked for 60 min at 400°C, in order to obtain a silica layer at solid state. The high temperature necessary to embed the cavity in a silica layer, requires a ramping temperature to prevent any mechanical stress that can affect the quality of the silica and, therefore, the efficiency of the process. So, an initial temperature of T = 100 °C is considered as the initial point and a rate of 4 °C/min is assumed to reach the end-point of 400 °C with 90 min for the ramping process (Fig. 6.1d).

The bowtie nanoantenna is then realized and the positive layer PMMA (polymethyl methacrylate) has been used for high resolution e-beam exposure. A first layer of PMMA 495K (6% in anisole) is spin coated at 5000 rpm and baked at 180°C for 5 min, obtaining a thickness of 250 nm. Then a second layer of PMMA 950K (6% in anisole) diluited 1:1 with xylene is spin coated on the first resist layer at 5000 rpm for 5 min, corresponding to a thickness of 150 nm (Fig. 6.1e). A total PMMA thickness of 400 nm is obtained. The choice of using two different chemical compositions of PMMA is very advantageous for the resolution of the final pattern of the nanoantenna, because a reverse T-shape can be obtained by using these PMMA with different molecular weight resins (495K and 950K), due to a different behaviour to the development (higher molecular weight corresponds to a fast resist remotion during the development process).

The pattern of the nanoantenna is defined by e-beam exposure of the PMMA layers, by using an electron dose of 480 $\mu C/mm^2$ with a current I = 80 pA. The resist development is done in a solution of 1:3 MIBK to IPA , which corresponds to the maximum resolution with high sensitivity, so requiring a development time of 3 min. A typical result of the development step is that shown in Fig. 6.1f. The reverse T-shape is very useful to obtain a high-resolution nanoantenna pattern, because it improves the lift-off process for the resist removal after the metal deposition.

The thermal evaporation is used to realize the bowtie structure. In particular, 3 nm Ni adhesion layer and then 30 nm Au layer are evaporated on the silica layer (Cr or Ti could be used as adhesion layer, confirming high affinity and efficiency for the adhesion of Au to the bottom silica layer, and also decreasing optical losses), as shown in Fig. 6.1g. PMMA removal is obtained with lift-off process, by soaking the sample in acetone for 30 min and then rinsed in deionized H_2O. It is evident the advantage of a reverse T-shape of the bilayers PMMA structure. The evaporation of metals with a total thickness of about 33 nm (Ni+Au) is much thinner than the first PMMA layer of 250 nm. This prevents the direct contact of metals to the upper PMMA layer, so minimizing issues during the PMMA removal, which becomes more critical with a single layer of PMMA. A comparison between the fabrication of the bowtie nanoantenna with a pattern defined by e-beam lithography on a single or two layers of PMMA has been reported in Fig. 6.3. The quality of the metal surface is much better by using the recipe proposed in this study with a reverse T-shape of the PMMA, rather than the results obtained with a single layer of PMMA, for which some residuals is typically observed after the lift-off process, particularly in small gap and at the edges of the metal structures.

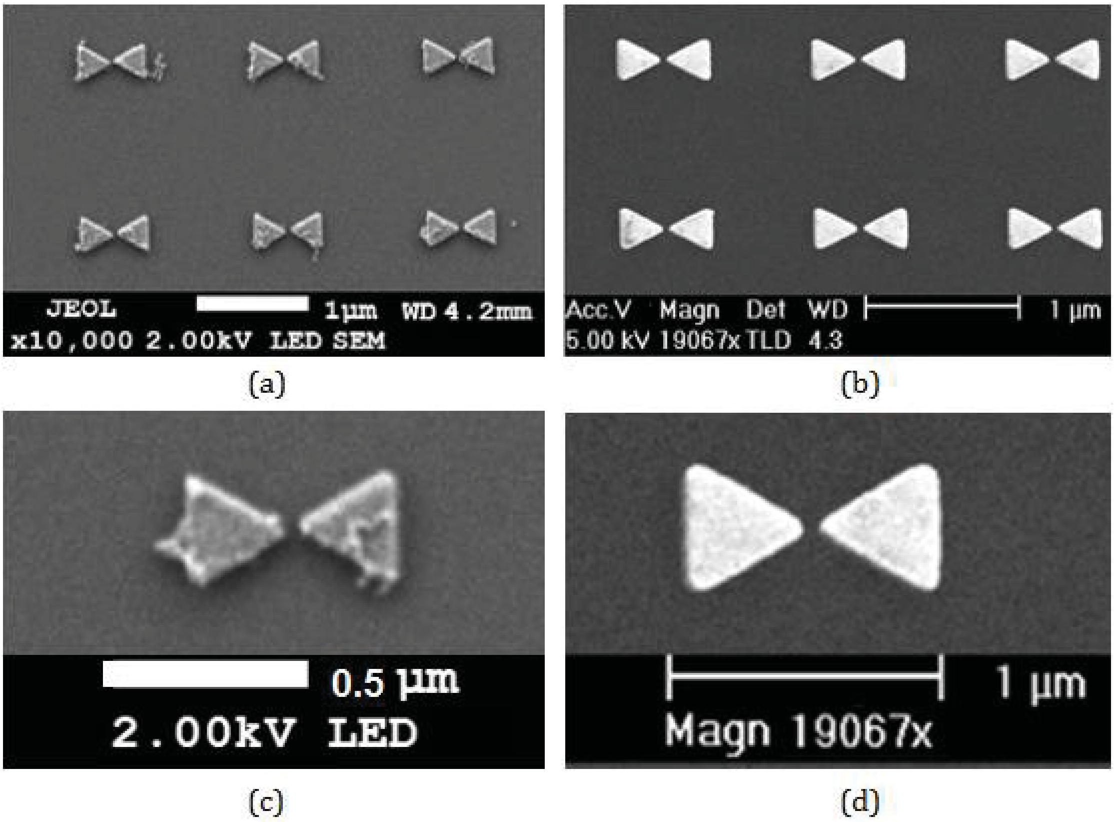

Fig. 6.3. SEM pictures of an array of bowtie nanoantennna obtained with an e-beam exposure of (a) single layer and (b) dual layer of PMMA resist. In (c) and (d) the magnification of the single bowtie for both cases has been reported.

The alignment between the PhC cavity and the bowtie is the most critical issue in the device fabrication, because a position of the nanoantenna exactly above the central holes is necessary to improve light coupling with the bowtie. Some markers have been used during the first exposure to align the bowtie to the PhC during the PMMA exposure. High accuracy has been obtained for the bowtie alignment to the PhC with a maximum misalignment of few tens nanometers, A SEM picture of the final photonic/plasmonic cavity has been reported in Fig. 6.4.

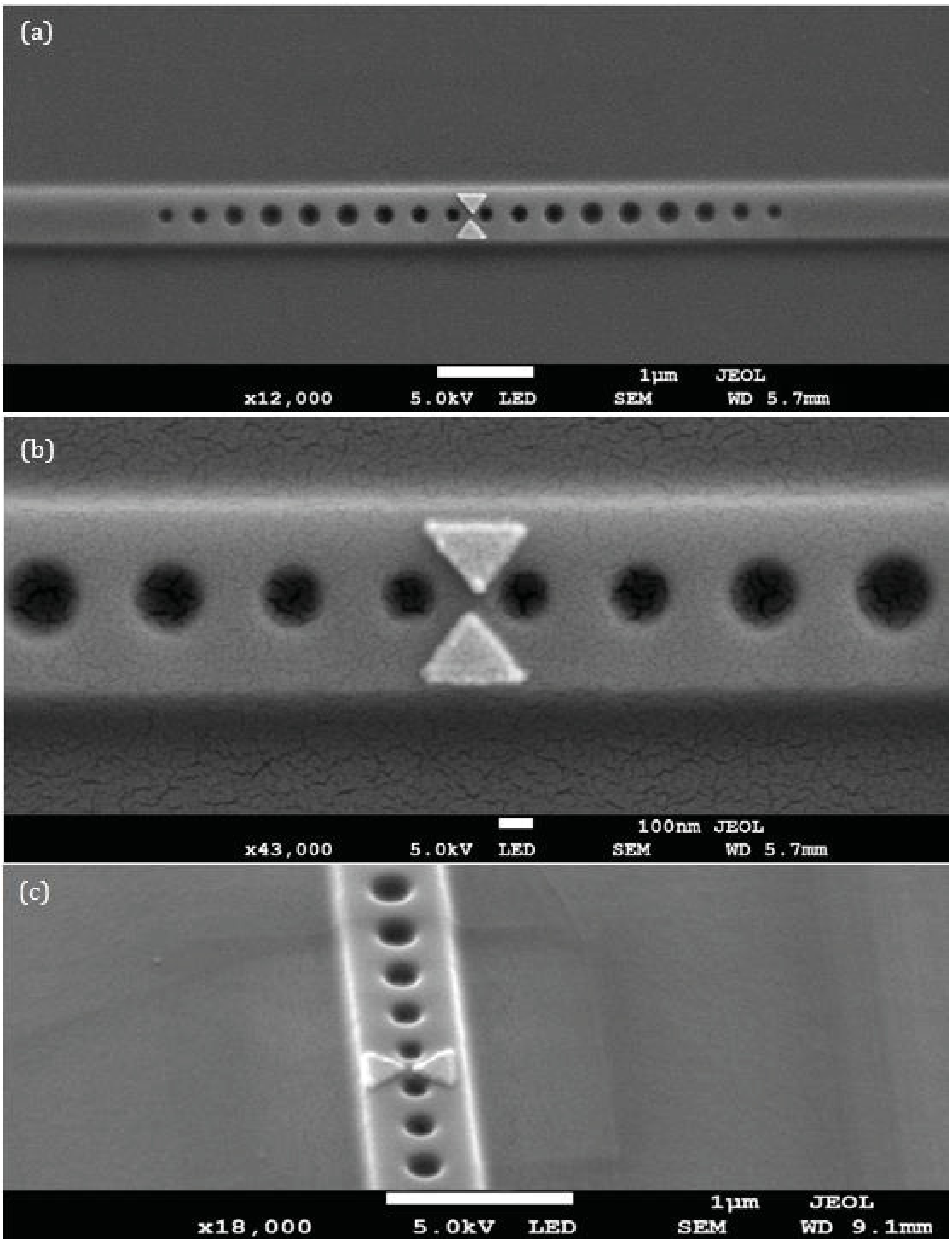

Fig. 6.4 (a) SEM picture of the photonic/plasmonic device with the bowtie nanoantenna placed on the PhC cavity, with (b) a magnification of the coupling region where the bowtie is aligned to the central holes of the PhC. (c) Top view of the hybrid cavity.

The accuracy of the thickness of the gold layer deposited on the PhC cavity has been previously verified by using a homemade ellipsometer, and its Graphical User Interface (GUI) has been reported in Fig. 6.5.

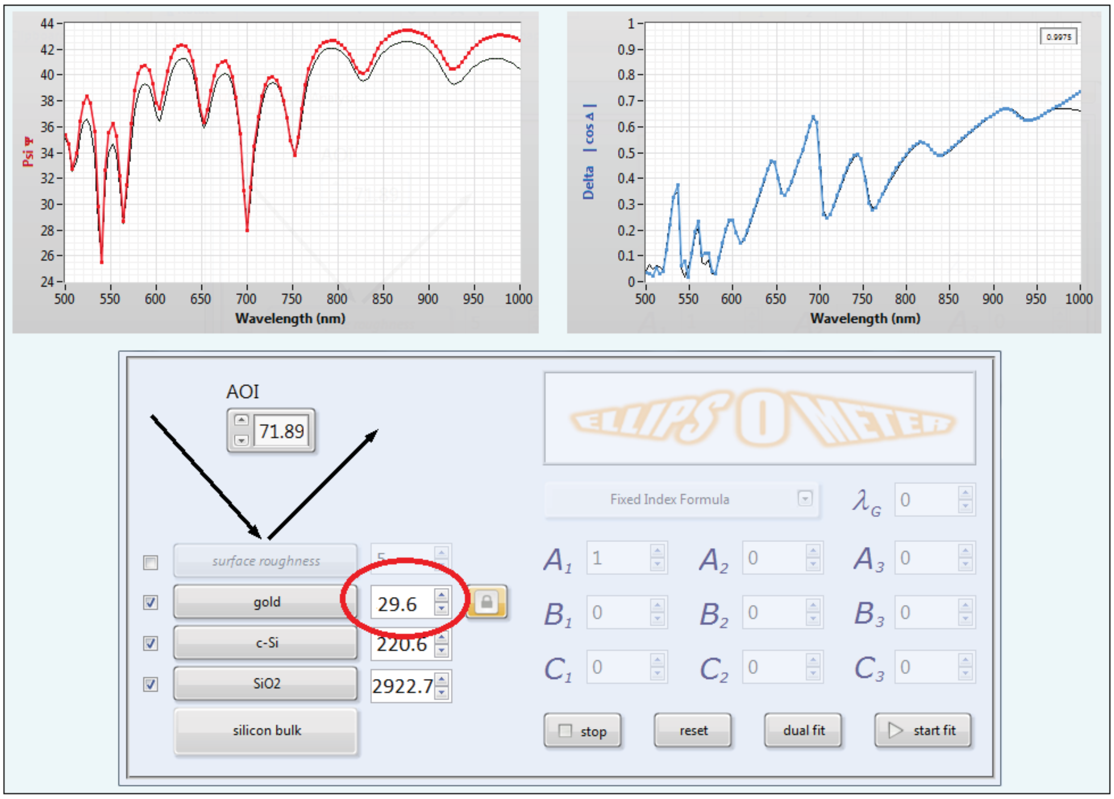

Fig. 6.5. GUI of the software of the ellipsometer used for measurements of the Au thickness.

The Au thickness has been also confirmed by using AFM method, which has been also used to evaluate the gold surface flatness, in order to control the bowtie resonance behavior.

The hybrid cavity has been integrated in a microfluidic chip to obtain a surrounding medium in water for the cavity, which is necessary for devices used for optical trapping applications to control the particles' motion around the trapping site.

The microfluidic channel has been realized in PDMS (Polydimethylsiloxane) with a rectangular section with a thickness of 10 µm and a width of 200 µm.

The fabrication steps have been reported in Fig. 6.6.

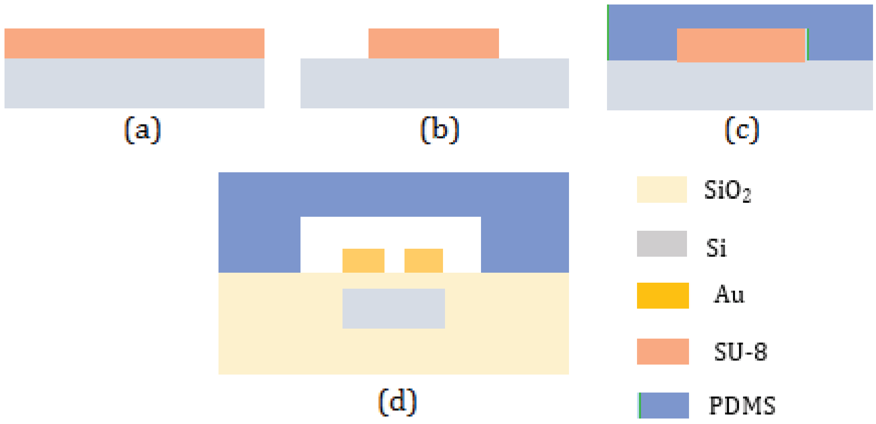

Fig. 6.6 (a-d) Fabrication process of the microfluidic channel used to integrate the hybrid cavity to realize the optofluidic chip.

We have spin coated the negative resist SU-8 (with a mixture of SU-8 2000.5:SU-8 2050 = 1:2) on a silicon substrate and baked at 95 °C for 10 min with an initial and final temperature of 65 °C for 2 min, to prevent undesired stress to the structure, for the realization of the mould for the microchannel. The final thickness of the resist is 10 µm. A third e-beam exposure has been done to define the pattern of the microchannel in the SU-8 (photolithography could be also used due to the large size of the channel). The dose used is 4 µC/mm^2 and the current I =200pA, after the resist has been developed for 3 min, aiming at defining the pattern of the microchannel (200 µm x 10 µm) (Fig. 6.6b). An example of SU-8 mould on a silicon substrate with a rectangular shape of the microchannels has been reported in Fig. 6.7.

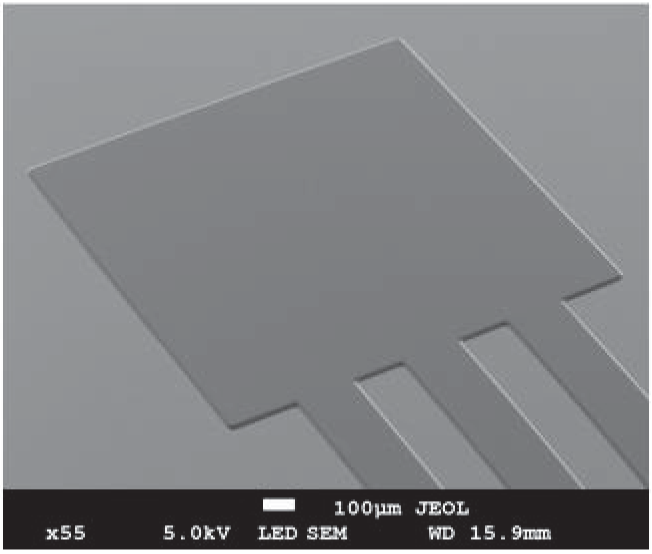

Fig. 6.7. SEM picture of a SU-8 mould on a silicon substrate

The following step is the PDMS deposition on Su-8 mould and after baking at 60°C for 3h (Fig. 6.6c). The PDMS is peeled off from the mould to realize the microchannel. Finally, the bonding between the chip with the hybrid cavity and the microfluidic channel is obtained by oxygen plasma (t = 20 s) (Fig. 6.6d), and the inlet and outlet sections are realized with a micropunch, so enabling the fluid flow inside the microchannel. In Fig. 6.8, a picture of the final optofluidic chip, with the integration of the photonic/plasmonic cavity in microfluidic channel, has been reported.

Fig. 6.8 Picture of the optofluidic chip with the hybrid cavities integrated in the same chip in a microfluidic channel with inlet/outlet section to allow the fluid flowing inside.

6.2 Optical setup

The optical setup used for the optical characterization of the hybrid cavities is shown in Fig. 6.9.

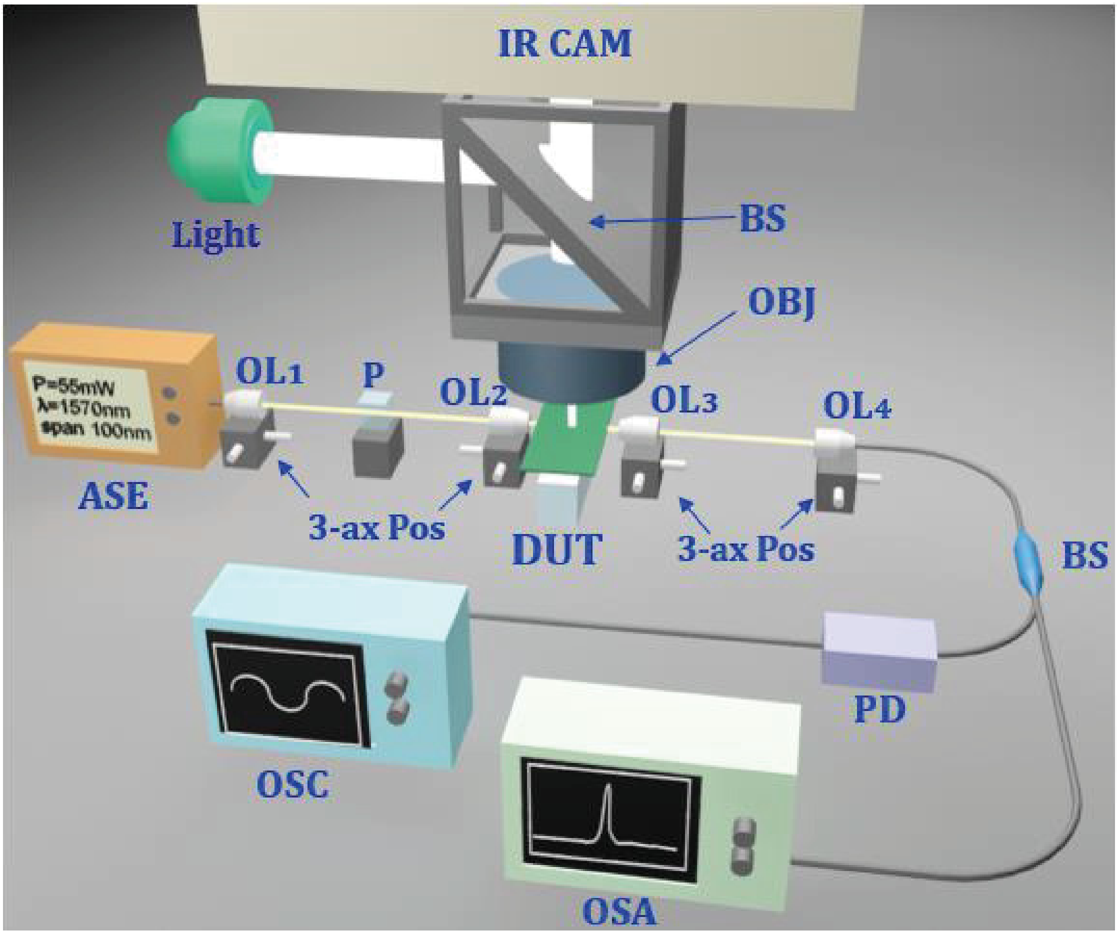

Fig. 6.9. Optical setup in end-fire technique used to characterize the hybrid cavity.

An "end-fire technique" has been considered to couple light in input and output of the device. An Amplified Spontaneous Emission (ASE) source has been used with a wavelength range from 1520 nm to 1620 nm with a scanning resolution of 40 pm and an optical power P ~ 55 mW. Light from ASE is fed to 16x optical lens (OL_1) and the collimated beam is delivered to a polarization beam splitter (P), where the TM polarized light is filtered out and the TE component is focused onto the input facet of the sample (DUT) by a 60x optical lens (OL_2). Then, at the output of the cavity light is collected by a 40x optical lens (OL_3).

An infrared camera (IR CAM) and a 20x objective (OBJ), placed above the sample, are used to visualize light propagating into the cavities, so facilitating the alignment between the input and output lenses with the device. Each optical lens is mounted on a three-axis stage (3-ax POS) to control the position of the lenses at the microscale for the alignment of the optical setup.

The collimated beam from OL_3 is then collected into an optical fiber by a 40x optical lens (OL_4). A fiber optical beam splitter (BS) is used to split light in an Optical Spectrum Analyser (OSA) to plot the transmission spectrum and in a photodetector (PD), directly connected to an oscilloscope (OSC), used to maximize the signal during the setup alignment.

The same optical setup has been used to characterize both PhC dielectric cavities and hybrid ones.

6.3. Experimental results

We have realized a simple nanowire and a PhC dielectric cavity without the bowtie in each optical chip, in addition to several hybrid cavities. This is useful because the spectra have been normalized to that of the nanowire, assumed as the reference point of maximum transmission, in order to evaluate the relative transmitted power at the output of each hybrid cavity.

For measurements, we have put deionized water (DI H_20) in the microchannel from the inlet and assumed a null flow. In Fig. 6.10, the experimental results of the PhC dielectric cavity have been reported, obtaining $Q = 1.7 x 10^3$ and resonance transmission T = 90%.

The good matching between the experimental results and 3D FEM simulations (Q = 1.8×10^3 and T = 93%) is evident. Furthermore, a high reliability has been also verified. This confirms the maturity of the fabrication process assumed for this configuration of PhC cavities, as discussed previously, which is necessary to realize several efficient nanotweezers in the same chip for the target application [238].

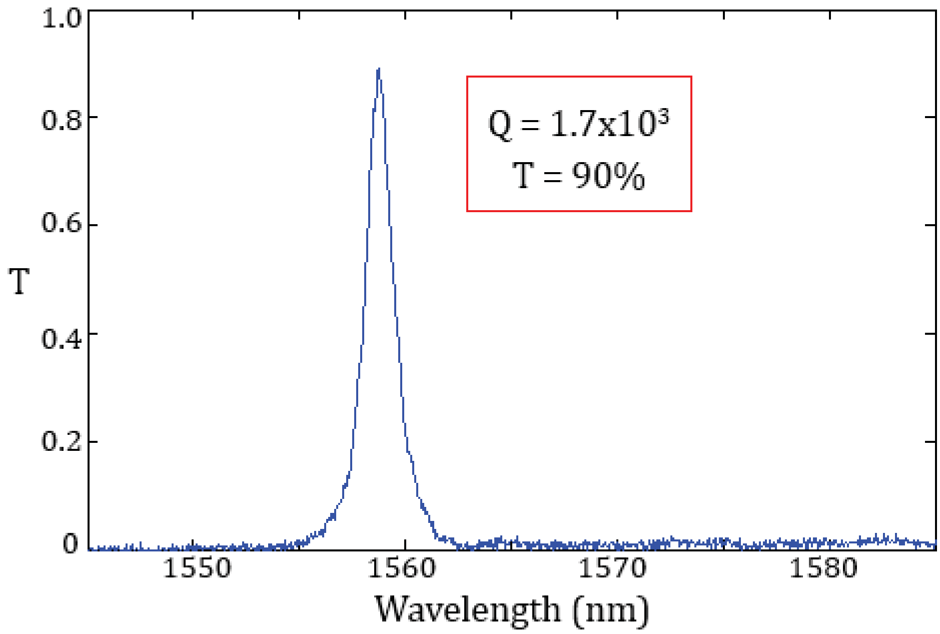

Fig. 6.10. Experimental transmission spectrum of the PhC dielectric cavity with $N = N_t = 3$.

The optical characterization of the hybrid cavity has been done with the same optical setup with in-plane light propagation in the cavity, so exploiting light coupling in input facet of the sample with the end-fire setup.

As calculated by simulations, a relevant drop in transmission has been measured due to the presence of the nanoantennna integrated in the hybrid configuration. Higher optical loss also affects the Q-factor of the cavity.

A Q-factor of $8x10^2$ and a resonance transmission of 22% have been calculated (see Fig. 6.11). As expected, a resonance red-shift of about 1 nm has been obtained in presence of the bowtie, due to the increase of the effective index of the hybrid cavity mode.
Experimental results demonstrate that Q-factor drops by a factor 2.1 compared to the PhC cavity. However, the mode volume of the hybrid structure is almost the same of the plasmonic nanoantenna ($V = 6x10^{-4}\ (\lambda/n)^3$), as calculated by 3D simulations, therefore this corresponds to $Q/V = 1.3\ x10^6\ (\lambda/n)^{-3}$, which is almost three orders of magnitude higher respect to the value obtained for the dielectric cavity ($Q/V = 2x10^3\ (\lambda/n)^{-3}$).
The enhancement of the optical loss due to the presence of the plasmonic nanoantenna has been also verified experimentally, with a transmission drop by a factor 4.2. Despite this decrease of the optical power, the cavity proposed in this study provides high detection resolution (T > 20%), which is a relevant advantage if compared with the performance obtained by simple plasmonic nanoantenna [238].

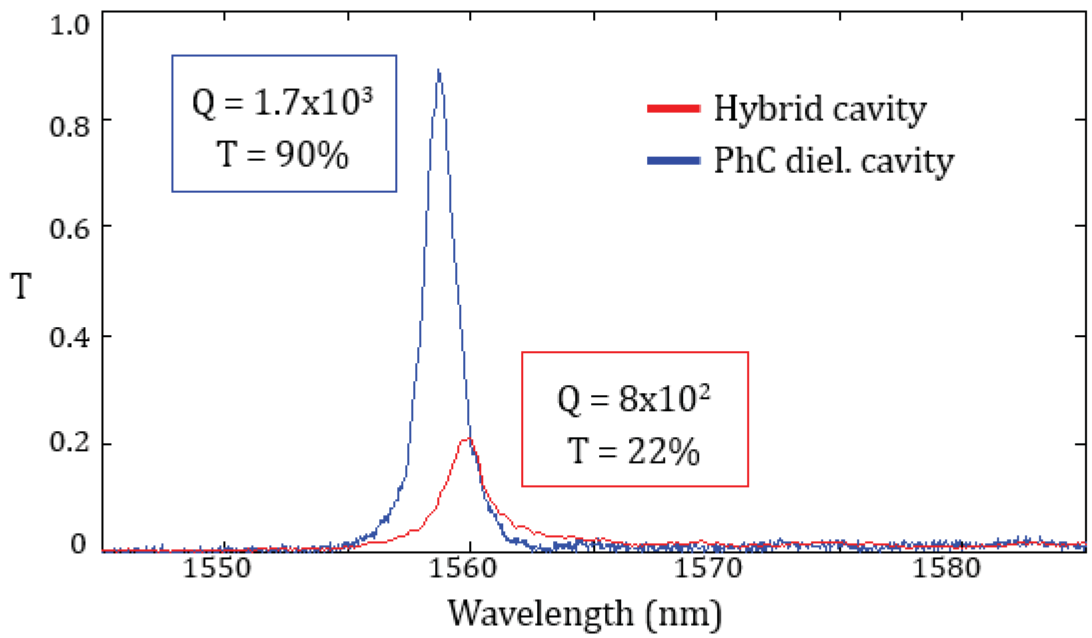

Fig. 6.11. Transmission spectra of the hybrid (red curve) and dielectric (blue curve) cavities.

The position of the bowtie nanoantenna and its separation from the PhC structure strongly affect the performance of hybrid cavity. A misalignment of the nanoantenna by about 100 nm along any direction increases the on-resonance transmission and the Q-factor, but it reduces the energy confined in the hotspot.

The energy confinement in the bowtie also depends on the gap with *s*. When *s* decreases from *s* = 60 nm to *s*=40 nm, the transmission and Q factor decrease slightly, but the energy density in the bowtie goes up, which is also reflected by an increase in the Q/V from 1.1 $x10^6$ $(\lambda/n)^{-3}$, with *s* = 60 nm, to $1.3x10^6$ $(\lambda/n)^{-3}$, with *s* = 40 nm (see Fig. 6.12). Given the added complexity of realizing the bowtie on top of a waveguide and requiring high yield, we found that *s* = 40 was a realistic lower bound for the gap width.

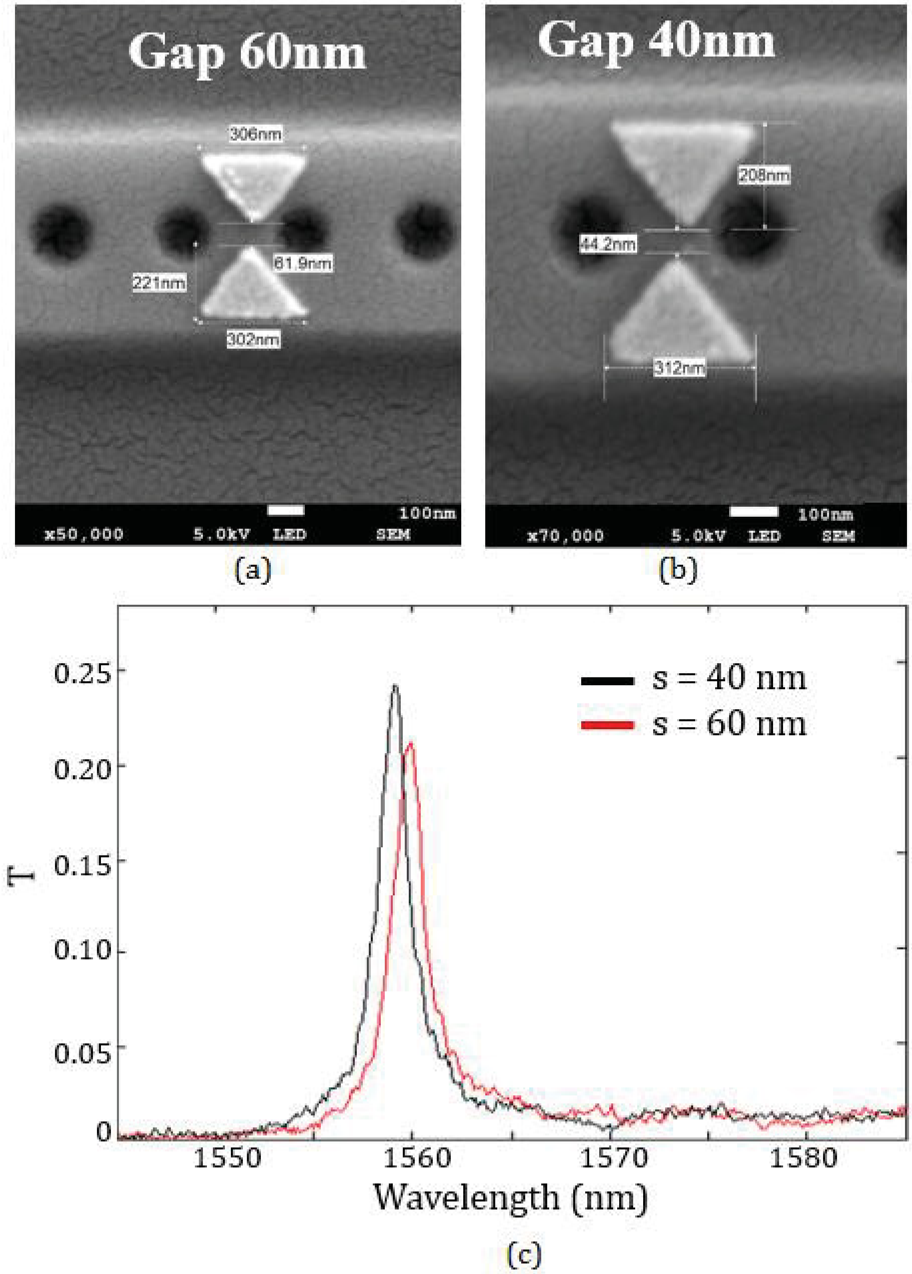

Fig. 6.12. Magnification of the vertical coupling region between the bowtie and the PhC with a nanoantenna slot of (a) 60 nm and (b) 40 nm. (c) Transmission spectra of the hybrid cavity with s = 60 nm (black curve) and s = 40 nm (red curve).

In Tab. 4 a comparison between the simulated results and experimental ones has been reported, in order to confirm the good matching between them.

Tab. 4. *Comparison between simulated and experimental results of the PhC dielectric cavity and the hybrid one.*

	PhC dielectric 3D FEM sim.	**Hybrid 3D FEM sim.**	**PhC dielectric Experimental**	**Hybrid Experimental**
Q	$1.8x10^3$	$9x10^2$	$1.7x10^3$	$8x10^2$
T	93%	26%	90%	22%

Similar performance confirms strong-light matter interaction, which makes the proposed photonic/plasmonic cavity suitable to be used as an efficient optical nanotweezer.

Chapter 7. Study and optical characterization of the nanotweezer for trapping at submicrometer scale

In this chapter, the study of the hybrid cavity as optical nanotweezer for trapping of submicrometer particles has been proposed.

Firstly, the results of 3D FEM simulations related to trapping of dielectric and metal nanoparticles have been reported, in order to define the range in which the hybrid cavity works as an efficient optical nanotweezer. Afterwards, the trapping system used for the experimental trapping of Au beads and the final results obtained with the photonic/plasmonic nanotweezer have been discussed.

7.1 Study of the photonic/plasmonic nanotweezer

The main advantage of the hybrid cavity proposed in this study is related to the strong energy confinement in the bowtie together with high detection resolution. These properties are fundamental for an efficient nanotweezer, because light-matter interaction is directly proportional to the values of optical force that can be exerted, while a high detection resolution allows to obtain information about the trapped object, because transmission changes are related to each trapping event and the entity of such changes is strongly affected by the object's properties.

The pattern of the photonic/plasmonic cavity proposed, discussed in Chapter 5, has been used to calculate the value of optical forces around the bowtie.

The presence of the plasmonic bowtie in the structure constrains the value of the optical power that can be used for nanoparticle trapping. In fact, thermal effects are stronger around the plasmonic nanoantenna and this causes an increase of temperature where there are the energy hotspots. A consequent increase of the Brownian motion is expected, which decreases the tweezer performance with a weaker attracting effect and shorter trapping time.

Therefore, a power $P_{in} \leq 1$ mW has been assumed in input to minimize the thermal effects, that is a necessary condition particularly for trapping in Rayleigh regime ($a \leq$ 100 nm), where Brownian motion becomes more relevant.

We carried out 3D FEM simulations to calculate the optical forces exerted by the hybrid cavity on 100 nm polystyrene and Au beads, using the Maxwell Stress Tensor (MST) method [32]. The results have been reported in Fig. 7.1.

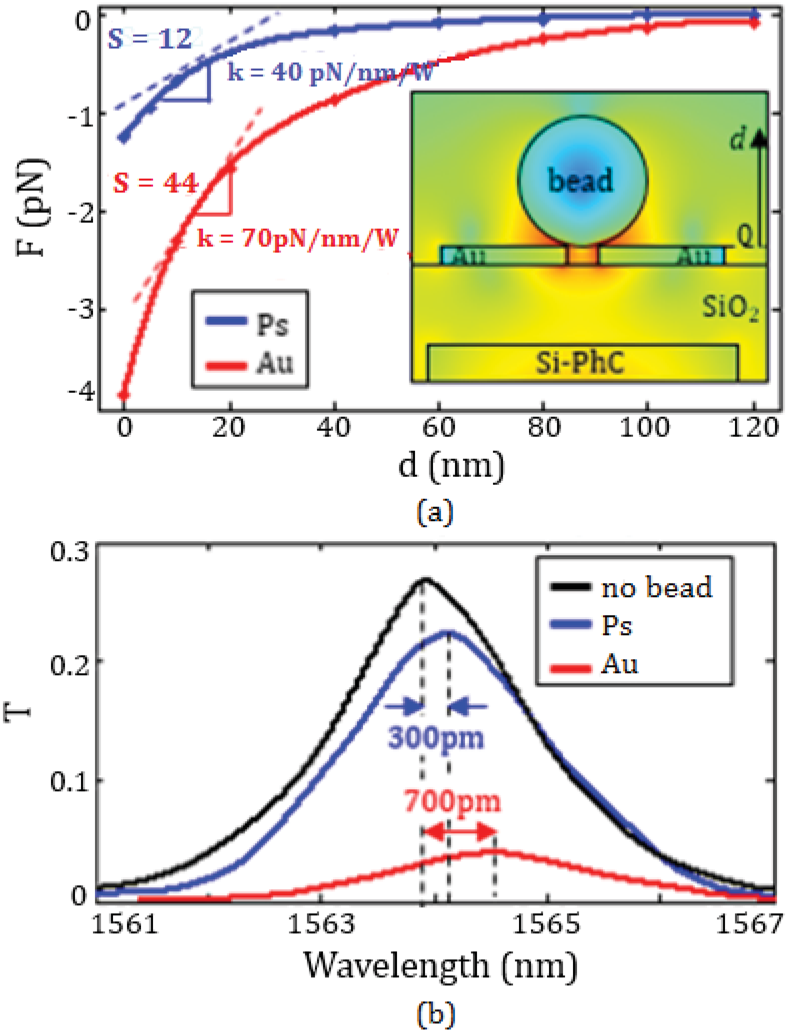

Fig. 7.1. (a) Optical forces exerted on 100 nm polystyrene (blue line) and Au (red line) nanoparticles by 3D FEM simulations. (b) Calculated transmission spectra of the hybrid cavity without (black line) and with 100 nm polystyrene (blue line) and Au (red line) beads. The resonance condition is red-shifted of about 300 pm and 700 pm, due to the presence of the PS and Au bead, respectively.

Values of optical force of few pN have been calculated with an input power P_{in} = 1 mW for both dielectric and metal beads. This results confirm the high efficiency of the proposed hybrid cavity to be used as optical nanotweezer. In fact, the optical stability, previously defined as $S = U/k_BT_c$, higher than 10 ($S > 10$) confirms a stable trapping condition, which corresponds to an action of the net force stronger than the opposite thermal energy k_BT_c, which means that we can assume the trapping force to be strong enough to completely overcome the Brownian motion of the particle [19, 34]. Such behavior is given by the strong hotspot obtained in the bowtie gap with low input power. Another relevant advantage of the hybrid cavity is the high value of the optical stiffness *k*, related to the strength of the restoring force to the equilibrium point in the bowtie gap; high values of *k* facilitate the attraction of the bead and make more difficult to push the particle away from the trapping site [35].

The trapping stiffness is k = 40 pN/(nm·W) for the dielectric particle and k = 70 pN/(nm·W) for the metal one. Such results are much higher than performance obtained with a simple PhC cavity [168], or simple plasmonic structures like the nanoantennna and the nanoholes. Furthermore, by comparison with performance obtained with the PhC cavity without the bowtie, a stability $S \ll 10$ has been calculated in that case, which highlights the advantage of the hybrid approach and its higher Q/V value.

Such performance confirms that the condition $S \geq 10$ can be obtained also with lower input power (P_{in} < 1 mW). In particular, the stable optical trapping of 100 nm dielectric beads is obtained with P_{in} < 800 μW, while the metal beads with the same size are trapped also with P_{in} ~ 200 μW.

7.2. Experimental trapping

The trapping efficiency of the hybrid nanotweezer has been verified experimentally for the manipulation of metal beads at submicrometer scale.

A similar optical setup proposed in Chapter 6 has been used to study the trapping action. In addition, a microfluidic pump has been used to control the fluid flow, in order to keep constant its motion in the microfluidic channel. This condition is necessary for trapping application, because with low values of the Reynolds number is possible to obtain a laminar flow, in order to minimize the Brownian motion of the beads in the microchannel. A flow of 10 μm/min is controlled with the microfluidic pump connected to the inlet.

Au beads have been dispersed in an aqueous solution. Two different solutions of 400 nm Au beads with a concentration of 1.9×10^8 particles/ml and 200 nm Au beads with 1.9×10^9 particles/ml (Sigma-Aldrich) have been used (see Fig. 7.2).

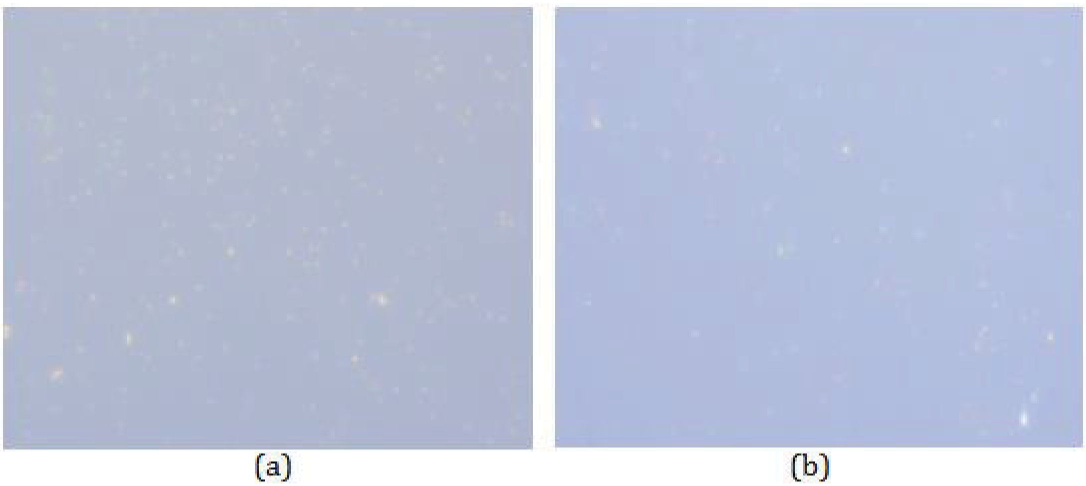

Fig. 7.2. Microscope image (50x magnification) of solutions of 400 nm Au beads with a concentration of 1.9×10^8 particles/ml and 200 nm Au beads with 1.9×10^9 particles/ml.

A tuneable laser is used for trapping measurements. The output power of the tunable laser is P_{las} = 8 mW. By 3D FEM simulations, we have calculated a red-shift of the resonance condition of about 700 pm and 850 pm with a trapping event of a 200 nm and 400 nm Au bead. Therefore, we have set the operating wavelength of the light source at the expected resonance condition in presence of the gold nanoparticle in the trapping site.

The optical power measured from a simple nanowire by the output photodetector in the optical setup is P_{out} = 4.8 μW. Therefore, the optical power in the cavity has been estimated to be $P_{cav} = \sqrt{P_{las} \cdot P_{out}}$ = 190 μW [170].

This setup has been used to observe experimentally trapping events in the cavity.

Once the metal nanoparticle flows very close to the bowtie, the gradient force draws the bead to the cavity, as described in Fig. 7.3.

At the same time, even if we have precompensated the expected red-shift of the resonance condition by setting the tuneable laser properly, however, a strong decrease of the transmission is observed at t = 0s (see Fig. 7.3) when a trapping event occurs, due to the absorption and scattering by the gold nanoparticles, as confirmed by simulations (see Fig. 5.13). This behavior confirms the ease of detection of a trapping event, by simply observing a fast change in the transmitted optical power.

In Fig. 7.3, the experimental results obtained for trapping of 200 nm Au beads have been reported [238].

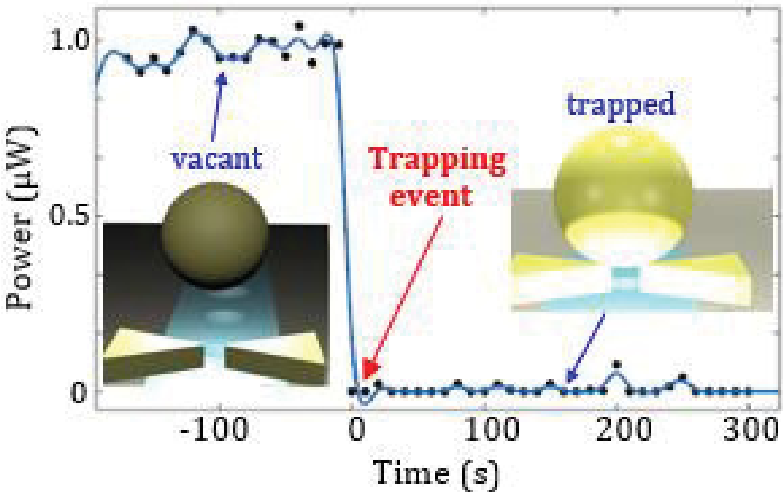

Fig. 7.3. Experimental results of trapping of a single 200 nm Au bead with the hybrid cavity for t > 5 min with P_{cav} = 190µW.

A long trapping time (t_{trap} > 5 min) has been verified, which confirms the strong trapping efficiency of the hybrid cavity as optical nanotweezer. Furthermore, the strength of the optical trap is also confirmed by the evidence that weak oscillations in transmission after the trapping event (t > 0 s) can be observed, which indicate the high trapping stiffness, as already calculated by 3D FEM simulations, and correspondingly reduced Brownian motion. Trapping of 400 nm Au beads has been also demonstrated and the experimental results have been reported in Fig. 7.4.

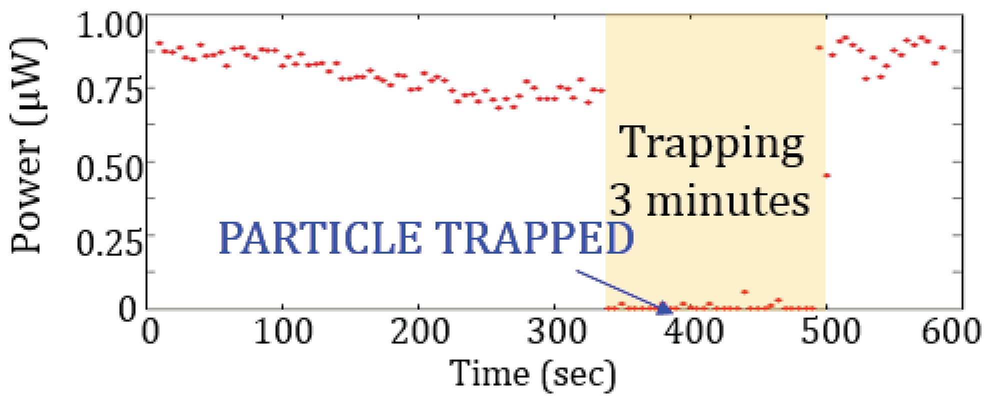

Fig. 7.4. Experimental results of trapping of a single 400 nm Au bead with the hybrid cavity for t ~ 3 min with P_{cav} = 190μW.

Trapping of 400 nm for 3 min has been verified. Then, the bead has been released from the trapping site, unlike the behavior observed for trapping of a smaller Au bead. It can be explained because the gradient force acting on a larger nanoparticle is not much stronger, due to the energy confinement in the bowtie slot in a region of few tens of nanometers. On the contrary, stronger effects of scattering and absorption are evident in this case, compared to the behavior observed with 200 nm Au bead. This corresponds to a more relevant thermal effect with a consequent decrease of the optical stability and, therefore, shorter trapping time [238].

We have also attempted to use the 1D cavity without bowtie for the same input optical power, but did not observe any particle deflection or trapping, again highlighting the benefit of the hybrid geometry.

Our results represent the first demonstration of a hybrid photonic crystal/bowtie plasmonic resonator cavity with in-plane light propagation. This allows to facilitate the nanotweezer integration in an on-chip system. We demonstrate high transmission and high-efficiency optical trapping, based on the ultra-high Q/V ($>10^6$ $(\lambda/n)^{-3}$) ratio of the device. The ability to confine a high fraction of the optical energy in the hotspot outside the cavity affords direct interaction with an analyte and increases the sensitivity for sensing applications. Moreover, high transmission ($T > 20\%$) makes it possible to detect any changes in the resonance condition easily.

Conclusions

An efficient photonic/plasmonic nanotweezer for trapping at the nanoscale has been proposed in this thesis.

The advantages of the optical manipulation compared to the performance obtained with other trapping methods have been discussed. In particular, the optically-based technique provides high values of optical forces with low power and prevents a direct contact with the target objects, so minimizing risks of damage and disruption.

The theory of the optical trapping regimes has been also proposed, in order to understand the physical effects that intervene in this process as a function of the properties of the target objects to trap with a more detailed description of the Rayleigh regime, suitable for the study of matter manipulation at the nanoscale.

The state-of-the-art of integrated optical, plasmonic and hybrid nanotweezers has been discussed to compare the performance of these devices, to put in evidence their advantages and drawbacks, in order to identify the most suitable configuration to exploit an efficient trapping condition at submicrometer scale and nanoscale.

The design, fabrication and optical characterization of the photonic/plasmonic cavity, realized by the 1D PhC dielectric cavity vertically coupled to a bowtie nanoantenna, has been proposed. The design of the 1D PhC cavity has been carried out to obtain a high resonance transmission and Q-factor. Instead, a very low mode volume and strong spatial energy confinement has been required to the bowtie nanoantenna. The matching of resonance condition has been also assumed to enhance the vertical coupling efficiency, so maximizing light-matter interaction in the hybrid configuration.

An ultra-high $Q/V > 10^6 (\lambda/n)^{-3}$ with a resonance transmission of 26% have been calculated by 3D FEM simulations. A good matching between simulated and experimental results has been verified. In fact, the $Q/V > 10^6 (\lambda/n)^{-3}$ and $T > 20$ % have been confirmed experimentally with the photonic/plasmonic cavity.

The strong light-matter interaction obtained with the hybrid cavity has been exploited to trap small particles with high efficiency and long trapping time. Trapping events of a single Au bead have been verified experimentally, with a trapping time longer than 5 minutes for a single 200 nm Au bead with an input power of only 190 μW. Similar performance confirms a high optical stability and low thermal effects in the system, so potentially enabling also the manipulation of living matter at the nanoscale.

The high efficiency of the proposed hybrid nanotweezer allows to continue the study for the optimization of the device performance and the improvement of the optical system used during trapping measurements. A key aspect could be represented by the integration in a handheld device of the hybrid nanotweezer with an efficient system for optical characterization, i.e. based on Surface-Enhanced Raman Spectroscopy (SERS). This enables the stable trapping of a single nanoparticle and also the detection and recognition of the trapped object by the study of the Raman signal collected. The hybrid cavity provides a strong enhancement of the Raman signal due to the presence of the bowtie in the trapping site, so improving the detection resolution, that is not suitable by using only a simple PhC dielectric structure.

Furthermore, the integration of a more efficient microfluidic channel in the optofluidic chip with some sections that enable the sorting of particles with different size and properties, will be very useful to carry only the target objects close to the trapping sites. Therefore, as future work we expect to improve the nanotweezer efficiency by implementing such system, so making the proposed device very suitable for several biomedical applications, for which trapping at the nanoscale without a direct contact is required and also a fast, accurate and selective detection of the target objects can facilitate the integration of such device in an efficient Lab on Chip microsystem to be used for treating and monitoring of several human diseases.

REFERENCES

[1] P. Y. Chiou, A. T. Ohta, and M. C. Wu, "Massively parallel manipulation of single cells and microparticles using optical images", Nature, 436(7049), pp. 370-372, 2005.

[2] D. G. Grier, "A revolution in optical manipulation", Nature, 424(6950), pp. 810-816, 2003.

[3] O. M. Maragò, P. H. Jones, P. G. Gucciardi, G. Volpe, and A. C. Ferrari, "Optical trapping and manipulation of nanostructures", Nat. Nanotech., 8(11), pp. 807-819, 2013.

[4] A. Ashkin, J. M. Dziedzic, "Optical trapping and manipulation of viruses and bacteria", Science, *v*ol. 235(4795), pp. 1517-1520, 1987.

[5] M. Righini, P. Ghenuche, S. Cherukulappurath, V. Myroshnychenko, F. J. Garcia de Abajo, and R. Quidant, "Nano-optical Trapping of Rayleigh Particles and Escherichia coli Bacteria with Resonant Optical Antennas", Nano Letters, 9(10), pp. 3387-3391, 2009.

[6] H. Zhang, K.-K. Liu, "Optical tweezers for single cells". Journ. of Royal Soc., 5(24), 2008.

[7] Y. Pang, H.Song, J. H. Kim, X. Hou, W. Cheng, "Optical trapping of individual human immunodeficiency viruses in culture fluid reveals heterogeneity with single-molecule resolution", Nat. Nanotech., 9(8), pp. 624-630, 2014.

[8] R. W Bowman, M. J. Padgett, "Optical trapping and binding", Reports on Progress in Physics, 76(2), 026401, 2013.

[9] X. Wang, S. Chen, M. Kong, Z. Wang, K. D. Costa, R. A. Li, D. Sun, "Enhanced cell sorting and manipulation with combined optical tweezer and microfluidic chip technologies", Lab on Chip, 11(21), pp. 3656-3662, 2011.

[10] S. M. Moghimi, A. C. Hunter and J. Clifford Murray, "Nanomedicine: current status and future prospects", The FASEB Journ., 19(3), pp. 311-330, 2005.

[11] M. L. Juan, R. Gordon, Y. Pang, F. Eftekhari and R. Quidant, "Self-induced back-action optical trapping of dielectric nanoparticles". Nat. Phys., 5, pp. 915-919, 2009.

[12] P. Jing, J. Wu, G. W. Liu, E. G. Keeler, S. H. Pun, and L. Y. Lin, "Photonic Crystal Optical Tweezers with High Efficiency for Live Biological Samples and Viability Characterization", Scient. Rep., 6, 19924 , 2016.

[13] T. van Leest and J. Caro, "Cavity-enhanced optical trapping of bacteria using a silicon photonic crystal", Lab on Chip, 13(22), pp. 4358-4365, 2013.

[14] S. Lin and K. B. Crozier, “Trapping-Assisted Sensing of Particles and Proteins Using On-Chip Optical Microcavities”, ACS Nano, 7(2), pp. 1725-1730, 2013.

[15] P. C. Chaumet, A. Rahmani, “Optical tweezers: dressed for success”, Nat. Nanotech., 9(4), pp. 252-253, 2014.

[16] F. Furno, K. S. Morley, B. Wong, B. L. Sharp, P. L. Arnold, S. M. Howdle, R. Bayston, P. D. Brown, P. D. Winship and H. J. Reid, “Silver nanoparticles and polymeric medical devices: a new approach to prevention of infection?”, Journal of Antimicrobial Chemotherapy, 54(6)6, pp. 1019–1024, 2004.

[17] D. Conteduca, F. Dell’Olio, C. Ciminelli, and M. N. Armenise, “New miniaturized exhaled nitric oxide sensor based on a high Q/V mid-infrared 1D photonic crystal cavity ”, App. Opt., 54(9), pp. 2208-2217, 2015.

[18] http://fortune.com/2015/05/08/cancer-drug-spending-100-billion-in-2014-headed-higher/

[19] A. Kotnala and R. Gordon, “Double nanohole optical tweezers visualize protein p53 suppressing unzipping of single DNA-hairpins”, Biom. Opt. Express, 5(6), pp. 1886-1894, 2014.

[20] A. A. Al Balushi and R. Gordon, “Label-Free Free-Solution Single-Molecule Protein–Small Molecule Interaction Observed by Double-Nanohole Plasmonic Trapping”, ACS Photonics, 1(5), pp. 389-393, 2014.

[21] K. C. Neuman and A. Nagy, “Single-molecule force spectroscopy: optical tweezers, magnetic tweezers and atomic force microscopy,” Nat. Methods, 5(6), pp. 491–505, 2008.

[22] JPK instruments Application Note: “Single-molecule DNA (over)stretching using optical tweezers”, http://www.jpk.com/optical-tweezers.233.en.html.

[23] M. J. Comstock, T. Ha, ock, T. Ha, R. Chemla, “Ultrahigh-resolution optical trap with single-fluorophore sensitivity”, Nature Methods, 8(4), pp. 335-340, 2011.

[24] M. Padgett, R. Di Leonardo, “Holographic optical tweezers and their relevance to lab on chip devices ”, Lab on Chip, 11(7), pp. 1196-1205, 2011.

[25] Optofluidics Documentation: “Experimental Tips and tricks”, http://docs.opfluid.com/documentation/.

[26] P. J. Pauzauskie, A. Jamshidi, J. K. Valley, J. H. Satcher, and M. C. Wu, “Parallel trapping of multiwalled carbon nanotubes with optoelectronic tweezers”, Appl. Phys. Lett., 95(11), 113104, 2009.

[27] M. S. Choi, G.-H. Lee, Y.-Jun Yu, D.-Y. Lee, S. H. Lee, P. Kim, J. Hone and W. J. Yoo, “Controlled charge trapping by molybdenum disulphide and graphene in ultrathin heterostructured memory devices”, Nat. Comm., 4(1624), 2013.

[28] K. Wang, E. Schonbrun, P. Steinvurzel, K. B. Crozier, “Trapping and rotating nanoparticles using a plasmonic nano-tweezer with an integrated heat sink”, Nature Comm., 2(1), 469, 2011.

[29] W.-Yi Tsai, J.-S. Huang, C.-Bin Huang, "Trapping and rotating nanoparticles using a plasmonic nano-tweezer with an integrated heat sink", Nano Letters, 14(2), pp. 547-552, 2014.
[30] B. J. Roxworthy, A. M. Bhuiya, V. V. G. K. Inavalli, H. Chen, K. C. Toussaint, "Multifunctional plasmonic film for recording near-field optical intensity", Nano Letters, 14(8), pp. 4687-4693, 2014.
[31] A. Ashkin, J. M. Dziedzic and T. Yamane, "Optical trapping and manipulation of single cells using infrared laser beams", Nature, 330(6150), pp. 769 – 771, 1987.
[32] M. Woerdemann, C. Alpmann, M. Esseling, C. Denz, "Advanced optical trapping by complex beam shaping", Laser Phot. Review, 7(6), pp. 839-854, 2014.
[33] V. H. Lieu, T. A. House, and D. T. Schwartz, "Hydrodynamic Tweezers: Impact of Design Geometry on Flow and Microparticle Trapping", Anal. Chem., 84(4), pp. 1963–1968.
[34] D. Di Carlo , N. Aghdam , L. P. Lee, "Single-Cell Enzyme Concentrations, Kinetics, and Inhibition Analysis Using High-Density Hydrodynamic Cell Isolation Arrays", Anal. Chem., 78(14), pp. 4925–4930, 2016.
[35] A. Winkleman, K. L. Gudiksen, D. Ryan, and G. M. Whitesides, "A magnetic trap for living cells suspended in a paramagnetic buffer", Appl. Phys. Lett., 85(12), pp. 2411-2413, 2004.
[36] M. A. M. Gijs, "Magnetic bead handling on-chip: new opportunities for analytical applications", Microfluid Nanofluid, 1(1), pp. 22-40, 2004.
[37] H. M. Hertz, "Standing-wave acoustic trap for nonintrusive positioning of microparticles", Journ. of App. Phys., 78(8), pp. 4845-4849, 1995.
[38] A. Rosenthal, J. Voldman, "Dielectrophoretic Traps for Single-Particle Patterning", Biophysical Journ., 88(3), pp. 2193–2205, 2005.
[39] N.G. Green , H. Morgan , J. J. Milner, "Manipulation and trapping of sub-micron bioparticles using dielectrophoresis", J. Biochem. Biophys. Methods, 35(2), 89–102, 1997.
[40] A. Karimi, S. Yazdi, and A. M. Ardekani , "Hydrodynamic mechanisms of cell and particle trapping in microfluidics", Biomicrofluidics, 7(2), 021501, 2013.
[41] D. Di Carlo, L. Y. Wu and L. P. Lee, "Dynamic single cell culture array", Lab on a Chip, 6(11), pp. 1445-1449, 2005.
[42] R. M. Johann, "Cell trapping in microfluidic chips", Anal. Bioanal. Chem., vol. 385, no. 3, pp. 408–412, 2006.
[43] S. Claire Hur, A. J. Mach, and D. Di Carlo, "High-throughput size-based rare cell enrichment using microscale vortices", Biomicrofluidics, 5, 022206, 2011.

[44] J. Nilsson, M. Evander, B. Hammarström, T. Laurell, "Review of cell and particle trapping in microfluidic systems", Analyt. Chim. Acta, 649(2), pp. 141–157, 2009.
[45] S. Kobel, A. Valero, J. Latt, P. Renaud, M. Lutolf, "Optimization of microfluidic single cell trapping for long-term on-chip culture", Lab on a Chip, 10(7), pp. 857-863, 2010.
[46] C. Probst, A. Grünberger, W. Wiechert, D. Kohlheyer, "Polydimethylsiloxane (PDMS) Sub-Micron Traps for Single-Cell Analysis of Bacteria", Micromachines, 4(4), 357-369, 2013.
[47] J.-S. Park, S.-H. Song and H.-Il Jung, "Continuous focusing of microparticles using inertial lift force and vorticity via multi-orifice microfluidic channels", Lab on a Chip, 9(7), pp. 939–948, 2009.
[48] S. Zheng, H. Lin, J.-Q. Liu, M. Balic, R. Datar, R. J. Cote, Y.-C. Tai, "Membrane microfilter device for selective capture, electrolysis and genomic analysis of human circulating tumor cells", Journ. of Chromat. A, 1162(2), pp. 154–161, 2007
[49] A. A. S. Bhagat, H. W. Hou, L. D. Li, C. T. Lim, J. Han, "Pinched flow coupled shear modulated inertial microfluidics for high throughput rare blood cell separation", Lab on a Chip, 11(11), pp. 1870-1878, 2011.
[50] S. P. Jang, S. U. S. Choi, "Role of Brownian motion in the enhanced thermal conductivity of nanofluids", Applied Phys. Lett., 2004, 84(21): 4316-4318.
[51] M. Tanyeri, E. M. Johnson-Chavarria, and C. M. Schroeder, "Hydrodynamic trap for single particels and cells", App. Phys. Lett., 2010, 96(22), 224101.
[52] S. Anandakumar, V. Sudha Rani, S. Oh, B.L. Sinha, M. Takahashi, C. Kim, "Translocation of bio-functionalized magnetic beads using smart magnetophoresis", Biosensors and Bioelectr., 26(4), pp. 1755-1758, 2010.
[53] L. Gao, M. A. Tahir, L. N. Virgin and B. B. Yelle, "Multiplexing superparamagnetic beads driven by multi-frequency ratchets", Lab on Chip, 11(24), pp. 4214–4220, 2011.
[54] M. Brzeska, M. Panhorst, P.B. Kamp, J. Schotter, G. Reiss, A. Pühler, A. Becker, H. Brückl, "Detection and manipulation of biomolecules by magnetic carriers", Journ. of Biotech., 112(1), pp. 25-33, 2004.
[55] T. Henighan, A. Chen, G. Vieira, A. J. Hauser, F. Y. Yang, J. J. Chalmers, and R. Sooryakumar, "Manipulation of Magnetically Labeled and Unlabeled Cells with Mobile Magnetic Traps", Biophys. Journal, 98(3), pp. 412-417, 2010.
[56] R. Venu, B. Lim, X. H. Hu, I. Jeong, T. S. Ramulu, C. G. Kim, "On-chip manipulation and trapping of microorganisms using a patterned magnetic pathway", Microfluid Nanofluid, 14(1), pp. 277-285, 2013.

[57] R. S. Conroy, G. Zabow, J. Moreland, and A. P. Koretsky, "Controlled transport of magnetic particles using soft magnetic patterns", App. Phys. Lett., 93(20), 203901, 2008.
[58] H. A. Pohl, and J. S. Crane, "Dielectrophoresis of cells", Nat. Methods, vol. 5, no. 6, pp. 491-505, 1971.
[59] B. Yafou, N. A. Kadri, and F. Ibrahim, "Dielectrophoretic Manipulation and Separation of Microparticles Using Microarray Dot Electrodes", Sensors, 14(4), pp. 6356-6369, 2014.
[60] N. G. Green, H. Morgan, J. J. Milner, "Manipulation and trapping of sub-micron bioparticles using dielectrophoresis", J. Biochem. Biophys. Methods, 35(2), pp.89-102, 1997.
[61] A. Nakano, T.-C. Chao, F. Camacho-Alanis, and A. Ros, "Immunoglobulin G and Bovine Serum Albumin Streaming Dielectrophoresis in a Microfluidic Device", Electrophoresis, 32(17), pp. 2314-2322, 2011.
[62] M. Li, W. Li, J. Zhang, G. Alici, W. Wen, "A review of microfabrication techniques and dielectrophoretic microdevices for particle manipulation and separat", Journal of Physics D: Applied Physics, 47(6), 063001, 2014.
[63] L. L. Rojas, P. Ebbinghaus, G. Vasan, M.-L. Chu, A. Erbe, and C.-F. Chou, "Low-Copy Number Protein Detection by Electrode Nanogap-Enabled Dielectrophoretic Trapping for Surface-Enhanced Raman Spectroscopy and Electronic Measurements", Nano Lett., 14(5), pp. 2242-2250, 2014.
[64] A. Kuzik, "Dielectrophoresis at the nanoscale", Electrophor., 32(17), pp. 2307-2313, 2011.
[65] K. A. Brown and R. M. Westervelt, "Triaxial AFM Probes for noncontact Trapping and Manipulation", Nano Lett., 11(8), pp. 3197-3201, 2011.
[66] K. J. Freedman, L. M. Otto, A. P. Ivanov, A. Barik, S.-H. Oh, and J. B. Edel, "Nanopore sensing at ultra-low concentrations using single-molecule dielectrophoretic trapping", Nat. Comm., 7, 10217, 2016.
[67] S. Strobel, R. A. Sperling, B. Fenk, W. J. Parak, and M. Tornow, "Dielectrophoretic trapping of DNA-coated gold nanoparticles on silicon based vertical nanogap devices", Phys. Chem., 13(21), pp. 9973-9977, 2011.
[68] C.-H. Chiou, L.-Ju Chien, and J.-N. Kuo, "Nanoconstriction-based electrodeless dielectrophoresis chip for nanoparticle and protein preconcentration", Appl. Phys., 8(8), 085201, 2015.
[69] P. Y. Chiou, A. Ohta, M. C. Wu, "Massively parallel manipulation of single cells and microparticles using optical images", Nature, 436(7049), pp. 370-372, 2005.

[70] S. L. Neale, M. Mazilu, J. I. B. Wilson, K. Dholakia, and T. F. Krauss, "The resolution of optical traps created by Light Induced Dielectrophoresis (LIDEP)", Opt. Exp., 15(20), pp. 12619-12626, 2007.

[71] S. Ota, S. Wang, Y. Wang, X. Yin, and X. Zhang, "Lipid Bilayer-Integrated Optoelectronic Tweezers for Nanoparticle Manipulations", Nano Letters, 13(6), pp. 2766-2770, 2013.

[72] J. S. Jeong, J. W. Lee, C. Y. Lee, S. Y. The, A. Lee, K. K. Shung, "Particle manipulation in a microfluidic channel using acoustic trap", Biomed. Microdevices, 13(4), pp. 779-788, 2011.

[73] J. Shi, D. Ahmed, X. Mao, Sz-C. S. Lin, A. Lawit, T. J. Huang, "Acoustic tweezers: patterning cells and microparticles using standing surface acoustic waves (SSAW)", Lab on chip, 9(20), pp. 2890-2895, 2009.

[74] X. Ding, Sz-Chin S. Lin, B. Kiraly, H. Yue, S. Li, I-Kao Chianga, J. Shi, S. J. Benkovic, and T. J. Huang, "On-chip manipulation of single microparticles, cells, and organisms using surface acoustic waves", PNAS, 109(28), pp. 11105-11109, 2012.

[75] M. Evander, L. Johansson, T. Lilliehorn, J. Piskur, M. Lindvall, S. Johansson, M. Almqvist, T. Laurell, and J.n Nilsson, "Noninvasive Acoustic Cell Trapping in a Microfluidic Perfusion System for Online Bioassays", Anal. Chem., 79(7), pp. 2984-2991, 2007.

[76] J. Shi, H. Huang, Z Stratton, Y. Huang, and T. J. Huang, "Continuous particle separation in a microfluidic channel via standing surface acoustic waves (SSAW)", Lab on Chip, 9(13), pp. 3354-3359, 2009.

[77] F. Guo, Z. Mao, Y. Chen, Z. Xie, J. P. Lata, P. Li, L. Ren, J. Liu, J. Yang, M. Dao, S. Suresh, and T. J. Huang, "Three-dimensional manipulation of single cells using surface acoustic waves", PNAS, 1524813113, 2015.

[78] D. J. Collins, B. Morahan, J. Garcia-Bustos, C. Doerig, M. Plebanski, and A. Neild, "Two-dimensional single-cell patterning with one cell per well driven by surface acoustic waves", Nat. Comm., 6(8686), 2015.

[79] M. Evander, O. Gidlöf, B. Olde, D. Erlinge, and T. Laurell, "Non-contact acoustic capture of microparticles from small plasma volumes", Lab on a Chip, 15(12), pp. 2588-2596, 2015.

[80] Bjorn Hammarstrom, T. Laurell and J. Nilsson, "Seed particle-enabled acoustic trapping of bacteria and nanoparticles in continuous flow systems", Lab on a Chip, 12(21), pp. 4296-4304, 2012.

[81] L. Bosnac, T. Aabo, P. M. Bendix, L. N. Oddershede, "Efficient Optical Trapping and visualization of silver nanoparticles", Nano Lett., 8(5), pp. 1486-1491, 2008.

[82] A. Ashkin, "Forces of a single-beam gradient laser trap on a dielectric sphere in the ray optics regime", Biophys. Journ., 61(2), pp. 569-582, 1992
[83] A. Ashkin, "Optical trapping and manipulation of neutral particles using lasers", Proceedings of the National Academy of Sciences of the United States of America, 94(10), pp. 4853-4860. 1997.
[84] JPK Instruments, "Nanotracker 2", http://www.jpk.com/nanotracker-2-overview.388.en.html
[85] http://www.prnewswire.com/news-releases/cell-robotics-launches-new-pathology-workstation-at-national-pathologists-meeting-73711107.html
[86] CellTool, "BioRam system", http://celltool.de/en/products/bioram.html
[87] http://www.azonano.com/equipment-details.aspx?EquipID=256
[88] http://www.prnewswire.com/news-releases/arryx-launches-bioryxr-200-infrared-system-75246752.html
[89] D. Erickson, "Optofluidics for Mobile Health, Bioenergy, and nanoparticle analysis", CLEO 2014, San Jose, California, 8-13 June 2014.
[90] H. Kawauchi, K. Yonezawa, Y. Kozawa, S. Sato, Calculation of optical trapping forces on a dielectric sphere in the ray optics regime produced by a radially polarized laser beam, Opt. Lett., 32(13), pp. 1839-1841, 2007.
[91] S. Sato, Y. Harada, Y. Waseda, "Optical trapping of microscopic metal particles", Opt. Lett., 19(22), pp. 1807-1809, 1994.
[92] L. P. Ghislain, N. A. Switz, W. W. Webb, "Measurement of small forces using an optical trap", Rev. Sci. Instrum., 65(2762), 1994.
[93] W. H. Wright, G. J. Sonek, M. W. Berns, "Radiation trapping forces on microspheres with optical tweezers", App. Phys. Lett., 63(715), 1993.
[94] L. Novotny, R. X. Bian, X. S. Xie, "Theory of nanometric optical tweezers", Phys. Rev. Lett., 79(645), 1997.
[95] J. A. Lock, "Calculation of the radiation trapping force for laser tweezers by use of generalized Lorenz-Mie theory", App. Opt., 43(12), pp. 2532-2544, 2004.
[96] A. Ashkin, "Acceleration and Trapping of Particles by Radiation Pressure", Phys. Review Lett., 24(4), pp. 156-159, 1970.
[97] J. Bergeron, A. Zehtabi-Oskuie, S. Ghaffari, Y. Pang, and R. Gordon, "Optical Trapping of Nanoparticles", J. Vis. Exp., 71(4424), 2013.
[98] J. E. Molloy, and M. J. Padgett, "Lights, action: Optical tweezers", Contemp. Physics, 43(4), pp 241-258, 2002
[99] A. Ashkin, J. M. Dziedzic, J. E. Bjorkholm, and S. Chu, "Observation of a single-beam gradient force optical trap for dielectric particles", Opt. Lett., 11(5), pp,288-290, 1986.

[100] K. Dholakia, P. Reece and M. Gu, “Optical micromanipulation”, Chem. Soc. Rev., 37(1): 42–55, 2008.
[101] M. Wördemann, “Structured Light Fields: Applications in Optical Trapping, Manipulation, and Organisation”, Springer theses (Verlag Berlin Heildenberg), ISSN: 2190-5053, 2012.
[102] P. Jones, O. Maragó, G. Volpe, “Optical Tweezers: Principles and Applications”, Cambridge University Press, New York, 2015.
[103] O. Brzobohaty, M. Siler, J. Trojek, L. Chvatal, V. Karasek, A. Patak, Z. Pokorna, F. Mika, P. Zemanek, “Three-Dimensional Optical Trapping of a Plasmonic Nanoparticle using Low Numerical Aperture Optical Tweezers”, Scientific Reports, 5(8106), 2015.
[104] K. Svoboda, and S. M. Block, “Optical trapping of metallic Rayleigh particles”, Optics Letters, 19(13), pp. 930-932, 1994.
[105] J. R. Arias-González, and M. Nieto-Vesperinas, “Optical forces on small particles: attractive and repulsive nature and plasmon-resonance conditions”, Journ. Opt. Soc. Am. A, 20(7), pp. 1201-1209, 2003
[106] D. Erickson, X. Serey, Y.-F. Chen, and S. Mandal, “Nanomanipulation using near field photonics”, Lab on a chip, 11(6), pp. 995-1009, 2011.
[107] S. Kawata, M. Ohtsu, M. Irie, “Near-Field Optics and Surface Plasmon Polaritons”, Springer Science & Business Media, 2003.
[108] M. Muradoglu, T. Le, C. Y. Lau, O. W. Liew, and T. Wah Ng, “Optical stirring in a droplet cell bioreactor”, Biom. Opt. Exp., 2012, 3(10): 2465-2470.
[109] T. A. Nieminen, V. L. Y. Loke, A. B. Stilgoe, G. Knöner, A. M. Brańczyk, N. R. Heckenberg, H. Rubinsztein-Dunlop, “Optical tweezers computational toolbox”, Journ. of Optics: Pure and Applied Opt., 2007, 9(8): S196-S203.
[110] G. Gouesbet, B. Maheu, and G. Grehan, “Light scattering from a sphere arbitrarily located in a Gaussian beam, using a Bromwich formulation”, J. Opt. Soc. Am., 1988, 5(9): 1427-1453.
[111] J. A. Lock, “Calculation of the radiation trapping force for laser tweezers by use of generalized Lorenz-Mie theory. I. Localized model description of an on-axis tightly focused laser beam with spherical aberration”, Appl. Optics, 2004, 43(12): 2532-2544.
[112] Y. Harada, T. Asakura, “Radiation forces on a dielectric sphere in the Rayleigh scattering regime”, Opt. Comm., 1996, 124(5): 529-541.
[113] L. Novotny and B. Hecht, “Principles of Nano-Optics”, Cambridge University Press, New York 2012.
[114] B. Sun, Y. Roichman, and D. G. Grier, “Theory of holographic optical trapping,” Opt. Express, 2008, 16(20): 15765–15776.

[115] M. Dienerowitz, M. Mazilu, and K. Dholakia, “Optical manipulation of nanoparticles: a review”, Journ. of Nanophotonics, 2, 021875., 2008
[116] L. Novotny and B. Hecht, “Principles of Nano-Optics”, Cambridge University Press, New York 2012.
[117] R. Huang, I. Chavez, K. M. Taute, B. Luki, S. Jeney, M. G. Raizen, and E.-L. Florin, “Direct observation of the full transition from ballistic to diffusive Brownian motion in a liquid”, Nat. Phys., 7(7), pp. 576-580, 2011.
[118] G. Volpe, and G. Volpe, “Simulation of a Brownian particle in an optical trap”, Am. Journ. of Phys., 81(3), pp. 224-230, 2013.
[119] X. Serey, S. Mandal and D. Erickson, “Comparison of silicon photonic crystal resonator designs for optical trapping of nanomaterials”, Nanotechnology, 21(30), 305202, 2010
[120] J. Wang, Z. Li, C. P. Yao, F. Xue, Z. X. Zhang, and G. Hüttmann, “Brownian Diffusion of Gold Nanoparticles in an Optical Trap Studied by Fluorescence Correlation Spectroscopy”, Laser Phys., 21(1), pp. 130-136, 2011.
[121] A. Kotnala and R. Gordon, “Quantification of High-Efficiency Trapping of Nanoparticles in a Double Nanohole Optical Tweezer”, Nano Lett., 14(2), pp. 853–856, 2014.
[122] M. Pelton, M. Liu, H. Y. Kim, G. Smith, P. Guyot-Sionnest, and N. F. Scherer, “Optical trapping and alignment of single gold nanorods by using plasmon resonances”, Opt. Lett., 31(13), pp. 2075-2077, 2006.
[123] X. Serey, S. Mandal, Y.-F. Chen, and D. Erickson, “DNA Transport and Delivery in Thermal Gradients near Optofluidic Resonators”, Phys. Review Lett., 108(4), 048102, 2012.
[124] E. J. G. Peterman, F. Gittes, and C. F. Schmidt, “Laser-Induced Heating in Optical Traps”, Biophys. Journ., 84(2), pp. 1308-1316, 2003.
[125] M. D. Wang, H. Yin, R. Landick, J. Gelles, and S. M. Block, “Stretching DNA with Optical Tweezers”, Biophys. Journ., 72(3): 1335-1346, 1997.
[126] S. N. S. Reihani, and L. B. Oddershede, “Optimizing immersion media refractive index improves optical trapping by compensating spherical aberrations”, Opt. Lett., 32(14), pp. 1998-2000, 2007.
[127] K. Dholakia, and T. Cizmar, “Shaping the future of manipulation”, Nat. Phot., 5(6), pp. 335-342, 2011.
[128] G. Rui, and Q. Zhan, “Trapping of resonant metallic nanoparticles with engineered vectorial optical field”, Nanophotonics, 2014, 3(6): 351-361.
[129] J. W. Taraska, “Simply Better Resolution in Live Cells”, Trends in Cell Biol., 25(11), pp. 636-638, 2015.

[130] S. F. Gibson, and F. Lanni, "Experimental test of an analytical model of aberration in an oil-immersion objective lens used in three-dimensional light microscopy", Journ. of the Opt. Soc. of Am. A, Optics and image science, 9(1), pp. 154-156, 1992.

[131] M. P Lee, and M. J Padgett, "Optical tweezers: a light in touch", Journ. of Microsc., 248(3), pp. 219-222, 2012.

[132] B. S. Schmidt, A. H. J. Yang, D. Erickson, and M. Lipson, "Optofluidic trapping and transport on solid core waveguides within a microfluidic device", Opt. Exp., 15(22), pp. 14322-14334, 2007.

[133] L. Kong, C. Lee, C. M. Earhart, B. Cordovez, and J. W. Chan, "A nanotweezer system for evanescent wave excited surface enhanced Raman spectroscopy (SERS) of single nanoparticles", Opt. Exp., 23(5), pp. 6793-6802, 2015.

[134] S. Kawata and T. Tani, "Optically driven Mie particles in an evanescent field along a channeled waveguide", Opt. Lett., 21(21), pp. 1768-1770, 1996.

[135] L. N. Ng, B. J. Luff, M. N. Zervas, and J. S. Wilkinson, "Propulsion of gold nanoparticles on optical waveguides", Opt. Comm., 208(1), pp. 117-124, 2002.

[136] B. S. Ahluwalia, P. McCourt, T. Huser, O. G. Helleso, "Optical trapping and propulsion of red blood cells on waveguide surfaces", Opt. Exp., 18(20), pp. 21053-21061, 2010.

[137] S. Gaugiran, S. Gétin, J. M. Fedeli, G. Colas, A. Fuchs, F. Chatelain, and J. Dérouard, "Optical manipulation of microparticles and cells on silicon nitride waveguides", Opt. Exp., 13(18), pp. 6956-6963, 2005.

[138] O. G. Hellesø, P. Løvhaugen, A. Z. Subramanian, J. S. Wilkinson, B. S. Ahluwalia, "Surface transport and stable trapping of particles and cells by an optical waveguide loop", Lab on a Chip, 12(18), pp. 3436-3440, 2012.

[139] D. Psaltis, S. R. Quake, and C. Yang, "Developing optofluidic technology through the fusion of microfluidics and optics", Nature, 442(7101), pp. 381-386, 2006.

[140] C. Yu, S. Mutlu, P. Selvaganapathy, C. H. Mastrangelo, F. Svec, and J. M. J. Frechet, "Flow Control Valves for Analytical Microfluidic Chips without Mechanical Parts Based on Thermally Responsive Monolithic Polymers", Anal. Chem., 75(8), pp. 1958-1961, 2003.

[141] J. Dai, T. Ito, L. Sun, and R. M. Crooks, "Electrokinetic Trapping and Concentration Enrichment of DNA in a Microfluidic Channel", Journ. of the Amer. Chem. SOc., 125(43), pp. 13026-13027, 2003.

[142] N. L. Jeon, D. T. Chiu, C. J. Wargo, H. Wu, I. S. Choi, J. R. Anderson, and G. M. Whitesides, Design and fabrication on integrated passive valvs and pumps

for flexible polymer3-Dimensional Microfluidic Systems“, Biom. Microd., 4(2), pp. 117-121, 2002.
[143] P. Domachuk, M. Cronin-Golomb, B. J. Eggleton, S. Mutzenich, G. Rosengarten, A. Mitchell, “Application of optical trapping to beam manipulation in optofluidics”, Opt. Exp. 13(19), pp. 7265-7275, 2005.
[144] D. J. Sirbuly, A. Tao, M. Law, R. Fan, and P. Yang, “Multifunctional Nanowire EvanescentWave Optical Sensors”, Adv. Mat. Vol. 19, no. 1, pp. 61-66, 2007.
[145] P. Schein, C. K. Ashcroft, D. O’Dell, I. S. Adam, B. Di Paolo, M. Sabharwal, C. Shi, R. Hart, C. Earhart, and D.Erickson, “Near-Field Light Scattering Techniques for Measuring Nanoparticle-Surface Interaction Energies and Forces”, Journ. of Ligthw. Tech., 33(16), pp. 3494-3502, 2015.
[146] M. Soltani, J. Lin, R. A. Forties, J. T. Inman, S. N. Saraf, R. M. Fulbright, M. Lipson, and M. D. Wang, “Nanophotonic Trapping for Precise Manipulation of Biomolecular Arrays”, Nat. Nanotech., 9(6), pp. 448-452, 2014.
[147] A. H. J. Yang, S. D. Moore, B. S. Schmidt, M. Klug, M. Lipson, and D. Erickson, “Optical manipulation of nanoparticles and biomolecules in sub-wavelength slot waveguides”, Nature, 457(7225), pp. 71-75, 2009.
[148] A. H. J. Yang, T. Lerdsuchatawanich, and D. Erickson, “Forces and Transport Velocities for a Particle in a Slot Waveguide”, Nano Lett., 9(3), pp. 1182-1188, 2009.
[149] S. Lin and K. B. Crozier, “An integrated microparticle sorting system based on near-field optical forces and a structural perturbation”, Opt. Exp., vol. 20, no. 4, pp. 3367-3374, 2012.
[150] C. Ciminelli, D. Conteduca, F. Dell'Olio, M. N. Armenise, “Design of an Optical Trapping Device Based on an Ultra-High Q/V Resonant Structure”, IEEE Phot. Journ., 6(6), 0600916, 2014.
[151] A. Rahmani, P. C. Chaumet, “Optical trapping near a photonic crystal”, Optics Express, 14(13), pp. 6353-6358, 2006.
[152] C. Ciminelli, C. M. Campanella, F. Dell’Olio, C. E. Campanella, M. N. Armenise, “Label-free optical resonant sensors for biochemical applications”, Progress in Quantum Electronics, 37(2), pp. 51-107, 2013.
[153] K. De Vos, I. Bartolozzi, E. Schacht, P. Bienstman1, R. Baets, “Silicon-on-Insulator microring resonator for sensitive and label-free biosensing”, Opt. Exp., 15(12), pp. 7610-7615, 2007.
[154] C. Ciminelli, F. Dell’Olio, D. Conteduca, C. M. Campanella, M. N. Armenise, “High performance SOI microring resonator for biochemical sensing”, Opt. and Las. Techn., 59, pp. 60-67, 2014.

[155] H. Wang, X. Wu, D. Shen, "Localized optical manipulation in optical ring resonators", Opt. Express, 23(21), pp. 27650-27660, 2015.
[156] H. Cai, and A. W. Poon, "Optical manipulation and transport of microparticles on silicon nitride microring-resonator-based add–drop devices", Opt. Lett., 35(17), pp. 2855-2857, 2010
[157] A. H. J. Yang and D. Erickson, "Optofluidic ring resonator switch for optical particle transport", Lab on a chip, 10(6), pp. 769-774, 2010.
[158] H. Cai, and A. W. Poon, "Optical manipulation of microparticles using whispering-gallery-modes in a silicon nitride microdisk resonator", Opt. Lett., 36(21), pp. 4257-4259, 2011
[159] S. Lin, E. Schonbrun, and K. Crozier, "Optical Manipulation with Planar Silicon Microring Resonators", Nano Lett., 10(7), pp. 2408-2411, 2010.
[160] S. Arnold, D. Keng, S. I. Shopova, S. Holler, W. Zurawsky, and F. Vollmer, "Whispering gallery mode carousel – a photonic mechanism for enhanced nanoparticle detection in biosensing", Opt. Exp., 17(8), pp. 6230-6238, 2009.
[161] T. F. Krauss, "Slow light in photonic crystal waveguides", Journ. of Phys D: App. Phys., 40, pp. 2666-2670, 2007.
[162] C. Ciminelli, H.M. Chong, F. Peluso, R.M. De La Rue, M.N. Armenise, High-Q Guided-Wave Photonic Crystal Extended Microcavity, in Proc. ECOC 2004, Post-deadline Paper Th. 4.2.6, Stockholm, (2004).
[163] M. Lee, and P. M. Fauchet, "Two-dimensional silicon photonic crystal based biosensing platform for protein detection", Opt. Exp., 15(8), pp. 4530-4535, 2007.
[164] M.G. Scullion, A. Di Falco, T.F. Krauss, "Slotted photonic crystal cavities with integrated microfluidics for biosensing applications", Biosens. and Bioelect., 27(1), pp. 101-105, 2011.
[165] C. Monat, P. Domachuk, and B. J. Eggleton, "Integrated optofluidics: a new river of light", Nat. Phot., 1(2), pp. 106-114, 2007.
[166] D. Conteduca, F. Dell'Olio, C. Ciminelli, and M. N. Armenise, "New miniaturized exhaled nitric oxide sensor based on a high Q/V mid-infrared 1D photonic crystal cavity", App. Opt., 54(9), pp. 2208-2217, 2015.
[167] B.-S. Song, S. Noda, T. Asano, Y. Akahane, "Ultra-high-Q photonic double heterostructure nanocavity", Nat. Mat., 4(3), pp. 207-210, 2005.
[168] M. G. Scullion, Y. Arita, T. F. Krauss, and K. Dholakia, "Enhancement of optical forces using slow light in a photonic crystal waveguide", Optica, 2(9), pp. 816-821, 2015.

[169] S. H. Mirsadeghi, J. F. Young, "Ultrasensitive Diagnostic Analysis of Au Nanoparticles Optically Trapped in Silicon Photonic Circuits at Sub-Milliwatt Powers", Nano Lett., 14(9), pp. 5004-5009, 2014.

[170] N. Descharmes, U. P. Dharanipathy, Z. Diao, M. Tonin, and R. Houdre, "Observation of Backaction and Self-Induced Trapping in a Planar Hollow Photonic Crystal Cavity", Phys. Review Lett.,, 110(12), 123601, 2013.

[171] P. Lalanne, C. Sauvan, J. P. Hugonin, "Photon confinement in photonic crystal nanocavities", Laser and Phot. Reviews, 2(6), pp. 514-526, 2008.

[172] Q. Quan, P. B. Deotare, and M. Loncar, "Photonic crystal nanobeam cavity strongly coupled to the feeding waveguide," Appl. Phys. Lett. 96, 203102, 2010.

[173] A. R. Md Zain, N. P. Johnson, M. Sorel, and R. M. De La Rue, "Ultra high quality factor one dimensional photonic crystal/photonic wire micro-cavities in silicon-on-insulator (SOI) ", Opt. Exp., 16(16), pp. 12084-12089, 2008.

[174] Q. Quan, M. Loncar, "Deterministic design of wavelength scale, ultra-high Q photonic crystal nanobeam cavities", Optics Exp., 19(19), 18529-18542, 2011.

[175] C. Wang, Q. Quan, S. Kita, Y. Li, and M. Lončar, "Single-nanoparticle detection with slot-mode photonic crystal cavities", App. Phys. Lett., 106(26), pp. 261105, 2015.

[176] F. Liang and Q. Quan, "Detecting Single Gold Nanoparticles (1.8 nm) with Ultrahigh-Q Air-Mode Photonic Crystal Nanobeam Cavities", ACS Photon., 2(12), pp. 1692-1697, 2015.

[177] S. Mandal, X. Serey, and D. Erickson, "Nanomanipulation Using Silicon Photonic Crystal Resonators", Nano Lett., 10(1), pp. 101-104, 2010.

[178] Y.-F. Chen, X. Serey, R. Sarkar, P. Chen, and D. Erickson, "Controlled Photonic Manipulation of Proteins and Other Nanomaterials", Nano Lett., 12(3), pp. 1633-1637, 2012.

[179] D. K. Gramotnev, and sS. I. Bozhevolnyi, "plasmonics beyond the diffraction limit", Nat. Phot., 4(2), pp. 83-91, 2010.

[180] M. Dragoman, D. Dragoman, "Plasmonics: Applications to nanoscale terahertz and optical devices", Prog. In Quant. Elect., 32(1), pp. 1-41, 2008.

[181] K. F. MacDonald, Z. L. Samson, M. I. Stockman and N. I. Zheludev, "Ultrafast active plasmonics", Nat. Phot., 3(1), pp. 55-58, 2008.

[182] N. Liu, M. Mesch, T. Weiss, M. Hentschel, and H. Giessen, "Infrared perfect absorber and its application as plasmonic sensor", Nano Lett., 10(7), pp. 2342-2348, 2010.

[183] T. Xu, Yi-K. Wu, X. Luo, and L. J. Guo, "Infrared Perfect Absorber and Its Application As Plasmonic Sensor", Nat. Comm., 1(59), 2010.

[184] H. A. Atwater, and A. Polman, “Plasmonics for improved photovoltaic devices”, Nat. Mat., 9(3), pp. 205-213, 2010.

[185] J. A. Conway, S. Sahni, and T. Szkopek. “Plasmonic interconnects versus conventional interconnects: a comparison of latency, crosstalk and energy costs”, Opt. Exp. 15(8), pp. 4474-4484, 2007.

[186] E. Ozbay, “Plasmonics: Merging Photonics and Electronics at Nanoscale Dimensions”, Science, 311(5758), pp. 189-193, 2006.

[187] J. N. Anker, W. P. Hall, O. Lyandres, N. C. Shah, J. Zhao and R. P. Van Duyne, “Biosensing with plasmonic nanosensors”, Nat. Mat., 7(6), pp. 442-453, 2008.

[188] C. Valsecchi, A. G. Brolo, “Periodic Metallic Nanostructures as Plasmonic Chemical Sensors”, Langmuir, 29(19), pp. 5638-5649, 2013.

[189] S. Lal, S. Link, and N. J. Halas, “Nano-optics from sensing to waveguiding”, Nat. Phot., 1(11), pp. 641-648, 2007.

[190] V. G. Kravets, F. Schedin, R. Jalil, L. Britnell, R. V. Gorbachev, D. Ansell, B. Thackray, K. S. Novoselov, A. K. Geim, A. V. Kabashin and A. N. Grigorenko, “Singular phase nano-optics in plasmonic metamaterials for label-free single-molecule detection”, Nat. Mat., 12(4), pp. 304-309, 2013.

[191] T. Lohmuller, L. Iversen, M. Schmidt, C. Rhodes, H.-L. Tu, W.-C. Lin, and J. T. Groves, “Single Molecule Tracking on Supported Membranes with Arrays of Optical Nanoantennas”, Nano Lett., 12(3), pp. 1717-1721, 2012.

[192] A. E. Çetin, A. A. Yanik, C. Yilmaz, S. Somu, A. Busnaina and H. Altug, “Monopole antenna arrays for optical trapping, spectroscopy, and sensing”, App. Phys. Lett., 98(11), 111110, 2011.

[193] T. V. Raziman, R. J. Wolke, and O. J. F. Martin, “Optical forces in nanoplasmonic systems: how do they work, what can they be useful for?”, Faraday Discuss., 178, pp. 421-434, 2015.

[194] M. L Juan, M. Righini, and R. Quidant, “Plasmon nano-optical tweezers”, Nat. Phot., 5(6), pp. 349-356, 2011.

[195] J. H. Kang, K. Kim, H. S. Ee, Y. H. Lee, T. Y. Yoon, M. K. Seo, H. G. Park, “Low-power nano-optical vortex trapping via plasmonic diabolo nanoantennas”, Nat. Comm., 2, 582, 2011.

[196] K. B. Crozier, W. Zhu, D. Wang, S. Lin, M. D. Best, and J. P. Camden, “Plasmonics for Surface Enhanced Raman Scattering: nanoantennas for Single Molecules”, IEEE Journ. on Selected Topics in Quant. Electr., 20(3), 6601645, 2014.

[197] D. Punj, R. Regmi, A. Devilez, R. Plauchu, S. B. Moparthi, B. Stout, N. Bonod, H. Rigneault, and J. Wenger, “Self-Assembled Nanoparticle Dimer Antennas for

Plasmonic-Enhanced Single-Molecule Fluorescence Detection at Micromolar Concentrations*",* ACS Photonics, 2(8), pp 1099–1107, 2015.

[198] D. P. Fromm, A. Sundaramurthy, P. J. Schuck, G. Kino, and W. E. Moerner, "Gap-Dependent Optical Coupling of Single "Bowtie" Nanoantennas Resonant in the Visible", Nano Lett., 4(5), pp. 957-961, 2004.

[199] C. M. Galloway, M. P. Kreuzer, S. S. Acimovic ,G. Volpe, M. Correia, S. Petersen, M. T. Neves-Petersen, and R. Quidant, "Plasmon-Assisted Delivery of Single Nano-Objects in an Optical Hot Spot", Nano Lett., 13(9), pp. 4299-4304, 2013.

[200] H. Fischer and O. J. F. Martin, "Engineering the optical response of plasmonic nanoantennas", Opt. Exp., 16(2), pp. 9144-9154, 2008.

[201] W. Zhang, L. Huang, C. Santschi and O. J. F. Martin, "Trapping and Sensing 10 nm Metal Nanoparticles Using Plasmonic Dipole Antennas", Nano Lett., 10(3), pp.1006-1011, 2010.

[202] M. B. Rasmussen, L. B. Oddershede and H. Siegumfeldt, "Optical Tweezers Cause Physiological Damage to Escherichia coli and Listeria Bacteria", Appl. Environ. Microbiol., 74(8), pp. *2441-2*446, 2008.

[203] M. Ploschner ; M. Mazilu ; T. F. Krauss; K. Dholakia, "Optical forces near a nanoantenna", Journ. of Nanophot., 4(1), 041570, 2010.

[204] B. Roxworthy, M. T. Johnston, F. T. Lee-Montiel, R. H. Ewoldt, P. I. Omoukhuede, K. C. Toussaint, "Plasmonic Optical Trapping in Biologically Relevant Media", Plos One, 9(4), 2014.

[205] H. Chen, Q. Ding, B. J. Roxworthy, A. M. Bhuiva, K. C. Toussaint, "Optical trapping with pillar bowtie nanoantennas", Proceedings of SPIE, the International Society of Optical Engineering, 9164, 91641M, 2014

[206] B. J. Roxworthy, K. D. Ko, A. Kumar, K. H. Fung, E. K. C. Chow, G. L. Liu, N. X. Fang, and K. C. Toussaint, Jr, "Application of Plasmonic Bowtie Nanoantenna Arrays for Optical Trapping, Stacking, and Sorting", Nano Lett., 12(2): 796-801, 2012.

[207] H. Chen, A. M. Bhuiya, R. Liu, D. M. Wasserman, and K. C. Toussaint, Jr, "Design, Fabrication, and Characterization of Near-IR Gold Bowtie Nanoantenna Arrays", The Journ. of Phys. Chem. C, 118(35)5, pp. 20553-20558, 2014.

[208] E.-S. Kwak, T.-D. Onuta, D. Amarie, R. Potyrailo, B. Stein, S. C. Jacobson, W. L. Schaich, and B. Dragnea, "Optical Trapping with Integrated Near-Field Apertures", J. Phys. Chem. B, 108(36), pp. 13607-13612, 2004.

[209] M. L. Juan, R. Gordon, Y. Pang, F. Eftekhari and R. Quidant, "Self-induced back-action optical trapping of dielectric nanoparticles". Nat. Phys., 5, pp. 915-919, 2009.

[210] A. Kotnala, and R. Gordon, "Double nanohole optical tweezers visualize protein p53 suppressing unzipping of single DNA-hairpins", Biom. Opt. Exp., 5(6), pp. 1886- 1894, 2014.

[211] J.-D. Kim and Y.-Gu Lee, "Trapping of a single DNA molecule using nanoplasmonic structures for biosensor applications", Biom. Opt. Exp., 5(8), 2471-2480, 2014.

[212] C. Chen, M. L. Juan, Y. Li, G. Maes G. Borghs, P. Van Dorpe, and R. Quidant, "Enhanced Optical Trapping and Arrangement of Nano-Objects in a Plasmonic Nanocavity", Nano Lett., 12(1), pp. 125-132, 2012.

[213] A. A. E. Saleh, and J. A. Dionne, "Toward Efficient Optical Trapping of Sub-10-nm Particles with Coaxial Plasmonic Apertures", Nano Lett., 12(11), pp. 5581-5586, 2012.

[214] Y. Pang and R. Gordon, "Optical trapping of a single protein", Nano Lett., 12(1), pp. 402-406, 2012.

[215] Y. Pang and R. Gordon, "Optical Trapping of 12 nm Dielectric Spheres Using Double-Nanoholes in a Gold Film", Nano Lett., 11(9), pp. 3763-3767, 2011.

[216] A. Kotnala, D. De Paoli and R. Gordon, "Sensing nanoparticles using a double nanohole optical trap", Lab on a Chip, 13(20), pp. 4142-4146, 2013.

[217] A. Zehtabi-Oskuie, A. A. Zinck, R. M. Gelfand, and R. Gordon, "Template stripped double nanohole in a gold film for nano-optical tweezers", Nanotech., 2014, 25(49): 495301.

[218] A. A. Al Balushi, A. Zehtabi-Oskuie, and R. Gordon, "Observing single protein binding by optical transmission through a double nanohole aperture in a metal film", Biom. Opt. Exp., 2013, 4(9): 1504-1511.

[219] A. Zehtabi-Oskuie, H. J., B. R. Cyr, D. W. Rennehan, A. A. Al-Balushi, and R. Gordon, "Double nanohole optical trapping: dynamics and protein-antibody co-trapping", Lab on a Chip, 2013, 13(13): 2563-2568.

[220] R. M. Gelfand, S. Wheaton, and R. Gordon, "Cleaved fiber optic double nanohole optical tweezers for trapping nanoparticles", Opt. Lett., 2014, 39(22): 6415-6417.

[221] J. Berthelot, S. S. Acimovic, M. L. Juan, M. P. Kreuzer, J. Renger, and R. Quidant, "Three-dimensional manipulation with scanning near-field optical nanotweezers", Nature Nanotech., 9(4), pp. 295-299, 2014.

[222] C. Tserkezis, R. Esteban, D. O. Sigle, J. Mertens, L. O. Herrmann, J. J. Baumberg, and J. Aizpurua, "Hybridization of plasmonic antenna and cavity

modes: Extreme optics of nanoparticle-on-mirror nanogaps", Phys. Review A, 92(5), 053811, 2015.

[223] D. Conteduca, F. Dell'Olio, C. Ciminelli, T. F. Krauss, and M. N. Armenise, "Design of a new photonic/plasmonic microcavity allowing a strong light-matter interaction", 3rd Mediterranean Photonics Conference, MePhoCo, May 7th-9th 2014, Trani (Italy).

[224] X. Yang, Y. Liu, R. F. Oulton, X. Yin, and X. Zhang, "Optical Forces in Hybrid Plasmonic Waveguides", Nano Lett, 11(2), pp. 321-328, 2011.

[225] S. Cui, X. Zhang, T. Liu, J. Lee, D. Bracher, K. Ohno, D. Awschalom, and E. L. Hu, "Hybrid Plasmonic Photonic Crystal Cavity for Enhancing Emission from near-Surface Nitrogen Vacancy Centers in Diamond", ACS Photonics, 2(4), pp. 465-469, 2015.

[226] M. Kauranen and A. V. Zayats, "Nonlinear plasmonics", Nat. Phot., 6(11), pp. 737-748, 2012.

[227] K. Roy, M. Padmanabhan, S. Goswami, T. Phanindra Sai, G. Ramalingam, S. Raghavan and A. Ghosh, "Graphene–MoS2 hybrid structures for multifunctional photoresponsive memory devices", Nat. Nanotech., 8(11), pp. 826-830, 2013.

[228] M. Fevrier, P. Gogol, A. Aassime, R. Megy, C. Delacour, A. Chelnokov, A. Apuzzo, S. Blaize, J.-M. Lourtioz, and B. Dagens, "Giant Coupling Effect between Metal Nanoparticle Chain and Optical Waveguide", Nano Lett., 12(2), pp. 1032-1037, 2012.

[229] M. A. Santiago-Cordoba, M. Cetinkaya, S. V. Boriskina, F. Vollmer, M. C. Demirel, "Ultrasensitive detection of a protein by optical trapping in a photonic-plasmonic microcavity", Journ. of Biophot., 5(8), pp. 629-638, 2012.

[230] C. Ciminelli, C. M. Campanella, F. Dell'Olio, C. E. Campanella, M. N. Armenise, "Label-free optical resonant sensors for biochemical applications", Progr. In Quant. Elect., 37(2), pp. 51-107, 2013.

[231] F. Vollmer, S. Arnold, "Whispering-gallery-mode biosensing: label-free detection down to single molecules", Nat. Meth., 5(7), pp. 591-596, 2008.

[232] V. R. Dantham, S. Holler, C. Barbre, D. Keng, V. Kolchenko, and S. Arnold "Label-Free Detection of Single Protein Using a Nanoplasmonic-Photonic Hybrid Microcavity", Nano Lett., 13(7), pp. 3347-3351, 2013.

[233] D. O'Dell, X. Serey, D. Erickson, "Self-assembled photonic-plasmonic nanotweezers for directed self-assembly of hybrid", App. Phys. Lett., 104(4), 043112, 2014.

[234] P.-T. Lin, H.-Y. Chu, T.-W. Lu, and Po-Tsung Lee, "Trapping particles using waveguide-coupled gold bowtie plasmonic tweezers", Lab on a chip, 14(24), pp. 4647-4652, 2014.

[235] G. Wang, Z. Ying, H.-pui Ho, Y. Huang, N. Zou, X. Zhang, "Nano-optical conveyor belt with waveguide-coupled excitation ", Opt. Lett., 41(3), pp. 528-531, 2016.

[236] D. Conteduca, F. Dell'Olio, C. Ciminelli, T. F. Krauss, and M. N. Armenise, "Design of a high performance optical tweezer for nanoparticle trapping", Applied Physics A, 122(4), 295, 2016.

[237] D. Conteduca, F. Dell'Olio, C. Ciminelli, T. F. Krauss, and M. N. Armenise, 3rd Mediterranean Photonics Conference, MePhoCo, May 7th-9th, 2014, Trani (Italy).

[238] D. Conteduca, F. Dell'Olio, C. Ciminelli, T. F. Krauss, M. N. Armenise, "Ultra-high Q/V hybrid cavity for strong light-matter interaction", manuscript in preparation.

List of publications

Publications related to the PhC activity

International Journals

1. C. Ciminelli, D. Conteduca, F. Dell'Olio, M. N. Armensise, "Design of an optical trapping device based on an ultra-high Q/V resonant structure", IEEE Phot. Journ, 6(6), 0600916, 2014;
2. D. Conteduca, F. Dell'Olio, F. Innone, C. Ciminelli, M. N. Armenise, "Rigorous design of an ultra-high Q/V photonic/plasmonic cavity to be used in biosensing applications", Optics and Laser Tech., 77, 2016;
3. D. Conteduca, F. Dell'Olio, C. Ciminelli, T. F. Krauss, M. N. Armenise, "Design of a high-performance optical tweezer for nanoparticle trapping", Applied Phys. A, 124(4), 2016.
4. D. Conteduca, F. Dll'Olio, T. F. Krauss, C. Ciminelli, "Photonic and plasmonic nanotweezing of nano- and microscale particles", in stampa su Applied Spectroscopy, 2016
5. D. Conteduca, F. Dell'Olio, C. Ciminelli, T. F. Krauss, M. N. Armenise, "Ultra-high Q/V hybrid cavity for strong light-matter interaction", manuscript in preparation.

International conferences

6. C. Ciminelli, F. Dell'Olio, D. Conteduca, T. F. Krauss, M. N. Armenise, "Hybrid photonic/plasmonic microcavities for Q/V ratio enhancement", 16th International Conference on Transparent Optical Networks (ICTON), Graz (Austria), 6 – 10 July, 2014, Invited Paper.

7. D. Conteduca, F. Dell'Olio, C. Ciminelli, T. F. Krauss, M. N. Armenise, "Design of a new photonic/plasmonic microcavity allowing a strong light-matter interaction", IEEE 3rd Mediterranean Photonics Conference (MEPHOCO), TRANI 7-9 May, 2014.

8. D. Conteduca, F. Dell'Olio, C. Ciminelli, T. F. Krauss, M. N. Armenise, "Design of a high-performance optical tweezer for nanoparticle trapping", META'15, the 6th International Conference on Metamaterials, Photonic Crystals and Plasmonics", New York, 4-7 Aug, 2015.

9. D. Conteduca, F. Dell'Olio, T. F. Krauss, C. Ciminelli, "Photonic-plasmonic nanotweezer for single nanoparticle optical trapping", PECS XII, York, July 17-21, 2016.

National conferences

10. D. Conteduca, F. Dell'Olio, C. Ciminelli, M. N. Armenise, "Optical forces control in photonic/plasmonic device for optical trapping", 46th annual meeting of the Associazione Gruppo Italiano di Elettronica (GE Association), Cagliari 16 – 20 June 2014.

11. M. N. Armenise, C. Ciminelli, D. Conteduca, I. De Bene, M. De Palo, F. Dell'Olio, F. Indiveri, F. Innone, D. Palmisano, N. Sasanelli and T. Tatoli, "Modelling and design of a new nanophotonic/plasmonic resonant biosensor for optical trapping and monitoring of nanoparticles", Workshop Score Poliba, 3-5 Dec. (Bari), 2014.

Other publications

International Journals

12. C. Ciminelli, F. Dell'Olio, D. Conteduca, C. M. Campanella, M. N. Armenise, "High performance SOI microring resonator for biochemical sensing", Optics & Laser Technology, 59, pp. 60-67, 2014.
13. F. Dell'Olio, D. Conteduca, C. Ciminelli, M. N. Armenise, "New ultrasensitive resonant photonic platform for label-free biosensing", Optics Express, 23(22), pp. 28593-28604, 2015.
14. D. Conteduca, F. Dell'Olio, C. Ciminelli, M. N. Armenise, "Novel graphene-based photonic devices for efficient light control and manipulation", IEEE Photonics Journal, 7(6), 7802409, 2015.
15. C. Ciminelli, D. D'Agostino, G. Carnicella, F. Dell'Olio, D. Conteduca, H.P.M.M. Ambrosius, M. K. Smit, M. N. Armenise, "A High-Q InP Resonant Angular Velocity Sensor for a Monolithically Integrated Optical Gyroscope", IEEE Photonics Journal, 8(1), 6800418, 2015.
16. D. Conteduca, F. Dell'Olio, C. Ciminelli, M. N. Armenise, "New miniaturized exhaled nitric oxide sensor based on a high Q/V mid-infrared 1D PhC cavity", Applied Optics, 54(9), pp. 2208-2217, 2015.
17. T. Tatoli, D. Conteduca, F. Dell'Olio, C. Ciminelli, M. N. Armenise, "Graphene-based fine-tunable optical delay line for optical beamforming in phased-array antennas", Applied Optics, 55(16), 2016
18. D. Conteduca, F. Dell'Olio, C. Ciminelli, M. N. Armenise, "Resonant plasmonic label-free biosensor for coronary artery disease detection", manuscript in preparation

International conferences

19. C. Ciminelli, D. Conteduca, F. Dell'Olio, M. N. Armenise, "Novel graphene-based photonic devices for efficient light control and manipulation", 17th International Conference on Transparent Optical Networks (ICTON), Budapest, 5-9 July 2015, Invited Paper.
20. D. Conteduca, T. Tatoli, F. Innone, F. Dell'Olio, C. Ciminelli, M. N. Armenise, "Reconfigurable optical beamformer with graphene-based fine-tunable optical delay line," sottomesso per la presentazione alla 18th Italian National Conference on Photonic Technologies, FOTONICA 2016, Roma 6-8 June.
21. C. Ciminelli, F. Innone, G. Brunetti, D. Conteduca, F. Dell'Olio, T. Tatoli, M.N. Armenise, "Rigorous model for the design of ultra-high Q-factor resonant cavities", 18th International Conference on Transparent Optical Networks ICTON 2016, Trento 10-14 July, 2016, Invited Paper.
22. Ciminelli, F. Dell'Olio, D. Conteduca, F. Innone, T. Tatoli, M. N. Armenise, "New microphotonic resonant devices for label-free biosensing," 18th International Conference on Transparent Optical Networks ICTON 2016, Trento 10-14 July, 2016. Invited Paper.
23. F. Dell'Olio, M. De Palo, D. Conteduca, C. Ciminelli, M. N. Armenise, "Resonant Nanoplasmonic Platform for Fast and Early Diagnosis of Cardiovascular Diseases," 2nd International Forum on Research and Technologies for Society and Industry (RTSI 2016), Bologna, 7-9 Sept., 2016.
24. C. Ciminelli, G. Brunetti, F. Dell'Olio, F. Innone, D. Conteduca, M.N. Armenise, "Emerging Applications of Whispering Gallery Mode Photonic Resonators," ApplePies International Conference (Applications in Electronics Pervading Industry, Environment and Society), Roma, 15-16 Sept., 2016.

National conferences

25. M. N. Armenise, G. Brunetti, G. Carnicella, C. Ciminelli, D. Conteduca, I. De Bene, M. De Palo, F. Dell'Olio, F. Indiveri, F. Innone, D. Palmisano, N. Sasanelli and T.Tatoli, "Miniaturized Optoelectronic Gyroscopes for Aerospace & Defense", Workshop Score Poliba, 3-5 Dec. (Bari), 2014.
26. T.Tatoli, G. D'Amato, D. Conteduca, F. Innone, M. De Palo, F. Dell'Olio, C. Ciminelli, G. Avitabile, M. N. Armenise, "Optoelectronic beamformer for spaceborne X-band synthetic aperture radar", 47th annual meeting of the Associazione Gruppo Italiano di Elettronica (GE Association), Siena 24 – 26 June 2015.
27. M. De Palo, D. Conteduca, F. Innone, T. Tatoli, F. Dell'Olio, C. Ciminelli, M. N. Armenise, "Plasmonic biosensor for cancer markers detection", 47th annual meeting of the Associazione Gruppo Italiano di Elettronica (GE Association), Siena 24 – 26 June 2015.
28. F. Dell'Olio, D. Conteduca, F. Innone, G. Brunetti, C. Ciminelli, M.N. Armenise, "Graphene-based vertically-stacked ring resonators for low power, fast and fine tunable delay line," Riunione Annuale del Gruppo di Elettronica (GE), Brescia, June 2016.
29. F. Innone, G. Brunetti, D. Conteduca, F. Dell'Olio, C. Ciminelli, M.N. Armenise, "Novel mathematical modelling for the design of ultra-high Q-factor ring resonators," Riunione Annuale del Gruppo di Elettronica (GE), Brescia, June 2016.
30. C. Ciminelli, F. Dell'Olio, D. Conteduca, F. Innone, G. Brunetti, M. N. Armenise, "Photonic sensors for hypersonic vehicle guidance/control and structural health monitoring," 2nd International Symposium Hypersonic Flight Proceedings, 2016.